Electrode Design for Improving Electrochemical Performances of Poor Electronic Conductive Active Materials

2013 年 9 月

関西大学審査学位論文

Electrode Design for Improving Electrochemical Performances of Poor Electronic Conductive Active Materials

Satoshi UCHIDA

Kansai University

September, 2013

博士論文要旨

理工学研究科総合理工学専攻
無機・物理化学研究領域
11D6008 内田悟史

Electrode Design for Improving Electrochemical Performances of Poor Electronic Conductive Active Materials

リチウムイオン電池は現在実用化されている二次電池の中で最もエネルギー密度が高い。現在のリチウムイオン電池のほとんどは正極にコバルト酸リチウムまたはマンガン酸リチウム、負極にグラファイト、電解液に $LiPF_6$ 塩を環状および直鎖カーボネートの混合溶媒に溶解させたものを用いており、これらの構成は開発当初からほとんど変更されていない。これまでリチウムイオン電池は携帯電話やノートパソコンなどの小型機器の電源として利用されてきたが、近年では電気自動車や電力貯蔵システムなどの大型機器へ用途が拡大しつつあり、今後、さらなる用途拡大が予想されている。それに伴って更なる高エネルギー密度化、高出力化、安全性の向上などが求められており、これらの要求に対応するためには用途ごとに適した性能を有するリチウムイオン電池を開発すべきであり、各材料を新規なものに置き換える必要がある。中でも電極活物質はリチウムイオン電池の性能を大きく左右するため、代替材料として様々な新規材料が提案されているが、現行のコバルト酸リチウムやグラファイトの性能 (容量、作動電位、高レート特性、サイクル寿命、熱安定性、電子伝導性、コストなど) のバランスが非常に優れているため、新規材料の用途は一部に限られている。特に、次世代材料と目されている正極ならびに負極材料は、諸特性に優れているにも関わらず、電子伝導性に乏しい、あるいは充放電により電子伝導性が維持できなくなる材料が多く、この点の抜本的な改善を可能とする材料設計指針の確立が強く求められている。

本論文では、非常に魅力的な性能を有しつつも電子伝導性に乏しく、その改善が難しいために広く実用化されるに至っていない新規正極材料 $LiFePO_4$ と新規負極材料シリコンに着目し、これらを次世代材料として利用するための材料および電極設計について報告する。

CHAPTER 1

Novel Synthesis Method for $LiFePO_4$ Cathode Material

リン酸鉄リチウム ($LiFePO_4$) の作動電位は 3.5 V vs. Li/Li^+ でありコバルト酸リチウム (3.9 V vs. Li/Li^+) と比べてやや低いが、熱安定性、サイクル寿命に優れ、永続的に原料の安定供給が可能な Fe を用いていることから、大型リチウムイオン電池用の正極材料として非常に魅力的である。他の材料と比べて電子伝導性とリチウムイオン電導性が極端に低いことが問題とされていたが、炭素との複合化による電子伝導性の付与と、微粒子化によるイオン拡散距離の短縮によって、これらの問題点はすでに解決され、現行材料よりも高レートで作動させることも可能になった。しかしながら、このように特性が改善された $LiFePO_4$ の合成は複雑で高コストであり、$LiFePO_4$ の普及を妨げている。この問題を解決するため

に、非常に簡便かつ低コストで電子伝導性とリチウムイオン電導性を付与しつつ、$LiFePO_4$を合成する方法を開発したので、本章で報告する。

Section I-1: A Rapid Synthesis Method of $LiFePO_4$/C Cathode Material Using High-frequency Induction Heating

リチウムイオン電池の正極材料は一般的に固相法で合成される。$LiFePO_4$の合成については様々な方法が報告されているが、簡便かつ実用的な方法はやはり固体原料を粉砕混合して数時間～数十時間焼成する固相法である。しかしながら、$LiFePO_4$に含まれる Fe は二価であり、原料には二価の Fe 化合物が用いられ、これらは容易に酸化して三価の Fe になってしまうため大気中で$LiFePO_4$を合成することが難しく、合成には Ar ガス中や真空中などの不活性雰囲気で長時間の焼成を必要とする。さらに、炭素との複合化や微粒子化に別のプロセスを必要とすることも多く複雑な合成法が多い。本節では原料にFe_2O_3を用いることで原料の取り扱いを簡便にし、さらに高周波誘導加熱法を用いることで焼成から炭素複合化および微粒子化のプロセスを短時間かつ一段階で行う方法について報告する。

Section I-2: Improvement of Heating Condition for $LiFePO_4$/C with High Electric Conductivity

前節で炭素複合化$LiFePO_4$ (以下 $LiFePO_4$/C) の短時間かつ簡便な合成法を報告したが、その電池特性は十分ではなかった。そこで合成した試料の電気伝導率を測定したところ、$LiFePO_4$の特性を十分に引き出すにはやや不十分な値であった。この原因として、本研究で開発した方法が非常に短時間で$LiFePO_4$相を生成させることが可能であるため、炭素複合化のために原料に添加したクエン酸が十分に炭化する前に焼成プロセスが終了してしまうことが予想される。そこで、クエン酸の炭化を促進する必要があるが、高温での焼成時間の延長は生成した$LiFePO_4$相の分解につながる。本節では高温焼成で$LiFePO_4$相を生成させた後、炭化促進のために$LiFePO_4$の分解が起こらない程度の温度に下げて熱処理を続けることで、$LiFePO_4$/C の電気伝導率を向上させることに成功したので、改善された電池化学特性とともに報告する。

Section I-3: Optimized Synthesis Process for Ideal Crystal Structure of $LiFePO_4$

前節で$LiFePO_4$/C に十分な電子伝導性を付与し、高い電池特性を引き出す方法について報告した。しかしながら、前節の方法で合成した $LiFePO_4$/C 容量は理論容量と比較してやや劣っており、レート特性についてもまだ改善の余地があると思われる。そこで、前節の材料の XRD を測定し、リートベルト法で構造を解析したところ、理想的であると思われる構造と比較してやや歪みを持っていることが分かった。これは焼成時の熱伝導が不均一であるためと考えられ、本節では均一な熱伝導を実現し、理想的な構造の$LiFePO_4$を得るための焼成方法と$LiFePO_4$/C のさらに向上した電池特性について報告する。

CHAPTER II

Improving Cycle Stability of High Capacity Silicon Negative Electrode Composed of μm-Silicon Particles

シリコンは最大で $Li_{4.4}Si$ の組成までリチウムを取り込むことが可能で、現行のグラファイト (最大 LiC_6) と比較して、重量規格で 10 倍以上の理論容量を有することから、非常に魅力的な負極材料である。炭素であるグラファイトと比べると電子伝導性が著しく低いが、一度リチウムを取り込み合金化すればその電子伝導性は負極材料として利用可能なレベルに引き上げられる。しかしながら、シリコンは大量のリチウムを取り込むため、充電の際に最大で 400% に膨張し、放電時に収縮する。この繰り返しにより、電極構造が崩壊してシリコン粒子同士の接触が失われ、電子接点が消失する。また、シリコン粒子自体もその応力に耐えられず、クラックの発生とともに微粉化して広表面積化するため、電解液の過剰な分解を招く。この電解液の分解生成物は不動態膜としてシリコン粒子上に堆積して電極の抵抗を増加させる。本章では、活物質であるシリコンに複雑な処理を施すことなく、シリコン電極の電子伝導性を低下させるこれらの問題を解決する方法について報告する。

Section II-1: Electrochemical Properties of Silicon Negative Electrodes Prepared with Polyimide Binder

シリコン電極の電子接点の消失は主にシリコンの膨張収縮による電極構造の崩壊が原因であるため、膨張収縮時の応力を緩和して電極構造を維持するために炭素との複合化やシリコン自体のナノ化による応力の低減が主に研究され、サイクル寿命は改善されてきたが、実用化に際してはまだ十分とはいえない。また、炭素との複合化プロセスが複雑であり、ナノシリコンの大量製造が非常に難しいということも問題である。これらの研究は主に活物質であるシリコンに着目して研究されてきたが、本節ではシリコン粒子と導電助剤を集電箔に結着する役割を担うバインダーに着目した。強力な接着力を持ちながら、破断しやすいポリイミドをバインダーとして用いることで、ナノシリコンを用いることなく膨張収縮時の電子接点の消失を抑制することができ、サイクル安定性を劇的に改善することができたので、本節で報告する。

Section II-2: Effect of Electrolyte Additives on Silicon Negative Electrode Prepared with Polyimide Binder

前節で、シリコン負極の構造の崩壊を抑制することができ、サイクル安定性を劇的に改善することができたが、μm オーダーのシリコン粒子自体にかかる応力を低減することができていないため、シリコン粒子の微粉化抑制が達成できていない。一般的にリチウムイオン電池の負極活物質であるリチウムとの反応電位において熱力学的に安定な電解液は存在しないものの、一度目の充電時に電解液が分解して負極活物質表面に固体電解質界面 (SEI)

膜と呼ばれる不動態膜を形成し、負極活物質と電解液成分の接触を妨げることで、その後の電解液の分解が抑制される。しかしながら、シリコン負極ではシリコンの微粉化によって SEI 膜で覆われていない新生面が発生するため、このような電解液の分解を抑制するメカニズムがうまく働かない。μm オーダーのシリコン粒子の微粉化を抑制することは困難を極めるので、本節では電解液にシリコン電極に対応できる SEI 膜を形成させるための添加剤を使用し、電解液の過剰分解を抑制する方法について報告する。

以上

CONTENTS

GENERAL INTRODUCTION

Principle of Li-ion batteries and their characteristics

Lithium (Li) -ion batteries are generally composed of Li-containing transition metal oxide positive electrode such as $LiCoO_2$ [1-5] and $LiMn_2O_4$ [6-9], graphite [10-14] negative electrode, and $LiPF_6$ dissolved in mixed solvent of linear carbonates and cyclic carbonate [15-18] as electrolyte. Li-ion batteries have highest energy density among secondary batteries commercially available because Li-ion battery has voltage of 3.7 – 3.8 V per single cell due to use the organic electrolyte [19, 20]. Its charge and discharge mechanism is that Li ions and electrons move between positive and negative electrode through the electrolyte, which is relatively simple [19, 21] compared to other secondary batteries. Therefore, deterioration of electrodes of Li-ion batteries is less compared with conventional secondary batteries with dissolution and deposition of electrodes and it has long cycle life [22-24].

Li-ion batteries with high energy density that can be downsized have been contributed the development of portable devices since it was first released by SONY in 1991 [25] and they are mounted on most portable device such as mobile phone and laptop computer even today [26, 27].

Demands of further high-performance Li-ion batteries and their development statue

In recent years, the applications of Li-ion batteries are spreading in large equipment such as plugin hybrid vehicles and electronic vehicles [28-30] and those markets were considered to grow significantly [31, 32]. Moreover, we are currently facing energy issues on a global scale, breaking away from dependence on fossil fuels and power generation using renewable energy have attracted attention[33, 34]. Power generation using renewable energy [35] requires a large energy storage system or household storage battery for power smoothing because the amount of power generation of this system is highly dependent on the weather [36, 37] and environment and application of the Li-ion batteries is also expected in these large applications.

Therefore, the development of Li-ion battery with further high energy density, high power and safety is urgent. However, , the configurations of the Li-ion batteries

currently on the market has not changed almost since the beginning of development because the balance of the performance of $LiCoO_2$ positive electrode and graphite negative electrode (capacity, operating potential, high-rate performances, cycle life, thermal stability, electric conductivity, and cost) are very good [22, 30]. Diversification of the configuration of Li-ion battery and development of Li-ion battery with a performance that is suitable for each application are important in order to meet the demands from diversified applications of Li-ion batteries [28, 38]. A new variety of electrode active materials which directly involved in electrochemical reaction has been proposed as an alternative material because it greatly affects the performance of the Li-ion battery. However, their applications are limited to a small part yet due to the reasons described above. In particular, the electrode materials leading the next generation often have poor electric conductivity or cannot maintain electric conductivity with charge and discharge [39-42]. Accordingly, the establishment of material design guidelines to enable a drastic improvement of these points is strong demand.

Detailed characteristics of the positive electrode materials which are dealt with in this study

Various materials have been proposed so far which involves the primary next generation positive electrode materials such as $LiCo_{1-x}M_xO_2$ (M = Ni, Mn, Al) as alternative materials of $LiCoO_2$, $LiMn_{2-x}M_xO_4$ (x = 0 – 0.5, M = Ni, Cr) as 5 V vs. Li/Li^+ class materials, xLi_2MnO_3-$(1-x)LiNi_{1/3}Mn_{1/3}Co_{1/3}O_2$ solid solution as high capacity materials, and $LiMPO_4$ (M = Fe, Mn, Co) as materials for long cycle life.

The $LiCo_{1-x}M_xO_2$ synthesized by substitution of cobalt in $LiCoO_2$ with another element is most accessible materials [43-45]. The crystal structure and its mechanism of Li insertion and de-insertion are similar to $LiCoO_2$. Substitution of rare and expensive cobalt element can solve the problem of strategic elemental strategy and leads to the reduction of cost. Among these materials, $LiNi_{1/3}Mn_{1/3}Co_{1/3}O_2$ reported by Ohozuku et al. [46, 47] has good thermal stability and its balance of characteristics is excellent. In addition, this material can be reversible charge-discharge in the potential range of over

4.2 V (vs. Li/Li^+), which is difficult in the case of using $LiCoO_2$ due to its irreversible phase transition. Therefore, $LiNi_{1/3}Mn_{1/3}Co_{1/3}O_2$ allows the construction of Li-ion battery with further high capacity and voltage [48, 49]. We also use this material as positive electrode toward the Si negative electrode in this study (Section 5).

Li*M*PO_4 is one of the groups of poly-anionic material. For the poly-anionic materials, the characteristic called inductive effect as shown below has been reported. The redox potential related to Li insertion and de-insertion of poly-anionic materials are significantly raised to positive side by the presence of the *M*O_4 tetrahedron and *M*O_6 octahedron in the structure due to strong polarization of the oxygen atoms toward the *M* cation and subsequent decrease the covalent component in the *M*-O bond [50, 51]. $LiFePO_4$ reported by Padhi et al. [52] in 1997 has relatively high redox potential around 3.5 V vs. Li/Li^+ despite the redox species is Fe. In addition, the crystal structure of $LiFePO_4$ is very stable even if all the Li were de-intercalated from structure by the presence of P-O covalent bond. Therefore, $LiFePO_4$ has good thermal stability and extremely long cycle life compared with $LiCoO_2$ [53-55]. The drawbacks of $LiFePO_4$ are low electric conductivity [39, 52] derived from lattice structure including P-O covalent bonds and poor Li ion diffusion through $LiFePO_4/FePO_4$ interface [56, 57]. The solutions to these problems have been reported already. These problems can be solved by modifying the surface of $LiFePO_4$ particles with carbon [58, 59] and decreasing the particle size to nano-scale [60, 61].

Most prominent advantage of Li-ion cells including nano-sized $LiFePO_4$ modified with carbon ($LiFePO_4$/C) which has been removed the drawbacks described above is quite long cycle life. The cycle life (which is generally defined the cycle number until the cell capacity below 80% of nominal capacity) of typical Li-ion cells composed of $LiCoO_2$ and graphite is about 500 cycles. On the other hand, the cells composed of $LiFePO_4$/C and graphite have overwhelmingly long cycle life more than thousands of cycles [53-55]. In addition, high thermal stability of the cell including $LiFePO_4$/C becomes apparent by suppressing the electrolyte decomposition [53, 62]. Therefore, the Li-ion battery including $LiFePO_4$/C is suitable for the applications

requiring long cycle life and high temperature operating such as large storage system or electric vehicles. In this study, we propose a novel solution method in order to improve the drawbacks of $LiFePO_4$ (CHAPTER I).

Detailed characteristics of the negative electrode materials which are dealt with in this study

The primary next generation negative electrode materials are $Li_4Ti_5O_{12}$ for high power application and silicon (Si) or tin (Sn) as high capacity material. The specific capacity of positive electrode difficult to significantly increase materials due to limited Li storage site and the presence of heavy transition metals in their structure which are required to obtain a high redox potential. Therefore, the demand for higher capacity is directed to the negative electrode which can be used a light element. For this reason, the attention to the Sn and Si increases naturally.

The Li storage mechanism of Si and Sn is alloying reaction [63, 64] which is different from intercalation into layer structure such as graphite. Accordingly, Si and Sn can store large amount of Li compared to graphite. Especially, the theoretical capacity of Si is 4200 mAh g^{-1} (correspond to $Li_{4.4}Si$) [64, 65] which is ten times higher than that of graphite. In addition, Si has relatively low potential of alloying/de-alloying with Li [64]. Therefore, Si is most an attractive negative electrode material for further improvement of energy density. In generally, the electrodes for Li-ion batteries are prepared by applying the slurry including active material, conductive carbon and binder the on current collector and drying it. The active material is fixed tightly to the collector with conductive carbon and electric conductivity of the electrodes is generally maintained during charge and discharge. However, the electric conductivity of Si negative electrode is easily lost because the electronic contacts between Si particles cannot be maintained by electrode structure collapses [41, 66, 67] with large volume expansion (max. 400%) and contraction which relate to alloying/de-alloying with Li ion [68-70] during charge/discharge. In generally, the effective methods to solve this drawback are downsizing (nano-Si particle) [67, 71] and morphology controls (nano-wire, nano-plate) [72-74]. These methods can reduce stress on electrode caused by volume expansion/contraction and suppress the electrode collapse during

charge/discharge. If Si becomes to be used mainly as negative electrode material by improving cycle stability, we will able to develop the thinner negative electrode and obtain the further high energy density. In this study, we try to improve the cycle stability of Si negative electrode without optimization of Si by focusing on binder method (CHAPTER II).

The objective of this study

The $LiFePO_4$ as positive electrode material and Si as negative electrode material have not practically used widely regardless of its extremely attractive battery performances because $LiFePO_4$ has quite poor electric conductivity and electronic contacts in Si electrode are difficult to maintain during cycles even though the improvement methods to overcome these drawbacks have been reported. Therefore, the barrier of practical use of these materials is not presence or absence of improve methods. In other words, this situation means that the proposed methods to overcome drawbacks so far which need complex process and lead to high-cost are not practical. In this thesis, we report the practical material and electrode design for using $LiFePO_4$ and Si as next generation electrode material.

A brief outline of this thesis on material and electrode design for practical use of $LiFePO_4$ and Si electrode is as follows:

CHAPTER I deals with novel synthesis method for $LiFePO_4$ cathode material by using high-frequency induction heating method.

In Section I-1, a rapid synthesis method of $LiFePO_4$/C cathode material using high- frequency induction heating is described. This report has focused on the significant reduction of heating time for the synthesis of $LiFePO_4$ and the detailed heating condition to obtain the single-phase $LiFePO_4$.

In Section I-2, improvement of heating condition for $LiFePO_4$/C with high electric conductivity is described.

In Section I-3, optimizing synthesis process for ideal crystal structure of

$LiFePO_4$ is described. The approaches to theoretical capacity and further improved rate performance of $LiFePO_4$/C by improving the crystal structure of $LiFePO_4$ phase have been discussed.

CHAPTER II deals with improving cycle stability of high capacity silicon negative electrode composed of μm-Si particles.

In Section II-1, electrochemical properties of silicon negative electrodes prepared with polyimide binder are described. This report has proposed a novel improvement method of cycle stability without optimization of Si active material by focusing on binder.

In Section II-2, effect of electrolyte additives on silicon negative electrode prepared with polyimide binder is described. The solutions to problem of electrolyte decomposition with pulverization of Si particles which cannot be avoided even though using polyimide binder have been discussed.

Section I-1. A Rapid Synthesis Method of $LiFePO_4$/C Cathode Material Using High-frequency Induction Heating

The positive electrode materials are generally synthesized by solid-state reactions following grinding and mixing of raw materials which is simple and practical. Various synthesis methods for $LiFePO_4$ have been reported and most of them require eventually long-time heating (550 – 600°C, 6 – 48 h) to obtain $LiFePO_4$ phase with good crystallinity. The heating process of $LiFePO_4$ synthesis cannot be carried out in air because the divalent iron compounds as raw materials of $LiFePO_4$ is easily oxidized and becomes trivalent iron in air. Therefore, the heating process needs inert atmosphere such as Ar flow and vacuum. In addition, another complex processes are often needed for surface modification with carbon and downsizing of $LiFePO_4$ particle to improve electronic and ionic conductivity. These processes lead to high-cost. In this section, novel rapid synthesis method is described, which is developed to achieve the $LiFePO_4$ phase generation, carbon modification and downsizing in one-step heating process by using high-frequency induction heating.

Section I-2. Improvement of Heating Condition for $LiFePO_4$/C with High Electric Conductivity

The $LiFePO_4$ modified with carbon ($LiFePO_4$/C) obtained in Section I-1 shows insufficient battery performances. Accordingly, electric conductivity measurement of obtained sample is carried out and its value is slightly not enough to bring out the good battery performances of $LiFePO_4$. The cause of low electric conductivity is seemed that the heating process is terminated before sufficient carbonization of citric acid which is mixed with raw materials as carbon source because the $LiFePO_4$ phase is generated in a few minutes by high-frequency induction heating. Although the carbonization of citric acid has to be promoted, the extension of high-temperature heating time leads to decompose of $LiFePO_4$ phase. In this section, the annealing process for improving electric conductivity of $LiFePO_4$/C is described. The heat treatment is continued with low temperature of which the decomposition of $LiFePO_4$ phase does not occur in order to promote carbonization of citric acid following $LiFePO_4$ phase generation at high temperature.

Section I-3. Optimizing Synthesis Process for Ideal Crystal Structure of $LiFePO_4$.

The $LiFePO_4$/C with sufficient electric conductivity and battery performance can be obtained by the method referred to in Section I-2. However, the discharge capacity at low rate of $LiFePO_4$/C obtained in Section I-2 is slightly inferior compared to its theoretical capacity and the rate performance seems to be able to improve. From the results of the crystal structure analysis by Rietveld refinement, the lattice parameter of obtained $LiFePO_4$ phase slightly different from that of ideal crystal structure. The slight distortion of the crystal structure prevents the Li ion conduction and limits battery performance of $LiFePO_4$/C, which is caused by inhomogeneous heating in synthesis process. The cause inhomogeneous heating is attributed to shape of the carbon crucible used in the heating process. Therefore, the heating process to obtain $LiFePO_4$/C with ideal crystal structure by using carbon crucible shape which enable to homogeneous heating is proposed in this section.

Section II-1. Electrochemical Properties of Silicon Negative Electrodes Prepared with Polyimide Binder

The decrease in electric conductivity (lost contact between Si particles) of Si electrode is caused by the collapse of electrode structure occurring together with expansion and contraction of Si electrode. Therefore, to maintain the electrode structure with relax the stress during expansion and contraction, downsizing, morphology controls (ca. nano-Si powder, Si nano-wire, and nano-plate) and combination of carbon composite with them have been studied mainly. Unfortunately, these methods are difficult to practical use because the fabrication process of Si-carbon composite is usually complex and mass production of nano-Si is very difficult. Therefore, conventional μm-Si particles should be used as active material and its cycle stability should be improved without optimization of Si or Si-carbon composite active materials. In this section, the improving method for cycle stability focusing on binder is proposed.

Section II-2. Effect of Electrolyte Additives on Silicon Negative Electrode Prepared with Polyimide Binder

In Section II-1, the cycle stability of μm-Si negative electrode is significantly improved by the application of polyimide having small breaking elongation and strong adhesion to the Si. But, the pulverization of Si particle is not prevented, which is certainly occurred as long as using μm-Si particles. The increase in surface area by pulverization of Si particle leads to excessive electrolyte decomposition. In generally, the inactive solid-electrolyte interface (SEI) layer formed by initial electrolyte decomposition prevents further decomposition. However, the electrolyte decomposition continues on Si electrode because the new surface which is not covered with the SEI layer constantly appears while the pulverization of Si is occurring. Therefore, the effect of electrolyte additives to prevent electrolyte decomposition on Si electrode should be investigated. In this section, effective electrolyte additive for Si negative electrode prepared with polyimide binder is selected and further improvement of cycle stability is reported.

References

[1] K. Mizushima, P.C. Jones, P.J. Wiseman, J.B. Goodenough, Mat. Res. Bull. 15 (1980) 783.

[2] T. Ohzuku, A. Ueda, J. Electrochem. Soc. 141 (1994) 2972.

[3] H. Wang, Y. I. Jang, B. Huang, D. R. Sadoway, Y. M. Chiang, J. Electrochem. Soc. 146 (1999) 473.

[4] K. Dokko, M. Mohamedi, Y. Fujita, T. Itoh, M. Nishizawa, M. Umeda, I. Uchida, J. Electrochem. Soc. 148 (2001) A422.

[5] H. Tukamoto, A. R. West, J. Electrochem. Soc. 144 (1997) 3164.

[6] M.M. Thackeray, P.J. Johnson, L A de Picciotto, P.G. Bruce, J.B. Goodenough, Mat. Res. Bull. 19 (1984) 179.

[7] M. M. Thackeray, A de Kock, M. H. Rossouw, D. Liles, J. Electrochem. Soc., 139 (1992) 363.

[8] Y. Xia and M. Yoshio, J. Electrochem. Soc. 143 (1996) 825.

[9] Y. Xia and M. Yoshio, J. Electrochem. Soc. 144 (1997) 4186.

[10] A. Yoshino, K. Sanechika, T. Nakajima, Jpn. Patent No. 90863/87 (1987).

[11] T. Ohzuku, Y. Iwakoshi, K. Sawai, J. Electrochem. Soc. 143 (1996) 2490.

[12] D. Aurbach, Y. Ein-Eli, J. Electrochem. Soc. 142 (1995) 1746.

[13] D. Aurbach, B. Markovsky, I. Weissman, E. Levi, Y. Ein-Eli, Electrochimica Acta 45 (1999) 67.

[14] S. K. Jeong, M. Inaba,R. Mogi, Y. Iriyama, T. Abe, Z. Ogumi, Langmuir 17 (2001) 8281.

[15] D. Aurbach, M. L. Daroux, P. W. Faguy, E. Yeager, J. Electrochem. Soc. 134 (1987) 1611.

[16] R. Fong, U. von Sacken, J. R. Dahn, J. Electrochem. Soc. 137 (1990) 2009.

[17] D. Aurbach Y. Gofer, M. B. Zion, P. Aped, J. Electroanal. Chem. 339 (1992) 451.

[18] M. Ue, J. Electrochem. Soc. 141 (1994) 3336.

[19] K. Xu, Chem. Rev. 104 (2004) 4303.

[20] S. S. Zhang, J. Power Sources 162 (2006) 1379.

[21] K. Ozawa, Solid State Ionics 69 (1994) 212.

[22] J. Li, E. Murphy, J. Winnick, P.A. Kohl, J. Power Sources 102 (2001) 294.

[23] D. Aurbach, Y. Ein-Eli, B. Markovsky, A. Zaban, J. Electrochem. Soc. 142 (1995) 2882.

[24] S. Megahed, B. Scrosati, J. Power Sources 51 (1994) 79.

[25] M. Wakihara, Mater. Sci. Eng. R 33 (2001) 109.

[26] M. Endo, C. Kim, K. Nishimura, T. Fujino, K. Miyashita, Carbon 38 (2000) 183.

[27] B. Scrosati, Electrochimica Acta 45 (2000) 2461.

[28] N. Omar, B. Verbrugge, G. Mulder, P. V. den Bossche, J. V. Mierlo, M. Daowd, M. Dhaens, S. Pauwels, Vehicle Power and Propulsion Conference (VPPC), 2010 IEEE.

[29] M. Dubarry, C. Truchot, B. Y. Liaw, K. Gering, S. Sazhin, D. Jamison, C. Michelbacher, J. Power Sources 196 (2011) 10336.

[30] M. Dubarry, C. Truchot, B. Y. Liaw, K. Gering, S. Sazhin, D. Jamison, C. Michelbacher, J. Electrochem. Soc. 160 (2013) A191.

[31] S. Brown, D. Pyke, P. Steenhof, Energy Policy 38 (2010) 3797.

[32] S. B. Peterson, J.F. Whitacre, J. Apt, J. Power Sources 195 (2010) 2377.

[33] R. F. Aguilera, R. G. Eggert, Gustavo Logos C. C., J. E. Tilton, The Energy Journal 30 (2009) 141.

[34] S. Sorrell, J. Speirs, R. Bentley, A. Brandt, R. Miller, Energy Policy 38 (2010) 5290.

[35] M. Z.Jacobson, M. Delucchi, Energy Policy 39 (2011) 1154.

[36] H. Mousazadeh, A. Keyhani, A. Javadi, H. Mobli, K. Abrinia, A. Sharifi, Renewable and Sustainable Energy Rev. 13 (2009).

[37] U. Focken, M. Lange, K. Monnich, H. P. Waldl, H. G. Beyer, A. Luig, J. Wind Eng. Ind. Aerodyn. 90 (2002) 231.

[38] T. Iwahori, I. Mitsuishi, S. Shiraga, N. Nakajima, H. Momose, Y. Ozaki, S. Taniguchi, H. Awata, T. Ono, K. Takeuchi, Electrochimica Acta 45 (2000) 1509.

[39] S. Chung, J. T. Bloking, Y, Chiang, Nat. Mater. 1 (2002) 123.

[40] K. Rissouli, K. Benkhouja, J.R. Ramos-Barrado, C. Julien, Mater. Sci. Eng. B 98 (2003) 185.

[41] J. H. Ryu, J. W. Kim, Y. Sung, S. M. Oh, Electrochem. Solid-State Lett. **7** (2004) A306.

[42] I. A. Courtney, J. R. Dahn, J. Electrochem. Soc. 144 (1997) 2045.

[43] T. Ohzuku, A. Ueda, M. Nagayama, Y. Iwakoshi, H, Komori, Electrochimica Acta 38 (1993) 1159.

[44] S. H. Kang, J. Kim, M. E. Stoll, D. Abraham, Y. K. Sun, K. Amine, J. Power Sources 112 (2002) 41.

[45] T. Ohzuku, Y. Makimura, Chem. Lett. (2001) 744.

[46] T. Ohzuku, Y. Makimura, Chem. Lett. (2001) 642.

[47] N.Yabuuchi, T. Ohzuku, J. Power Sources 119–121 (2003) 171.

[48] M. H. Lee, Y. J. Kang, S. T. Myung, Y. K. Sun, Electrochimica Acta 50 (2004) 939.

[49] K.M. Shaju, G.V. Subba Rao, B.V.R. Chowdari, Electrochimica Acta 48 (2002) 145.

[50] A. K. Padhi, K. S. Nanjundaswamy, C. Masquelier, S. Okada, J. B. Goodenough, J. Electrochem. Soc. 144 (1997) 1609.

[51] A. Yamada, S. C. Chung, K. Hinokuma, J. Electrochem. Soc. 148 (2001) A224.

[52] A.K. Padhi, K.S. Nanjundaswamy, J.B. Goodenough, J. Electrochem. Soc. 144 (1997) 1188.

[53] M. Takahashi, H. Ohtsuka, K. Akuto, Y. Sakurai, J. Electrochem. Soc. 152 (2005) A899.

[54] J. Liu, J. Wang, X. Yan, X. Zhang, G. Yang, A. F. Jalbout, R. Wang, Electrochimica Acta 54 (2009) 5656.

[55] J. Kim, S. C. Woo, M. Park, K. J. Kim, T. Yim, J. Kim, Y. Kim, Journal of Power Sources 229 (2013) 190.

[56] N. Meethong, Y. Kao, M. Tang, H. Huang, W. C. Carter, Y. Chiang, Chem. Mater. 20 (2008) 6189.

[57] N. Meethong, H. Huang, W. C. Carter, Y. Chiang, Electrochem. Solid-State Lett. 10 (2007) A134.

[58] H. Huang, S. C. Yin, L. F. Nazar, Electrochem. Solid-State Lett. 4 (2001) A170.

[59] R. Dominko, M. Bele, M. Gaberscek, M. Remskar, D. Hanzel, S. Pejovnik, J. Jamnik, J. Electrochem. Soc. 152 (2005) A607.

[60] X. Ou, H. Gu, Y. Wu, J. Lu, Y. Zheng, Electrochimica Acta 96 (2013) 230.

[61] S. Yang, X. Zhou, J. Zhang, Z. Liu, J. Mater. Chem. 20 (2010) 8086.

[62] A. Yamada, M. Yonemura, Y. Takei, N. Sonoyama, R. Kanno, Electrochem. Solid-State Lett. 8 (2005) A55.

[63] C. J. Wen, R. A. Huggins, J. Solid State Chem. 37 (1981) 271.

[64] R. A. Huggins, J. Power Sources 81–82 (1999) 13.

[65] J. P. Maranchi, A. F. Hepp, P. N. Kumta, Electrochem. Solid-State Lett. 6 (2003) A198.

[66] J. Li, A. K. Dozier, Y. Li, F. Yang, Y. Cheng, J. Electrochem. Soc. 158 (2011) A689.

[67] H Li, X Huang, L Chen, Z. Wu, Y. Liang, Electrochem. Solid-State Lett. 2 (1999) 547.

[68] L. Y. Beaulieu, K. W. Eberman, R. L. Turner, L. J. Krause, J. R. Dahn, Electrochem. Solid-State Lett. 4 (2001) A137.

[69] M. T. McDowell, S. W. Lee, J. T. Harris, B. A. Korgel, C. Wang, W. D. Nix, Y, Cui, Nano Lett. 13 (2013) 758.

[70] M. Green, E. Fielder, B. Scrosati, M. Wachtler, J. S. Moreno, Electrochem. Solid-State Lett. 6 (2003) A75.

[71] H. Kim, M. Seo, M. Park, J. Cho, Angew. Chem. Int. Ed. 49 (2010) 2146.

[72] C K. Chan, H. Peng, G. Liu, K. McIlwrath, X. F. Zhang, R. A. Huggins, Y. Cui, Nat. Nanotech. 3 (2008) 31.

[73] C. K. Chan, R. Ruffo, S. S. Hong, R. A. Huggins, Y. Cui, J. Power Sources 189 (2009) 34.

[74] K. Nakai, I. Tsuchioka, M. Saito, A. Tasaka, T. Takenaka. M. Hirota, M. Inaba, Electrochemistry 78 (2010) 438.

CHAPTER I

Novel Synthesis Method for $LiFePO_4$ Cathode Material

Section I-1

A Rapid Synthesis Method of $LiFePO_4$/C Cathode Material Using High-frequency Induction Heating

I-1-1. Introduction

Lithium iron phosphate ($LiFePO_4$) with olivine-type structure reported by Padhi et al. [1] is an attractive cathode material for Li-ion batteries due to its good electrochemical characteristics such as flat potential around 3.5 V vs. Li/Li^+ for Li insertion/extraction and the theoretical capacity of 170 mAh g^{-1}, together with its long cycle stability, high thermal stability, low environmental impact. $LiFePO_4$ is also an excellent material in a view point of elemental strategy because $LiFePO_4$ does not contain rare metals [2]. The low electric conductivity [3] and low Li-ion diffusivity [4] which causes low battery performances of $LiFePO_4$ has been already improved by modifying the surface of $LiFePO_4$ particles with carbon and decreasing the particle size, respectively [5, 6]. The advantage of $LiFePO_4$ cathode material described above may be able to significantly reduce the costs and extend the cycle life of Li-ion batteries. Therefore, the Li-ion batteries including $LiFePO_4$ modified with carbon ($LiFePO_4$/C) [7, 8] as cathode are suitable than for large scale applications such as electric vehicles (EVs), hybrid electric vehicles (HEVs), and large storage systems for natural energy generation such as wind power or solar power.

In order to improve battery performances of $LiFePO_4$/C cathode material, various synthesis methods have been reported. The solid-state reactions [9], polyol process [10], sol-gel process [11, 12], hydrothermal method [13, 14], solvothermal method [15], splay pyrolysis [16], mechanical activation [17], and co-precipitation [18] are useful for the synthesis of $LiFePO_4$/C with excellent battery performances. However, most of these methods use relativity expensive divalent iron compounds as iron source and require quite complex synthesis process or long-time (several hours) heating process to obtain $LiFePO_4$ phase in inert gas or vacuum state to suppress oxidation of iron (from Fe^{2+} to Fe^{3+}). As a result, $LiFePO_4$/C becomes an expensive material and has not come to be widely commercialized despite having excellent battery performances.

Although such problems are present, the low cost synthesis methods for $LiFePO_4$/C are not so much reported. The microwave synthesis is one of the few low-cost methods [19, 20, 21], but controllability of the microwave is not enough to obtain $LiFePO_4$/C with high battery performances. Thus microwave synthesis cannot be applied to mass production.

In this study, we propose the novel low-cost synthesis method to obtain $LiFePO_4$/C with high battery performances which combines a high-frequency induction heating with carbothermal reduction [22]. The carbon sources were added beforehand to precursor for carbothermal reduction and carbon modification of $LiFePO_4$ surface. The high frequency induction heating which allows a very fast temperature rise to the desired temperature is adopted to reduce heating time. Furthermore, carbothermal reduction allows using quite inexpensive Fe_2O_3 as iron source. The novel synthesis method which we propose in this paper reduces the manufacturing costs of $LiFePO_4$/C in terms of both process cost and material cost. The $LiFePO_4$/C composite generates via carbothermal reduction of Fe_2O_3. First, the carbon sources thermal decompose and carbonize. The resulting carbon deprives oxygen from Fe_2O_3 in vacuum state or inert gas. Then $LiFePO_4$ phase generates from divalent iron and other raw materials according to reaction as

$$Li_2CO_3 + Fe_2O_3 + 2NH_4H_2PO_4 + 0.5C \rightarrow 2LiFePO_4 + 2NH_3 + 3H_2O + 1.5CO_2 \text{ [23]}$$

The residual carbon which is not consumed during carbothemal reduction remains on surface of $LiFePO_4$ particles and functions as conductive agent.

I-1-2. Experimental

$LiFePO_4$/C samples were synthesized by solid-state reaction of stoichiometric amount of Li_2CO_3 (Kanto Chemical Co., 99.0%), Fe_2O_3 (Kishida Chemical Co., 98.5%) and $NH_4H_2PO_4$ (Kanto Chemical Co., 99.0%). The starting materials were mixed with 10 wt.% citric acid (Kanto Chemical Co., 99.0%) or sucrose (Kanto Chemical Co., 99.0%) as carbon source by planetary ball-milling for 5 h in ethanol medium. The rotating speed was 400 rpm and the ball to powder weight ratio

was 20:1. After drying at 80°C over 6 h in air to remove ethanol, the obtained mixture was pressed into pellet with 2-3 mm thickness at 21 MPa (30 kN). The pellet was placed in a carbon crucible, and the carbon crucible including pellet precursor was placed in a vacuum chamber. The carbon crucible was rapidly heated to 700 or 900°C at a heating rate of 1500 - 3000°C min^{-1} by high-frequency induction heating, and held for 1h or few minutes at the upper temperature in vacuum state. After heating process, the carbon crucible rapidly cooled down to room temperature. The resulting gray or black pellets were ground thoroughly in a mortar, and the obtained power was used as cathode active materials.

The cathodes for electrochemical performances test were prepared in dry-room with dew point of -55°C. The synthesized cathode active materials were mixed with ketjen black (Lion Corp., Carbon ECP) and polyvinylidene fluoride (Kureha Corp., #1100) with a weight ratio of 85:8:7 in adequate amount of *N*-methyl-2-pyrrolidone (Kishida Chemical Co., 99.5%) solvent and the obtained slurry was casted onto Al-foil current collector and dried at 100°C for 10 h in vacuum oven. The prepared cathode sheets were cut into disks with diameter of 12 mm as the test cathodes. The mass loading of active material in the electrodes was 4.2-4.7 mg cm^{-2}.

Electrochemical measurements were carried out using flat type cell (Hosen Co.) assembled in argon-filled globe box with the prepared test cathode, Li foil (Honjo Metal Corp.) disk with a diameter of 13 mm as an anode, 1M $LiPF_6$ solution with ethylene carbonate-dimethyl carbonate (1:1 v/v)(Kishida Chemical Co., LBG) as the electrolyte, and polypropylene porous film as the separator. The charge-discharge measurement including cycle performance tests was carried out in the voltage range of 2.5-4.2 V on galvanostatic charge-discharge unit (BTS2004W, Intex Co.). The rate performance test was carried out at 1/10, 1/5, 1/2, 1, 3, 5, and 10 C-rates (1 C = 170 mAh g^{-1}) by every 5 cycles. The cycle stability for high-rate charge-discharge was assessed by the cells retested back to the initial 1/10 C-rate after the various rate tests.

X-ray diffraction (XRD, Ultima IV, Rigaku Co.) with Cu Kα radiation was used to identify the phases of synthesized samples. A graphite monochromator was used for diffracted beams. The diffraction data were collected between 10-50° by a step scan mode with a scanning step of 0.02° and a sampling time of 5 s. The morphology of

second particles was observed using scanning electron microscope (SEM, SU-1500, Hitachi Co.). The particle size of synthesized samples was observed in second electron (SE) images, and the compositional information was obtained from back scatter electron (BSE) images. The morphology of primary particles and residual carbon on the surface of particles were observed using transmission electron microscope (TEM, , JEOL Co.). The chemical state of the iron in synthesized samples was analyzed by Mossbauer spectroscopy (measured by Toray Research Center Inc.) with ^{57}Co/Rh radiation and the spectrometer works in constant acceleration mode. The transition between the ground state and the lowest excited state of ^{57}Fe was used for analysis. The synthesized sample powder and small amount of polyethylene powder were mixed and molded into tablet. The tablets were sealed in an aluminum laminate pack in argon filled glove box to suppress the oxidation of sample during the measurement. The primary particle distribution of synthesized samples was determined by small-angle X-ray scattering (SAXS, Ultima IV, Rigaku Co.); 30 - 70% of the direct beam was scattered by adjusting thickness of the samples and scattering profile was collected between 0.08 - 2.00°. The X-ray scattering derived from air was deducted as a back ground. The particle size distributions were determined by curve fitting for scattering profiles using parameters such as background intensity, average particle size, normalized distribution ratio, scale factor, and true density of $LiFePO_4$ (3.60 g cm^{-3}).

I-1-3. Results and discussion

Fig. I-1-3-1 shows XRD patterns of synthesized samples sintered at 700°C for 1 h with 10wt.% citric acid (LFP-C) and 10wt.% sucrose (LFP-S). The orthorhombic olivine phase (Space group: Pnma) is observed in both samples, which indicates that $LiFePO_4$/C can be generated in far less time than conventional method by using high-frequency induction heating. However, the LFP-C contains a slight impurity phase and LFP-S contains large amount of impurities. These impurities are Fe_2P or Fe_3P phase generated by over reduction of $LiFePO_4$ phase [24, 25]. The presence of impurities contained in synthesized samples implies inhomogeneously progress of carbothermal reduction and the difference in the amount of impurities indicates that the homogeneity of the carbothermal reduction varies depending on the carbon sources. The citric acid

can be dissolved in ethanol would disperse homogeneously in the overall precursor during ball-milling, while sucrose cannot be dissolved in ethanol would present inhomogeneously in the precursor. Therefore, we consider that the carbothermal reduction proceeded locally and large amount of impurities were generated in LFP-S. The peak intensity of LFP-S is quite smaller than that of LFP-C. The generation of impurities due to inhomogeneous carbothermal reduction probably reduces significantly the amount of $LiFePO_4$ phase in LFP-S.

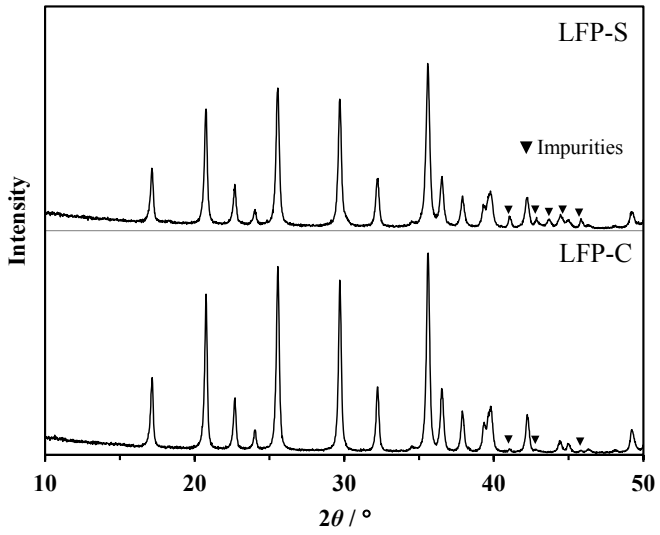

Fig. I-1-3-1 XRD patterns of synthesized samples heated at 700°C with sucroce (LFP-S) and citric acid (LFP-C) as carbon source.

Fig. I-1-3-2 shows the SEM images of LFP-S (a, b) and LFP-C (c, d). The second electron (SE) images (a) and (c) shows the difference of particle size between LFP-C and LFP-S. The large particles observed in Fig. I-1-3-2 (a) are not aggregate because synthesized pellet samples have been carefully crushed in a mortar. In other words, the observed large particles are very hard sintered particles which cannot be crushed. any more. The LFP-C particles are far smaller compared with LFP-S particles. Since the particle growth due to sintering is suppressed by the residual carbon which was not used during carbothermal reduction prevents the contact between $LiFePO_4$

particles, the distribution of carbon source in the precursor is very important. Inhomogeneous distribution of sucrose in precursor would be not enough to suppress particle growth. The back scattered electron (BSE) images (b) and (d) shows the compositional information. The bright spots labeled with circles means the concentration of relatively heavy elements, and it seems to be a collection of Fe in those samples. Many large bright spots observed in Fig. I-1-3-2 (b) probably correspond to crystalline impurity phases such as Fe_2P or Fe_3P in LFP-S confirmed in XRD pattern. Judging from the results shown so far, we consider that the sucrose is inappropriate as carbon source in our method. On the other hand, the bright spots are hardly observed in Fig. I-1-3-2 (d), which indicates almost absence of Fe_2P or Fe_3P phase in LFP-C. This result also is in good agreement with the results of XRD.

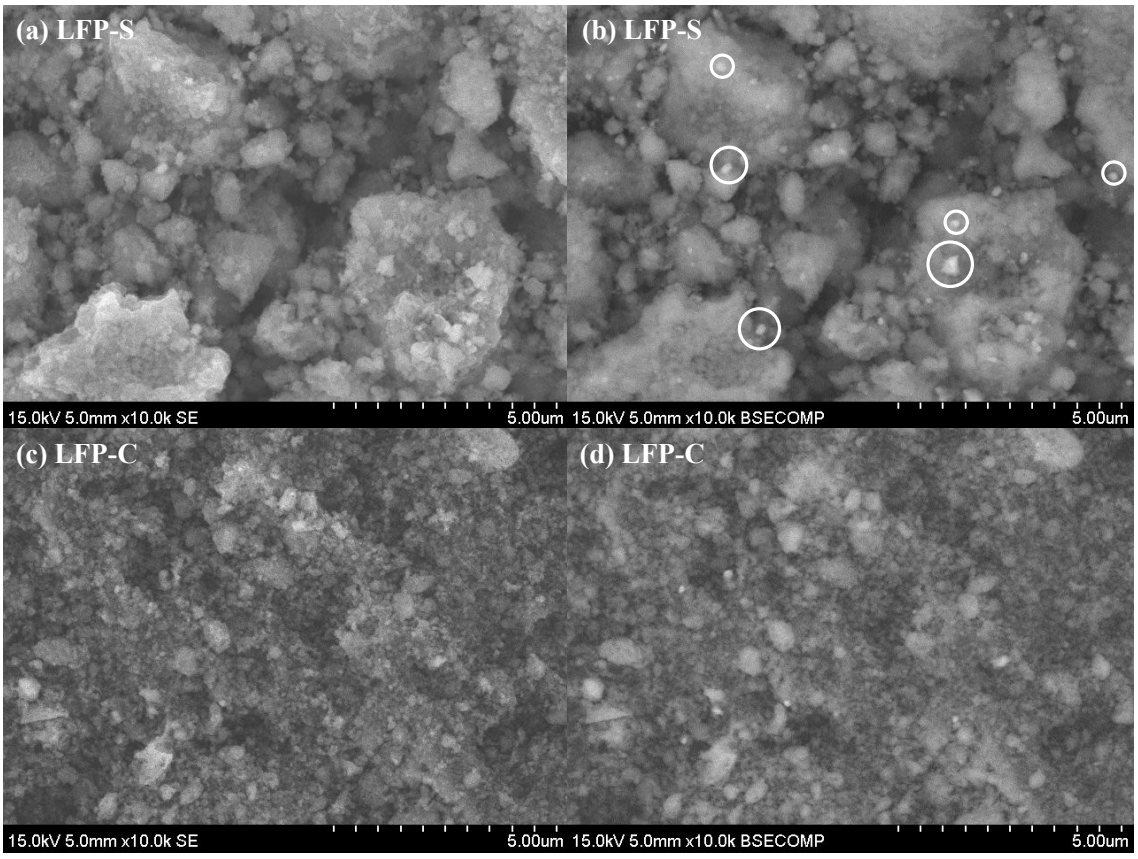

Fig. I-1-3-2 SEM images of (a, b) LFP-S, (c, d) LFP-C. Left side shows SE images, and right side shows BSE images.

Fig. I-1-3-3 shows the charge-discharge curves at 1/10 C-rate (1C = 170 mA g^{-1}) of prepared cathodes containing LFP-C or LFP-S. The voltage plateau around 3.5 V based on Fe^{2+}/Fe^{3+} redox couple in olivin structure is observed in both cathodes. LFP-C and LFP-S cathode show discharge capacities of 71.6 and 118.6 mAh g^{-1} in the initial cycle respectively, and continue to show equivalent discharge capacities in subsequent cycles. Although the Fe_2P or Fe_3P phase contained in each samples does not adversely affect the cycle performances, the generation of impurities cannot be tolerated because the generation of large amount impurities directly relates to loss of $LiFePO_4$ proportions and decrease of charge-discharge capacity of synthesized samples. The LFP-C shows the larger charge-discharge capacity than LFP-S, but it far from theoretical capacity (170 mAh g^{-1}). The LFP-C should hardly contain the crystalline impurities such as Fe_2P or Fe_3P phase in the result of XRD and BSE observation. However, the XRD and BSE observation cannot detect except for crystalline impurities and concentration of relatively heavy elements. Thus the concept that the charge-discharge performance of LFP-C is limited by other undetected impurities is appropriate.

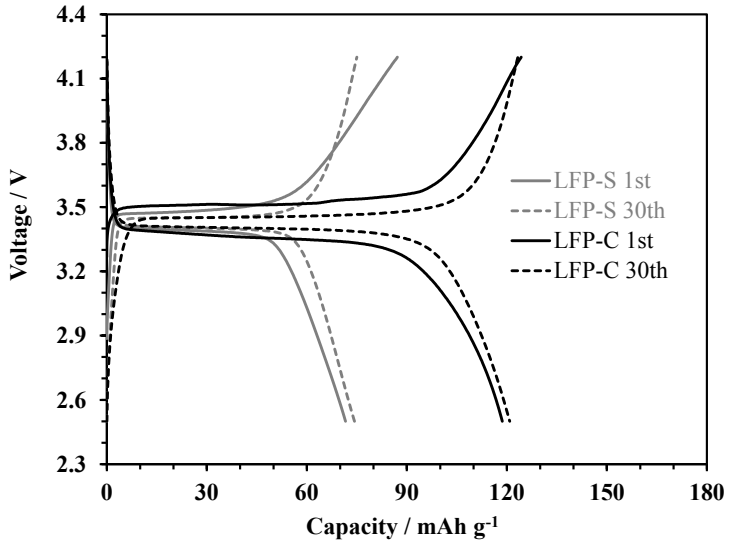

Fig. I-1-3-3 Charge-discharge curves of the cathodes containing LFP-S and LFP-C at 1/10 C-rate (1 C-rate = 170 mAh g^{-1}).

In order to found the other causes for low charge-discharge capacity of LFP-C, we investigated the chemical state of Fe in the LFP-C. Fig. I-1-3-4 shows Mossbauer spectrums obtained from LFP-C. The results of curve fitting, the spectrums can be divided into three types of doublet. The isomer shift, quadrupole splitting, chemical state of Fe, and abundance corresponding to each doublet are summarized in Table I-1-3-1. The isomer shift and quadrupole splitting for strong doublet labeled "State 1" can be attributed to typical divalent iron. The other doublets are attributed to Fe^{3+} labeled "State 2" or "State 3". However, "State 2" and "State 3" seems to close to the state of Fe^{2+} because their isomer shift is larger than that of typical Fe^{3+} (δ = 0.3 mm s^{-1}). Moreover, the quadrupole splitting of "State 2" is quite larger compared with that of typical Fe^{3+}, which indicates low symmetry of electron orbital. The 3d orbital of typical Fe^{3+} is half-filled subshell and spherical symmetry. In other words, the lower symmetry of 3d orbital means the existence of the sixth electron, which suggests that "State 2" is more close to the state of Fe^{2+} than "State 3". According to the above interpretation, the Fe labeled "State 2"and "State 3" derives from raw material (Fe_2O_3) or its decomposition products. Since the slight over reduction byproducts is confirmed in XRD pattern, the LFP-C would seem to not contain so much impurity. But actually, 2%

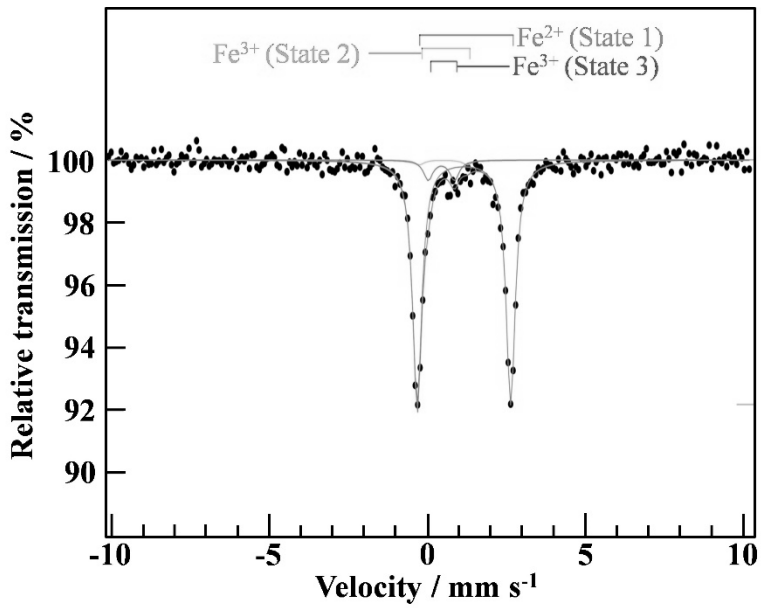

Fig. I-1-3-4 Mossbauer spectrum of LFP-C.

Fe^{3+} labeled "State 2" and 7% of Fe^{3+} labeled "State 3" deriving from Fe_2O_3 or its decomposition products remains in LFP-C. The results of Mossbauer analyze suggests a possibility that carbothermal reduction and generation of $LiFePO_4$ have not partially completed.

Table I-1-3-1 Summary of various parameters obtained by curve fitteing of Mossbauer spectrum for LFP-C.

Component	Isomer shift δ / mm s^{-1}	Quadrupole splitting Δ / mm s^{-1}	Fe / %	Explanation
State 1	+ 1.23	2.96	91	Typical Fe^{2+}
State 2	+ 0.57	1.51	2	Low-symmetry Fe^{3+}
State3	+0.51	0.83	7	Fe^{3+}

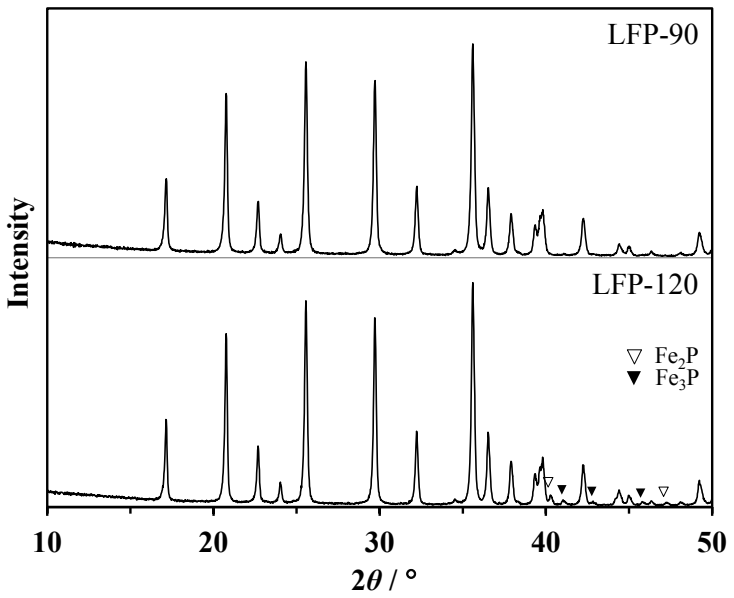

Fig. I-1-3-5 XRD patterns of synthesized samples heated at 900°C for 120 s (LFP-120) and 90 s (LFP-90).

The synthesis of $LiFePO_4$ phase is generally carried out under 700°C [9, 11, 16] to avoid generation of over reduction byproducts, but we think that the rate-limiting

step of the generation of $LiFePO_4$ phase in our method is carbothermal reduction and its reaction kinetic is very slow around 700°C. Therefore, we attempted to raise the heating temperature to 900°C for synthesis of $LiFePO_4$/C containing no impurities more quickly. The only citric acid is adopted as carbon source. Fig. I-1-3-5 shows XRD patterns of synthesized samples sintered at 900°C for 120 s with a heating-rate of 1500°C min^{-1} (LFP-120) and for 90 s with a heating-rate of 3000°C min^{-1} (LFP-90). Since we knew that the reaction kinetic of the carbothermal reduction at 900°C is extremely fast from other preliminary experiments, the heating time at 900°C was set a very short. The olivine phase is confirmed in both LFP-90 and LFP-120 and their peak intensity are larger than that of LFP-C. In addition, the LFP-120 includes Fe_2P and Fe_3P which generated by decomposition of $LiFePO_4$ due to excessive reaction. Therefore, we conclude that the 120 seconds of heating time is too long at 900°C to obtain the $LiFePO_4$/C includes no impurities, and reduce the heating time 90 s to adjust the progress of carbothermal reduction. Moreover, we applied faster heating rate (3000°C min^{-1}) considering the carbothermal reduction starts around 700°C and rapidly proceeds during temperature rising from 700 to 900°C. The XRD pattern of LFP-90 shows single-phase of $LiFePO_4$, and generation of Fe_2P or Fe_3P can be suppressed.

Fig. I-1-3-6 shows the SEM and TEM images of LFP-120 (a, b) and LFP-90 (c, d). The LFP-120 contains the secondly particles with diameter of submicron size and a few micrometer (Fig. I-1-3-6 (a)), while the LFP-90 contains only submicron particles (Fig. I-1-3-6 (c)). The heating condition of 900°C using a high-frequency induction heating significantly increases the kinetics of reaction and sintering, and the secondary particle morphology varies considerably in just 30 s. The TEM image shows the morphology of primary particles. The primary particle size of LFP-120 seems to be slightly larger than that of LFP-90 (Fig. I-1-3-6 (b) and (d)). The difference of just 30 s at 900°C seems to cause increase in the primary particle size. The residual carbon which has not been consumed during carbothermal reduction exists on the surface of $LiFePO_4$. However, the residual carbon does not cover the surface and the exposed surface of $LiFePO_4$ is observed in TEM images. This result does not mean inhomogeneous distribution of citric acid as a carbon source in the precursor. The shapes of all $LiFePO_4$/C samples obtained by heating at 900°C become porous pellets, which imply

fierce gas (CO_2, NH_3 or ethanol vapor) generation. The gases partially blow off the citric acid covering the precursor and the surface of $LiFePO_4$ particles partially expose. If the exposed surface is in contact with each other, the primary particle size is expected to grow rapidly by sintering, but the particle size growth can be suppressed, which suggests that the porous shapes formed by fierce gas generation prevents the contact between the $LiFePO_4$ particles. As a result, fierce gas generation acts effectively to suppress the particle size growth.

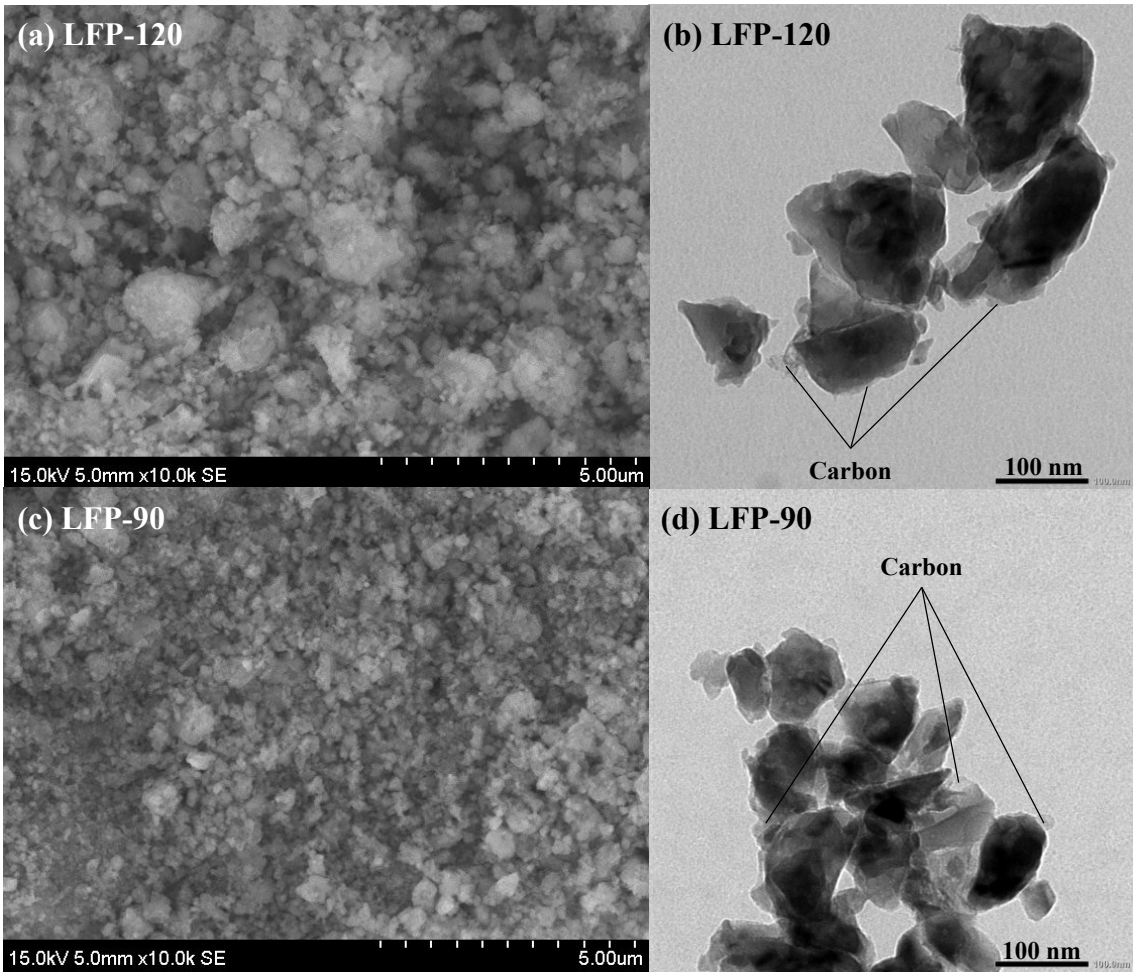

Fig. I-1-3-6 SEM (SE) images of (a) LFP-120, (b) LFP-90 and TEM images of (b) LFP-120, (d) LFP-90.

The primary particle size greatly affects the charge-discharge performances in $LiFePO_4$ with poor Li-ion conductivity. Fig. I-1-3-7 shows the primary particle size distributions calculated by SAXS profiles. The average particle diameters of LFP-90 and LFP-120 are 54.5 and 72.8 nm, respectively. Although there is not so much difference in average particle size, it is clear that LFP-120 contained the particles larger than 200 nm whereas LFP-90 hardly contains the particles larger than 100 nm. The primary particle size distributions correspond to the difference in particle size observed in the TEM images.

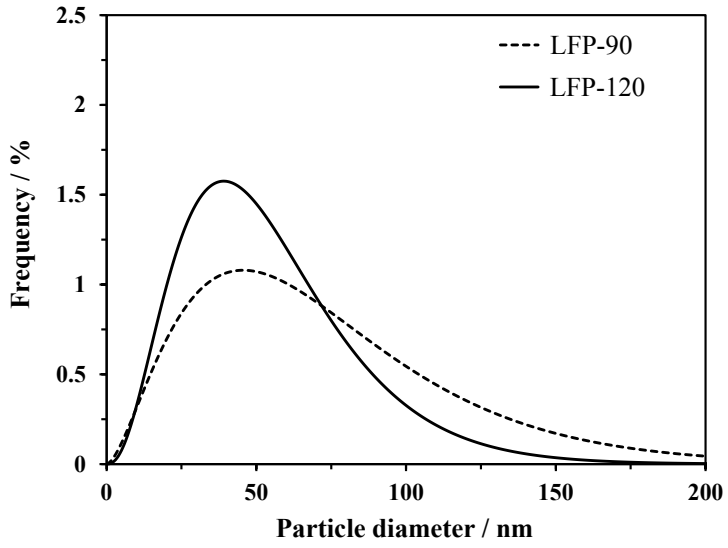

Fig. I-1-3-7 Primary particle size distributions of LFP-120 and LFP-90 calculated from SAXS profiles.

Fig. I-1-3-8 shows the charge-discharge curves of the cathodes containing LFP-120 and LFP-90 at 1/10 or 10 C-rate. The voltage plateau region based on Fe^{2+}/Fe^{3+} redox couple extends in both cathodes compared to LFP-C cathode. The LFP-120 and LFP-90 cathodes shows discharge capacities of 136.7 and 153.3 mAh g^{-1} at 1/10 C-rate, respectively, and LFP-90 cathode reaches 90% of the theoretical capacity. As a result of much improving the reaction kinetic of carbothermal reduction by heating at 900°C, the generation of $LiFePO_4$ phase completes within 120 s, and the charge-discharge capacity significantly improves. The lower discharge capacity of

LFP-120 than that of LFP-90 seems to be attributed to decrease in content of $LiFePO_4$ phase in LFP-120 by generation of Fe_2P and Fe_3P phase. At 10 C-rate, LFP-120 and LFP-90 cathodes shows discharge capacities of 74.1 and 100.1 mAh g^{-1}, respectively, and the voltage plateau is kept.

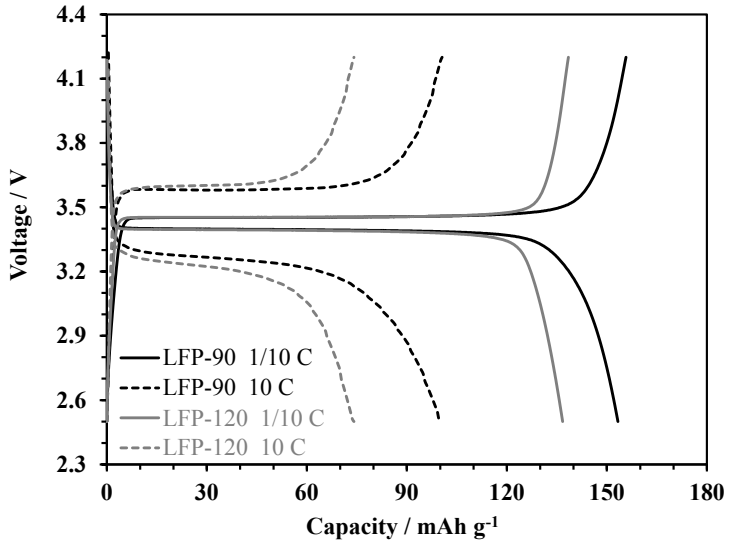

Fig. I-1-3-8 Charge-discharge curves of the cathodes containing LFP-120 and LFP-90 at 1/10 and 10 C-rate (1 C-rate = 170 mAh g^{-1}).

Fig. I-1-3-9 shows the charge-discharge rate performances of LFP-120 and LFP-90 cathodes. As is also clear from charge-discharge curves of 10 C-rate, charge-discharge rate performances of LFP-90 is consistently higher than that of LFP-120. The Fe_2P with relatively good electrical conductivity acts as conductive agent [26], and seems to improve the rate performance of LFP-120. However, the LFP-120 has significantly disadvantage of relatively low Li-ion diffusion because of the larger primary particle size than that of LFP-90. The charge-discharge rate performance test also serves as a test of the cycle stability at high rate. Comparing the discharge capacity of initial 5 cycles (1/10 C-rate) and last 5 cycles (1/10 C-rate) after various rate tests, its values of LFP-120 and LFP-90 dose not degrade a bit. The LFP-120 and LFP-90 has excellent cycle stability inherent in $LiFePO_4$.

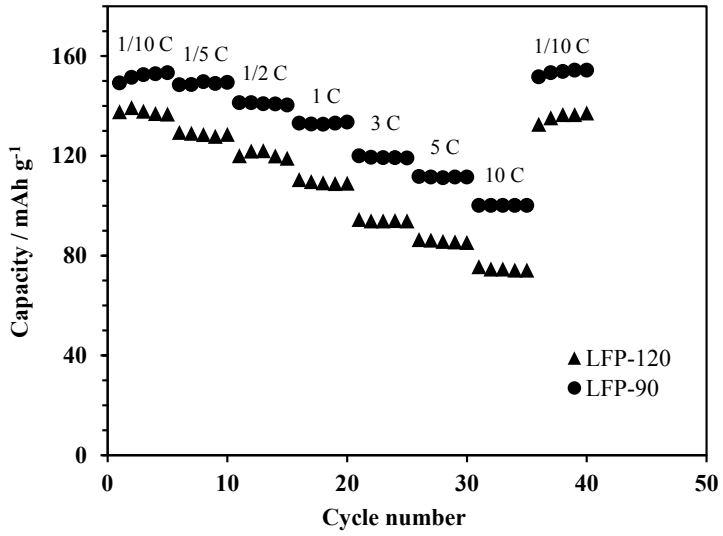

Fig. I-1-3-9 Charge-discharge rate performances of the cathodes containing LFP-120 and LFP-90 at various C-rate.

I-1-4. Conclusions

We successfully synthesize the $LiFePO_4$/C composite using Fe_2O_3 in far less time (within a few minutes) compared to conventional method by combination carbothermal reduction with high-frequency induction heating. The carbon source should be homogeneously dispersed and the citric acid is suitable as carbon source in our method. The LFP-C synthesized by heating at 700°C for 1 h contains large amount of Fe^{3+} species deriving from Fe_2O_3 because the carbothermal reduction is not completed and the cathode containing LFP-C shows low charge-discharge capacity (118.6 mAh g^{-1}) compared to theoretical capacity. The application of a higher heating temperature to improve the reaction kinetic increases charge-discharge capacity by suppressing the remaining of Fe^{3+} species. The generation of over reduction byproducts such as Fe_2P or Fe_3P can be suppressed by adjustment of heating time. Even if adjustment of heating time is required in seconds scale, high-frequency induction heating satisfies the request by its excellent controllability. The LFP-90 synthesized in optimized conditions contains no impurities, and the particle size is sufficiently small to achieve the high battery performances. The charge-discharge rate performance and cycle stability of the cathode containing LFP-90 is excellent and the discharge capacity

is 153.3 and 100.1 mAh g^{-1} at 1/10 and 10 C-rate, respectively. In our method, the $LiFePO_4$/C with high battery performances is obtained in extremely short time. Therefore, we believe that this synthesis method is possible to reduce the cost of $LiFePO_4$/C cathode material drastically, and can contribute to further applications of Li-ion batteries in various fields.

I-1-5. References

[1] A.K. Padhi, K.S. Nanjundaswamy, and J.B. Goodenough, J. Electrochem. Soc. 144 (1997) 1188.

[2] A.K. Padhi, K.S. Nanjundaswamy, C. Masquelier, S. Okada, and J.B. Goodenough, J. Electrochem. Soc. 144 (1997) 1609.

[3] S. Y. Chung, Y. M. Chiang, Solid-State Lett. 6 (2003) A278.

[4] P. P. Prosini, M. Lisi, D. Zane, M. Pasquali, Solid State Ionics 148 (2002) 45.

[5] C. Delacourt, P. Poizot, S. Levasseur, and C. Masquelier, Electrochem. Solid-State Lett. 9 (2006) A352.

[6] P. Gibot, M. Casas-Cabanas, L. Laffont, S. Levasseur, P. Carlach, S. Hamelet, J.-M.Tarason, and C. Masquelier, Nat. Mater. 7 (2008) 741.

[7] Z. Chen and J.R. Dahn, J. Electrochem. Soc. 149 (2002) A1184.

[8] H. Huang, S.C. Yin, and L.F. Nazar, Electrochem. Solid State Lett. 4 (2001) A170.

[9] A. Yamada, S.C. Chung, and K. Hinokuma, J. Electrochem. Soc. 148 (2001) A224.

[10] D. H. Kim and J. Kim, Electrochem. Solid-State Lett 9 (2006) A439.

[11] M. Koltypin, D. Aurbach, L. Nazar, and B. Ellis, J. Power Sources 174 (2007) 1241.

[12] D. Choi and P.N. Kumta, J. Power Sources 163 (2007) 1064.

[13] K. Dokko, S. Koizumi, H. Nakano, K. Kanamura, J. Mater. Chem. 17 (2007) 4803.

[14] B. Ellis, W. H. Kan, W. R. M. Makahnouk, L. F. Nazar, J. Mater. Chem. 17 (2007) 3248.

[15] T. Muraliganth, A. V. Murugan, and A. Manthiram, J. Mater. Chem. 18 (2008) 5661.

[16] M. Konarova, I. Taniguchi, J. Power Sources 194 (2009) 1029.

[17] J. K. Kim, G. Cheruvally, J. W. Choi, J. U. Kim, J. h. Ahn, G. B. Cho, K. W. Kim,

H. J. Ahn, J. Power Sources 166 (2007) 211.

[18] G. Arnold, J. Garche, R. Hemmer, S. Strobele, C. Vogler, and M. W. Mehrens, J. Power Sources 119-121 (2003) 247.

[19] M. Higuchi, K. Katayama, Y. Azuma, M. Yukawa, M. Suhara, J. Power Sources 119-121 (2003) 258.

[20] Y. Zhang, H. Feng, X. Wu, L. Wang, A. Zhang, T. Xia, H. Dong, M. Liu, Electrochim. Acta 54 (2009) 3206.

[21] L. Wang, Y. Huang, R. Jiang, D. Jia, Electrochim. Acta 52 (2007) 6778.

[22] J. Barker, M. Y. Saidi, J. L. Swoyer, Electrochem. Solid-State Lett., 6 (2003) A53.

[23] H. P Liu, Z. X. Wang, X. H Li, H. J. Guo, W. J Peng, Y. H Zhang, Q. Y Hu, J. Power Sources, 184 (2008) 469.

[24] Y. Lin, H. Pan, M. Gao, Y. Liu, J. Electrochem. Soc. 154 (2007) A1124.

[25] Y. Lin, M.X. Gao, D. Zhu, Y.F. Liu, H.G. Pan, J. Power Sources, 184 (2008) 444.

[26] C. W. Kim, J. S Park, K. S. Lee, J. Power Sources, 163 (2006) 144.

Section I-2

Improvement of Heating Condition for $LiFePO_4$/C with High Electric Conductivity

I-2-1. Introduction

Lithium iron phosphate ($LiFePO_4$) with an olivine-type structure is considered an attractive cathode material for Li-ion batteries due to its good electrochemical characteristics such as flat potential at 3.5 V vs. Li/Li^+ for Li insertion/extraction and the acceptable theoretical specific capacity of 170 mAh g^{-1}, together with its long cycle stability, high thermal stability, low environmental impact, and especially an ideal composition as realization of elemental strategy [1, 2]. The low electric conductivity and low Li-ion diffusivity, which are drawbacks of $LiFePO_4$, have been improved by modifying the surface of $LiFePO_4$ particles with carbon and by decreasing the particle size, respectively [3, 4]. $LiFePO_4$ modified with carbon ($LiFePO_4$/C) [5, 6] will be applied to large-scale applications such as electric vehicles (EVs), hybrid electric vehicles (HEVs), and large storage systems for power generation from natural energy as wind, solar power and so on.

To improve battery performance of $LiFePO_4$/C cathode material, various synthesis methods involving solid-state reactions [7, 8], a polyol process [9], sol–gel process [10], solvothermal method [11], mechanical activation [12], and co-precipitation [13] have been reported. However, most of reported methods need a relatively expensive divalent iron compound as iron source. Furthermore, to obtain a $LiFePO_4$ phase, most methods eventually require long-time (typically several hours) sintering in an inert gas or vacuum to suppress oxidation of iron (from Fe^{2+} to Fe^{3+}). As a result, $LiFePO_4$/C synthesized by typical methods costs much, which would limit its practical application. In this context, we have reported a novel synthesis method for $LiFePO_4$/C [14], which combines a carbothermal reaction [15] with a high-frequency induction heating method as a solution for these problems.

In this study, $LiFePO_4$/C composite is synthesized via carbothermal reduction of quite inexpensive Fe_2O_3 as iron source to reduce raw material cost. Moreover, its

energy cost could be drastically reduced because our high-frequency induction heating as a sintering process is completed in a few minutes by rapid heating. Citric acid as a carbon source is decomposed thermally, and then the carbonaceous products remove oxygen from Fe_2O_3 to yield divalent iron in vacuum or an inert gas. The resulting $LiFePO_4$ phase is derived from reactions of divalent iron with other raw materials. The carbonaceous products have not been consumed completely during the carbothermal reduction; they remain at the surface of $LiFePO_4$ particles ($LiFePO_4$/C) and function as conductive auxiliary. In this paper, we optimize the annealing process following the sintering process in our high-frequency induction heating method in an attempt to improve the electrochemical properties of $LiFePO_4$/C.

I-2-2. Experimental

Synthesis - The present $LiFePO_4$/C samples were synthesized by a solid-state reaction of stoichiometric amounts of Li_2CO_3 (Kanto Chemical Co., 99.0%), Fe_2O_3 (Toda Kogyo Corp., 99.5%), and $NH_4H_2PO_4$ (Kanto Chemical Co., 99.0%) together with 10 wt.% citric acid (Kanto Chemical Co., 99.0%) as carbon source. The starting materials were mixed by planetary ball-milling for 5 h in ethanol medium. The rotating speed was 400 rpm and a ball to powder weight ratio was 20:1. After drying at 80°C over 6 h at atmospheric pressure to remove ethanol, the obtained precursor was pressed into pellet with 2-3 mm thickness at 14 MPa (20 kN). The pellet precursor was inserted into a carbon crucible, and this was placed in a vacuum chamber. The carbon crucible was rapidly heated to 900°C at a heating rate of 3000°C min^{-1} by high-frequency induction heating, and then held it for a few minutes in a vacuum. After the sintering process at 900°C, the temperature was reduced to 700°C and held the temperature for a few minutes for sufficient carbonization of citric acid as carbon source. At the end of heating process, the carbon crucible was rapidly cooled down to room temperature. The resulting gray pellet were ground thoroughly in a mortar, and the obtained powder ($LiFePO_4$/C) was used as cathode active material.

Cathode preparation - The cathode for electrochemical performance tests was prepared in a dry room with a dew point of -55°C. The obtained $LiFePO_4$/C was mixed with ketjen black (Lion Corp., Carbon ECP) and polyvinylidene fluoride (Kureha Corp.,

#1100) with a weight ratio of 85:8:7 in an adequate amount of *N*-methyl-2-pyrrolidone (Kishida Chemical Co., 99.5%) solvent and the obtained slurry was cast onto an Al-foil current collector and dried at 100°C for 10 h in a vacuum oven. The prepared cathode sheet was cut into disks with a diameter of 12 mm as test cathode. The mass loading of active material in an electrode was 5.2 mg cm^{-2}; this loading was intentionally set heavier than that on the cathode in our previous report [14] in order to prepare a realistic cathode with an enough mass loading.

Electrochemical measurements - Electrochemical measurements were performed using a CR2032 coin type cell assembled in an argon-filled globe box with the prepared test cathode, a Li foil (Honjo Metal Corp.) disk with a diameter of 13 mm as an anode, 1M $LiPF_6$ solution with ethylene carbonate - dimethyl carbonate (1:1 v/v) (Kishida Chemical Co., LBG) as an electrolyte, and porous polypropylene film as a separator. The charge and discharge measurement including rate performance test was carried out in a voltage range of 2.5-4.2 V using a galvanostatic charge and discharge unit (Intex Co., BTS2004W) at 1/10, 1/5, 1/2, 1, 3, 5, and then 10 C-rates (1C = 170 mA g^{-1}) by every 5 cycles. In order to assess the cycle stability for high-rate charge-discharge, the cells were retested back to the initial 1/10 C-rate after the above various rate tests.

Material analysis - The X-ray diffraction (XRD, Rigaku Co., Ultima IV) with Cu Kα radiation was used to identify the phases of synthesized samples. A graphite monochrometer was used for diffracted beams. The diffraction data were collected between 10-50° by a step scan mode with a scanning step of 0.02° and a sampling time of 5 seconds. The electric conductivity was measured by a four probe method. The obtained powder sample was pressed into pellet at 5 MPa, and four probes were pressed against the pellet. The measurement was performed 10 times for each sample; the average value was regarded as representative electrical conductivity.

The morphology of secondary particles was observed using scanning electron microscope (SEM, Hitachi Co., SU-1500). The primary particle-size distribution of synthesized samples was determined by small-angle X-ray scattering (SAXS, Rigaku Co., Ultima IV); 30 - 70% of the direct beam was scattered by adjusting thickness of the samples and the scattering profile was collected between 0.08 - 2.00°. The X-ray

scattering derived from air was deducted as a back ground. The primary particle-size distribution was determined by curve fitting for the scattering profile with several parameters such as background intensity, average particle size, normalized distribution ratio, scale factor, and true density of $LiFePO_4$ (3.60 g cm^{-3}).

I-2-3. Results and discussion

Fig. I-2-3-1 shows charge and discharge curves of the cathode containing $LiFePO_4$/C obtained by sintering at 900°C for 100 seconds without annealing. A typical voltage plateau based on Fe^{2+}/Fe^{3+} redox couple of $LiFePO_4$ with olivine structure is observed, and discharge capacities are 149.5 and 131.3 mAh g^{-1} at 1/10 and 1 C-rates (1 C-rate = 170 mA g^{-1}), respectively. However, discharge capacity is reduced to about 90.2 mAh g^{-1} at 10 C-rate. Furthermore, the polarization between the charge and discharge is too large; this should correlate with somewhat poor conductivity of the sample: 8.7×10^{-3} S cm^{-1} (Table I-2-3-1). To increase the conductivity, we added an annealing process in the high-frequency induction heating procedure because we thought that the primary cause of low electric conductivity is insufficient carbonization of decomposition products of citric acid.

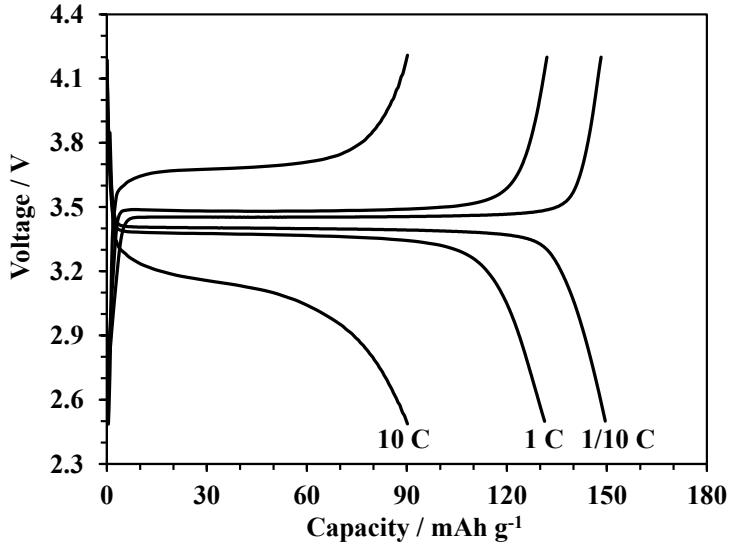

Fig. I-2-3-1 Charge and discharge curves of the cathode containing non-annealed $LiFePO_4$/C at 1/10, 1, 10 C-rates (1C = 170 mA g^{-1}). Cutoff voltages are 2.5 and 4.2 V.

Fig. I-2-3-2 shows XRD patterns of non-annealed and annealed $LiFePO_4$/C obtained by sintering at 900°C for 105 seconds, and for annealed $LiFePO_4$/C, followed by annealing at 700°C for 75 seconds. The obtained XRD profiles suggest that both samples are single-phase $LiFePO_4$ and contain no impurities. The reaction rate of carbothermal reduction is very fast at 900°C, and too long sintering easily leads to generation of Fe_2P by excessive reduction [16]. Thus, as we considered that the formation of $LiFePO_4$ phase is completed by sintering at 900°C for 105 seconds, the following annealing process was carried out at 700°C; the lower temperature should provide a significantly slow reaction rate of carbothermal reduction to suppress the formation of Fe_2P. The residual carbon on surface of $LiFePO_4$ particles was not observed in XRD patterns because of its amorphous characteristic. The electric conductivity of $LiFePO_4$/C is improved to 1.9×10^{-2} S cm^{-1} by adding such a short-time annealing process to the high-frequency induction heating procedure.

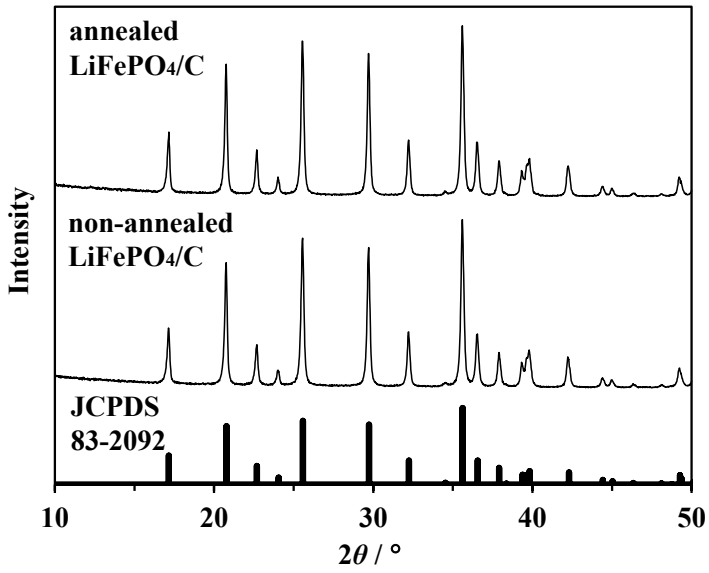

Fig. I-2-3-2 XRD patterns of annealed and non-annealed $LiFePO_4$/C and the reference pattern (JCPDS 83-2092).

Fig. I-2-3-3 shows the primary particle-size distributions calculated from SAXS profiles of annealed and non-annealed $LiFePO_4$/C. The primary particle-size

distributions are quite similar, and the mean primary particle diameters of annealed and non-annealed $LiFePO_4/C$ are 48.4 nm and 47.5 nm, respectively.

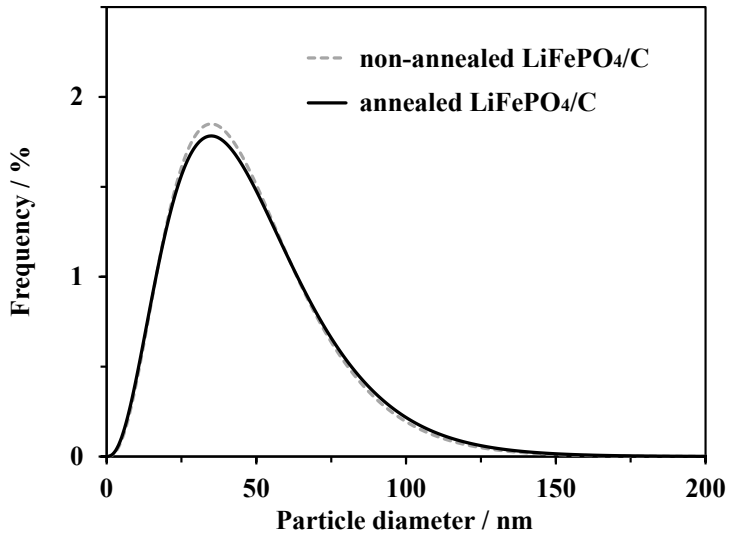

Fig. I-2-3-3 Primary particle size distribution of non-annealed and annealed $LiFePO_4/C$ calculated from SAXS profiles. Frequencies of the plots are accumulated at every 1nm.

Fig. I-2-3-4 shows the SEM images of annealed and non-annealed $LiFePO_4/C$. Various particle sizes from submicron to about 3 μm are observed in these images. Judging from the primary particle-size distributions and particle appearance observed in the SEM images, particles observed by SEM should be secondary particles that are formed by aggregation of primary particles. Comparing two images, the secondary particle diameters of both samples seem almost same. These results suggest that the annealing process never increase the primary and secondary particle diameters. Therefore, Li-ion diffusivity in both samples can be regarded as basically equivalent. Important physical properties of the annealed and non-annealed $LiFePO_4/C$ are summarized in Table I-2-3-1. Although there is no difference in the particle-size parameters between the samples, the electric conductivity is increased by the annealing probably due to enhanced amorphous carbon deposition on the particles.

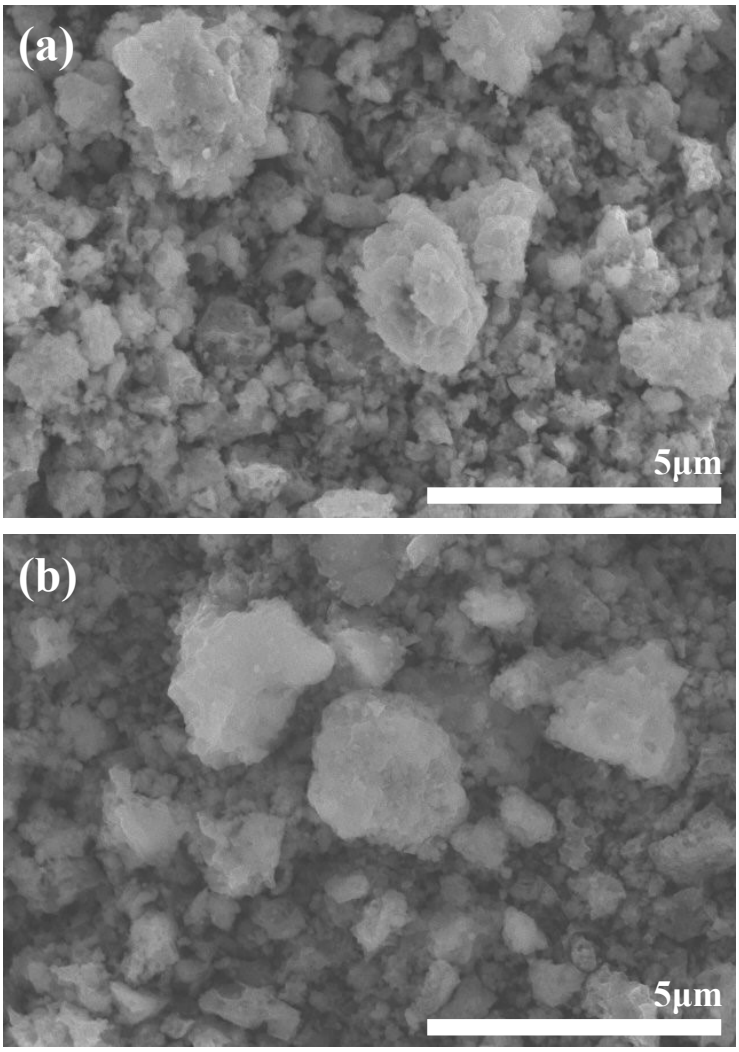

Fig. I-2-3-4 SEM images of (a) annealed and (b) non-annealed $LiFePO_4$/C. Magnification of the observation is x10,000.

Table I-1-3-1 Important physical properties of annealed and non-annealed $LiFePO_4$/C.

Sample	Electric conductivity	Secondary particle size	Mean primary particle size
annealed $LiFePO_4$/C	1.9×10^{-2} S cm^{-1}	< 3 μm	48.4 nm
non-annealed $LiFePO_4$/C	8.7×10^{-3} S cm^{-1}	< 3 μm	47.5 nm

Fig. I-2-3-5 shows the charge and discharge curves of the cathodes containing annealed $LiFePO_4$/C. The polarization voltages between charge and discharge curves of the cathodes containing non-annealed (Fig. I-2-3-1) and annealed $LiFePO_4$/C (Fig. I-2-3-5) at 50% state of charge (SOC) with various rates ($\Delta E_{\text{C-rate}}$) are summarized in Table I-2-3-2.

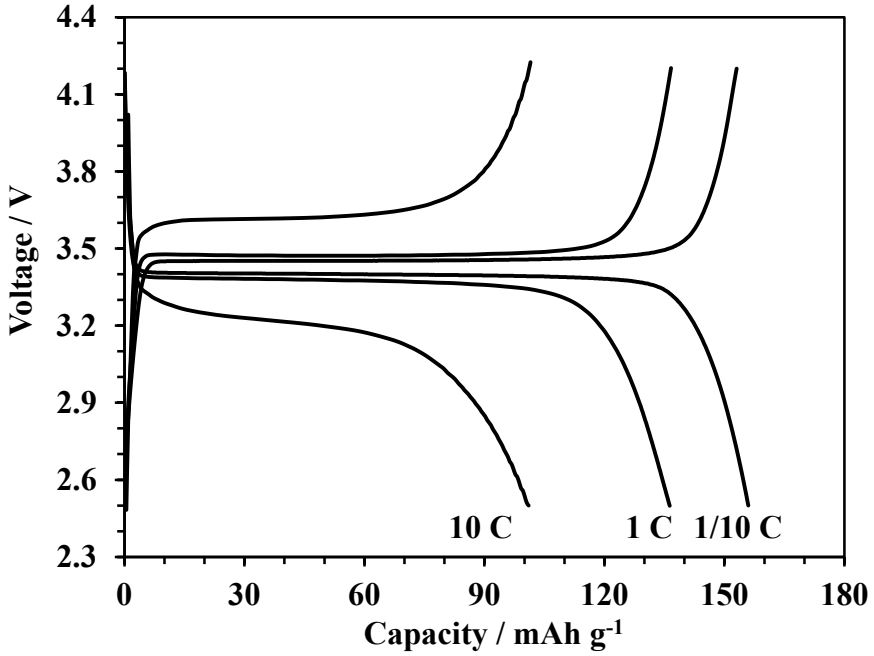

Fig. I-2-3-5 Charge and discharge curves of the cathode containing annealed $LiFePO_4$/C at 1/10, 1, 10 C-rates (1C = 170 mA g^{-1}). Cutoff voltages are 2.5 and 4.2 V.

Table I-2-3-2 Polarization between charge and discharge curves of the cathodes containing annealed and non-annealed $LiFePO_4$/C at 50% SOC with various rates.

Sample	$\Delta E_{1/10\,C}$	$\Delta E_{1\,C}$	$\Delta E_{10\,C}$
annealed $LiFePO_4$/C	57 mV	101 mV	422 mV
non-annealed $LiFePO_4$/C	57 mV	118 mV	576 mV

The polarization voltage between charge and discharge is relatively small when compared to that of the corresponding cathode with non-annealed $LiFePO_4$/C at 1/10 and 1 C-rate; the discharge capacities of annealed $LiFePO_4$/C cathode are 156.0 and 136.3 mAh g^{-1}, respectively, which are slightly larger than those of non-annealed $LiFePO_4$/C cathode. In addition, the polarization at 10 C-rate is significantly reduced when compared to that of non-annealed $LiFePO_4$/C cathode, and the discharge capacity of 100.1 mAh g^{-1} is achieved at 10 C-rate.

Fig. I-2-3-6 shows the charge and discharge rate performances of annealed and non-annealed $LiFePO_4$/C cathodes at 1/10-10 C-rates. The difference in the discharge capacity between both samples tends to become larger with increasing charge and discharge rate. With respect to the charge and discharge curves (Fig. I-2-3-1 and I-2-3-5), it is clear that the annealed $LiFePO_4$/C has superior charge and discharge performance to the non-annealed $LiFePO_4$/C. Furthermore, the annealed $LiFePO_4$/C synthesized in this study shows better cycle stability and charge-discharge rate performance than $LiFePO_4$/C reported in other papers using carbothermal reduction process [15-18].

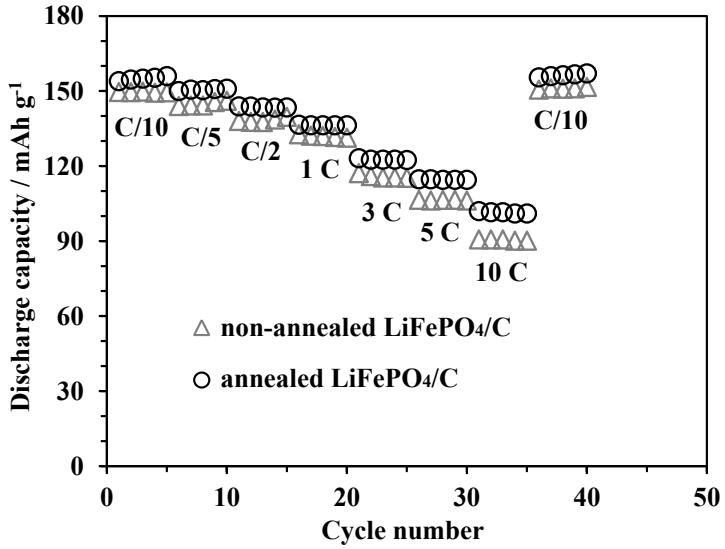

Fig. I-2-3-6 Charge and discharge rate performance of the cathodes containing annealed and non-annealed $LiFePO_4$/C at 1/10-10 C-rates (1C = 170 mA g^{-1}).

We have suggested that differences in observed electrochemical properties are derived from a difference in the electrical conductivity that is controllable by the short-time annealing process. In addition, our high-frequency induction heating method would be too aggressive for enough carbonization of residual decomposition products from citric acid as a carbon source because the electrical conductivity can be significantly improved by a relatively low-temperature short-time annealing. Therefore, the present annealing treatment following the main process is very important and effective to improve the electrochemical performances of $LiFePO_4$/C obtained by a high-frequency induction heating method.

I-2-4. Conclusions

We have successfully developed the synthesis of $LiFePO_4$/C in a few minutes by using high-frequency induction heating; inexpensive Fe_2O_3 is applicable as iron source in combination with a carbothermal reduction method. It was found that the electrical conductivity of $LiFePO_4$/C can be improved from 8.7×10^{-3} to 1.9×10^{-2} S cm^{-1} by introducing the short-time annealing process at 700°C following the sintering process at 900°C. The discharge capacities of the annealed $LiFePO_4$/C cathode at 1/10, 1, and 10 C-rates are 156.0, 136.3, and 100.1 mAh g^{-1}, respectively, which are somewhat larger than those of the non-annealed $LiFePO_4$/C cathode. The polarization between charge and discharge of the annealed $LiFePO_4$/C cathode is much smaller than that of the non-annealed cathode. Furthermore, the annealed $LiFePO_4$/C cathode is superior to the non-annealed cathode in charge and discharge rate performance. We consider that the difference in these electrochemical properties should be derived mainly from a difference in the electrical conductivity of residual carbon at the surface of $LiFePO_4$ particles. In fact, the conductivity is improved by the short-time annealing process while no formation of Fe_2P as impurity and no increase in primary and secondary particle sizes are observed. Therefore, the present annealing treatment is very effective in improving electrochemical performances of $LiFePO_4$/C in the synthesis process based on the high-frequency induction heating method.

I-2-5. References

[1] A.K. Padhi, K.S. Nanjundaswamy, and J.B. Goodenough, J. Electrochem. Soc. 144 (1997) 1188.

[2] A.K. Padhi, K.S. Nanjundaswamy, C. Masquelier, S. Okada, and J.B. Goodenough, J. Electrochem. Soc. 144 (1997) 1609.

[3] C. Delacourt, P. Poizot, S. Levasseur, and C. Masquelier, Electrochem. Solid-State Lett. 9 (2006) A352.

[4] P. Gibot, M. Casas-Cabanas, L. Laffont, S. Levasseur, P. Carlach, S. Hamelet, J.-M.Tarason, and C. Masquelier, Nat. Mater. 7 (2008) 741.

[5] Z. Chen and J.R. Dahn, J. Electrochem. Soc. 149 (2002) A1184.

[6] H. Huang, S.C. Yin, and L.F. Nazar, Electrochem. Solid State Lett. 4 (2001) A170.

[7] M. Koltypin, D. Aurbach, L. Nazar, and B. Ellis, J. Power Sources 174 (2007) 1241.

[8] A. Yamada, S.C. Chung, and K. Hinokuma, J. Electrochem. Soc. 148 (2001) A224.

[9] D.-H. Kim and J. Kim, Electrochem. Solid-State Lett. 9 (2006) A439.

[10] D. Choi and P.N. Kumta, J. Power Sources 163 (2007) 1064.

[11] T. Muraliganth, A. V. Murugan, and A. Manthiram, J. Mater. Chem. 18 (2008) 5661.

[12] A.Yamada and S.C. Chung, J. Electrochem. Soc. 148 (2001) A960.

[13] G. Arnold, J. Garche, R. Hemmer, S. Strobele, C. Vogler, and M. W. Mehrens, J. Power Sources 119-121 (2003)247.

[14] S. Uchida, M. Yamagata, and M. Ishikawa, The 51st Battery Symposium in Japan, Abstr., p.193 (2010) [in Japanese]; J. Power Sources, in contribution.

[15] H. P. Liu, Z. X. Wang, X. H. Li, H. J. Guo, W. J. Peng, Y. H. Zhang, Q. Y. Hu, J. Power Sources 184 (2008) 469.

[16] C. W. Kim, M. H. Lee, W. T. Jeong, K. S. Lee, J. Power Sources 146 (2005) 534.

[17] N. V. Kosova, E. T. Devyatkina, S. A. Petrov, J. Electrochem. Soc. 157 (2010) A1247.

[18] G. T. K. Feya, H. M. Kao, W. H. Li, J. Power Sources 196 (2011) 2810.

Section I-3

Optimizing Synthesis Process for Ideal Crystal Structure of $LiFePO_4$

I-3-1. Introduction

All the consistent materials of Li-ion batteries must be improved and diversified to expand use of Li-ion batteries. Majority of battery performances are dependent on the electrochemical properties of the electrode active materials, the application of novel active materials to commercial Li-ion batteries is a particularly pressing need. Currently, $LiCoO_2$ is most widely used as positive electrode material due to its high battery performances [1] but cobalt is very expensive. Thus, there is a need for inexpensive and high-performance positive electrode material instead of the $LiCoO_2$ [2, 3]. The lithium iron phosphate ($LiFePO_4$) which has been reported by Padhi et al. [4] has a theoretical capacity of 170 mAh g^{-1} and relatively high redox potential around 3.5 V vs. Li/Li^+ attributed Fe^{2+}/Fe^{3+} redox couple. In addition, $LiFePO_4$ have better thermal stability and long-term cycle performance than $LiCoO_2$ [5]. The drawbacks of $LiFePO_4$ are low electric conductivity derived from lattice structure including P-O covalent bonds [6] and poor Li ion diffusion through $LiFePO_4/FePO_4$ interface [4, 7], these problems have already been improved by modifying the surface of $LiFePO_4$ particles with carbon [5, 8] and decreasing the particle size to nano-scale [9, 10]. Although the $LiFePO_4$ modified with carbon ($LiFePO_4/C$) which has been removed the drawbacks described above is suitable as positive electrode material for large-scale Li-ion batteries used in electric vehicles, plugin hybrid electric vehicles and large power storage systems and does not seem to have any problem, the market price of $LiFePO_4/C$ is higher than that of $LiCoO_2$ even though it produced from an inexpensive iron, which interfere wide practical application of it.

The high cost of $LiFePO_4/C$ is mainly caused by high temperature heating process of synthesis method. Since the iron in the $LiFePO_4$ phase is divalent, heating process must be carried out in an inert gas or vacuum to suppress oxidation of iron (from Fe^{2+} to Fe^{3+}) and long-time (typically several hours) heating is required [4-6]. In addition, the use of divalent iron compounds as iron source, which enables the easy synthesis of

$LiFePO_4$ phase, slightly increases the cost of $LiFePO_4$/C. In order to synthesis $LiFePO_4$/C with superior electrochemical performances which has extremely small particle size and finely modified with carbon, various synthesis methods have been suggested in addition to typical solid-state reactions [4, 6, 11, 12]. The liquid phase synthesis methods such as hydrothermal method [13-15], solvothermal method [16-18] are very effective means for synthesis of $LiFePO_4$/C with excellent battery performances. However, these methods do no complete only liquid phase process, and eventually require long-time heating process in inert atmosphere or reducing gas flow such as mixed gas of H_2 and Ar. The spray pyrolysis method also requires the additional heating process in reducing gas containing H_2 except for pyrolysis process [19, 20]. As a result, these methods lead to increase the cost of $LiFePO_4$/C. Therefore, it is important to use inexpensive trivalent iron compounds as iron source and significantly reduce the heating time. The carbothermal reduction is necessary to use trivalent iron such as Fe_2O_3. When the trivalent iron compounds are heated with carbon or organic carbon source at high temperature in inert atmosphere, the trivalent iron compounds deprived of oxygen by carbon and divalent irons are generated [21, 22]. The microwave methods have been already reported as a method to significantly reduce the heating time [23, 24]. But, microwave technics is difficult to control because microwave makes target materials heat spontaneously, and there is little reported cases that could be synthesis $LiFePO_4$/C with good battery performance [25, 26].

Previously, we have reported a novel rapid synthesis method for $LiFePO_4$/C [27], which combines a carbothermal reaction with a high-frequency induction heating method to reduce material and process costs of $LiFePO_4$/C. In this method, conductive crucible which made of carbon or metal allowed to exotherm rapidly (> 1000°C min^{-1}) by High-frequency induction heating and the precursor of $LiFePO_4$ is heated indirectly by heated crucible. Our method is same as solid-state reaction and easily to control despite the rapid synthesis involves only a few minutes heating process. Then the $LiFePO_4$/C synthesized in our method shows the maximum discharge capacity of 156 mAh g^{-1} at 1/10 C-rate (1 C = 170 mA g^{-1}) and maintained 100.1 mAh g^{-1} at 10 C-rate. However, we had noticed the possibility that the $LiFePO_4$ phase synthesized in previous our method does not have ideal crystal structure and had thought that there is a point

should be improved in previous our method because the pellet precursor is heated from only one side due to the shape of used carbon crucible shown in Fig. I-3-3-1 (a) and further the heating time is quite short. In this paper, we report the optimized heating conditions using a crucible with improved shape shown in Fig. I-3-3-1 (b) to homogeneously heat the pellet precursor from both sides. Furthermore, we compared physical and electrochemical properties of $LiFePO_4/C$ synthesized in this work to those of previous sample.

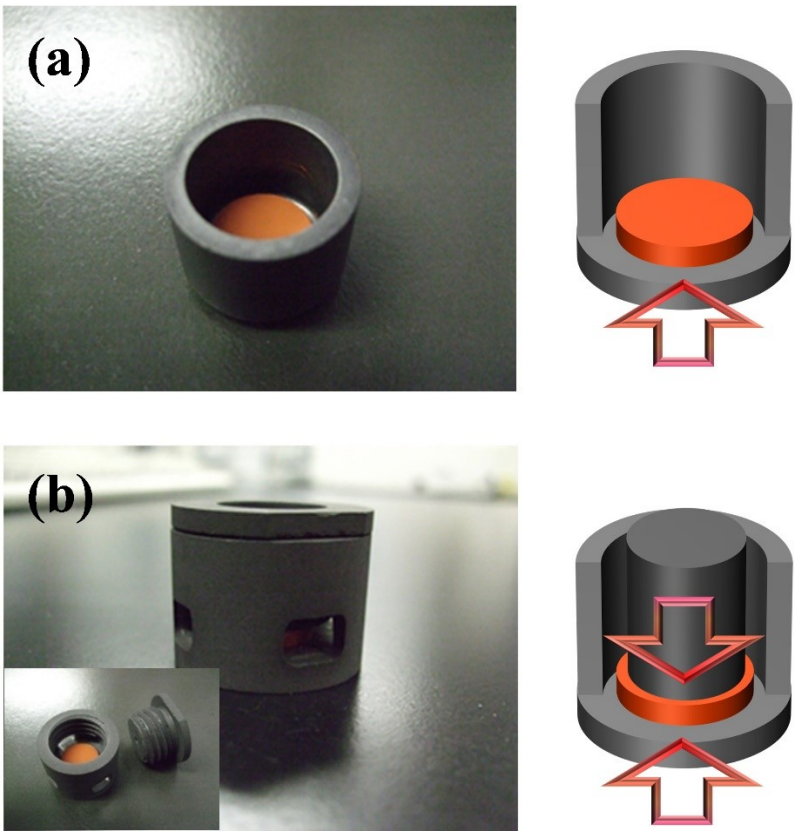

Fig. I-3-3-1 Photographs and schematic images of carbon crucibles using in previous work (a) and this work (b).

I-3-2. Experimental

The $LiFePO_4/C$ sample was synthesized by a solid-state reaction of stoichiometric amounts of Li_2CO_3 (Kanto Chemical Co., 99.0%), Fe_2O_3 (Toda Kogyo

Corp., 99.5%), and $NH_4H_2PO_4$ (Kanto Chemical Co., 99.0%) together with citric acid (Kanto Chemical Co., 99.0%) as carbon source. In this work, the addition amount of citric acid was increased to 12 wt.% (10wt.% in previous studies) because the loss of large amount of citric acid is expected due to enhancing thermal conduction to pellet precursor by using a carbon crucible for heating the pellet precursor from both sides. The mixing process of starting materials and the preparation process of pellet precursor are same as our previous work [27]. The pellet precursor was sandwiched between two parts of carbon crucible for both sides heating (Fig. I-3-3-1 (b)), and it was placed in a vacuum chamber. The carbon crucible was rapidly heated to 900°C at a heating rate of 1800°C min^{-1} by high-frequency induction heating, and then it held for 1 minute at elevated temperature. Since the reaction rate is improved due to enhancing thermal conduction to pellet precursor by using a carbon crucible for heating the pellet precursor from both sides, the holding time at 900°C was shorter than the previous work. After the sintering process at 900°C, the temperature was reduced to 700°C and held the temperature for 2 minutes for sufficient carbonization of citric acid. The resulting gray pellet was ground thoroughly in a mortar, and the obtained powder was used as active material.

The X-ray diffraction (XRD, Rigaku Co., Ultima IV) with Cu Kα radiation was used to identify the phases of synthesized samples. The diffraction data were collected in step scanning mode under the same conditions as previous work [27]. The carbon content of synthesized samples was measured by X-ray fluorescence (XRF, Rigaku Co., ZSX Primus II) analysis. The electric conductivity was measured by a four probe method. The obtained powder sample was pressed into pellet at 5 MPa, and four probes were pressed against the pellet. The measurement was performed 10 times; the average value was regarded as representative electrical conductivity. The morphology of primary particles was observed using transmission electron microscope (TEM, JEOL Ltd., JEM-2100). The electron accelerating voltage is 120 kV. The primary particle-size distribution of synthesized samples was determined by small-angle X-ray scattering (SAXS, Rigaku Co., Ultima IV). The measurement conditions of scattering profile were same as previous work [27]. The primary particle-size distribution was determined by curve fitting for the scattering profile with several parameters such as background

intensity, average particle size, normalized distribution ratio, scale factor, and true density of $LiFePO_4$ (3.60 g cm^{-3}).

The positive electrode for electrochemical measurement was prepared by using the obtained $LiFePO_4$/C, ketjen black (Lion Corp., Carbon ECP) and polyvinylidene fluoride (Kureha Corp., #1100) with respective weight ratio of 85:8:7 in the same way as previous work [27]. The prepared positive electrode sheet was cut into disks with a diameter of 12 mm as test electrode. The mass loading of active material in an electrode was approximately 6.0 mg cm^{-2}.

The electrochemical measurement was carried out using a CR2032 coin type cell assembled in an argon-filled globe box. The composition of positive electrode half cells was same as previous work [27]. The charge and discharge rate performance test was carried out in a voltage range of 2.5-4.2 V using a galvanostatic charge and discharge unit (Intex Co., BTS2004W) at 1/10, 1/5, 1/2, 1, 3, 5, 10 and then 20 C-rates (1C = 170 mA g^{-1}) by every 5 cycles. The charge and discharge cycle performance test was also carried out in a same voltage range at 5 C-rate for 100 cycles following pre-cycle which is each 5 cycles at 1/10 and 1 C-rate. The alternative current (AC) impedance spectra were measured by using frequency response analyzer (Solartron analytical, 1255B). The measurement cells were charged to 80 mAh g^{-1} (approximate half charging state) at 1/10 C-rate after fully charging and discharging of 5 cycles at 1/10 C-rate, and their voltage were relaxed for 10 h at open circuit condition for measurement in steady state. The measurement frequency range was 100 kHz – 10 mHz.

I-3-3. Results and discussion

Fig. I-3-3-2 shows the XRD profiles of $LiFePO_4$/C synthesized in previous work (Previous sample) and this work (Optimized sample). A reference pattern (JCPDS 83-2092) is displayed at the bottom. The crystalline impurities that can be confirmed by XRD are not included in previous sample. On the other hand, the XRD profiles obtained from optimized sample synthesized by using a carbon crucible for heating the pellet precursor from both sides include the peaks attributed to impurities. These peaks are related to Fe_2P phase formed by over reduction of $LiFePO_4$ phase. The Fe_2P content in

optimized sample obtained by Rietveld refinement is 1.1 wt.% (Table I-3-3-1). The Fe_2P improves the conductivity of $LiFePO_4$ and dose not affects cycle stability [28]. Large amount of Fe_2P forming decreases the $LiFePO_4$ phase in the sample, which leads to decrease in maximum specific capacity, but the presence of a small amount of Fe_2P is not a problem [28]. The lattice parameters of $LiFePO_4$ phase calculated from the each XRD profiles of shown in Table I-3-3-1. The lattice parameter is important factor which significantly affect the electrochemical properties of $LiFePO_4$ phase [29]. The lattice parameters of previous sample deviated that reported by Padhi et al. We considered that this result is due to heating from only one side of pellet precursor. Thus, we improved the shape of the carbon crucible to achieve homogeneous heating. The optimized sample synthesized by using a carbon crucible for heating the pellet precursor from both sides has ideal lattice parameters close to report of Padhi et al. It found that the $LiFePO_4$ phase with ideal crystal structure generates despite a short heating time such as 3 minutes.

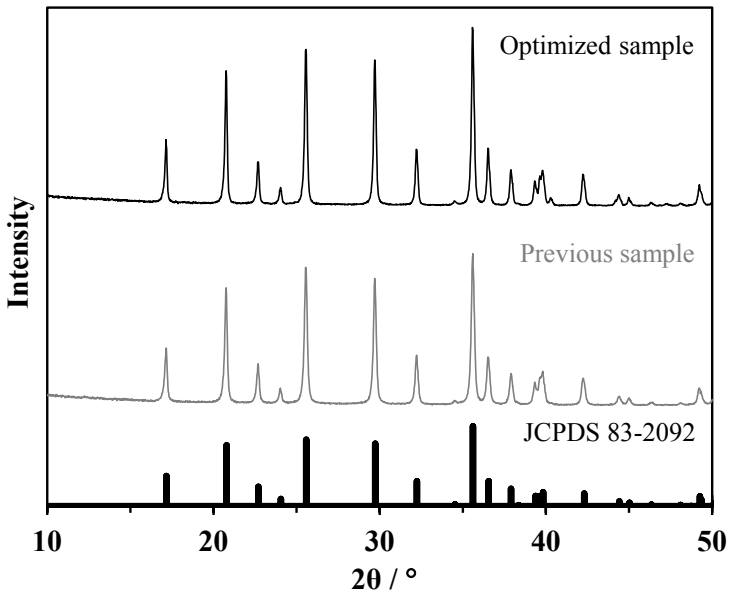

Fig. I-3-3-2 XRD profiles of synthesized samples and reference pattern of $LiFePO_4$ (JCPDS 83-2092)

Table I-3-3-1 Phase compositions obtained by Rietveld refinement and lattice parameters of $LiFePO_4$ phase calculated from the XRD profiles.

Sample	Compositions (wt.%)		Lattice parameters (Å)		
	$LiFePO_4$	Fe_2P	*a*-axis	*b*-axis	*c*-axis
Previous sample	98.9	1.1	10.327	6.011	4.697
Optimized sample	100.0	0.0	10.335	6.008	4.695
Padhi et al.[1)]	---	---	10.335	6.008	4.693

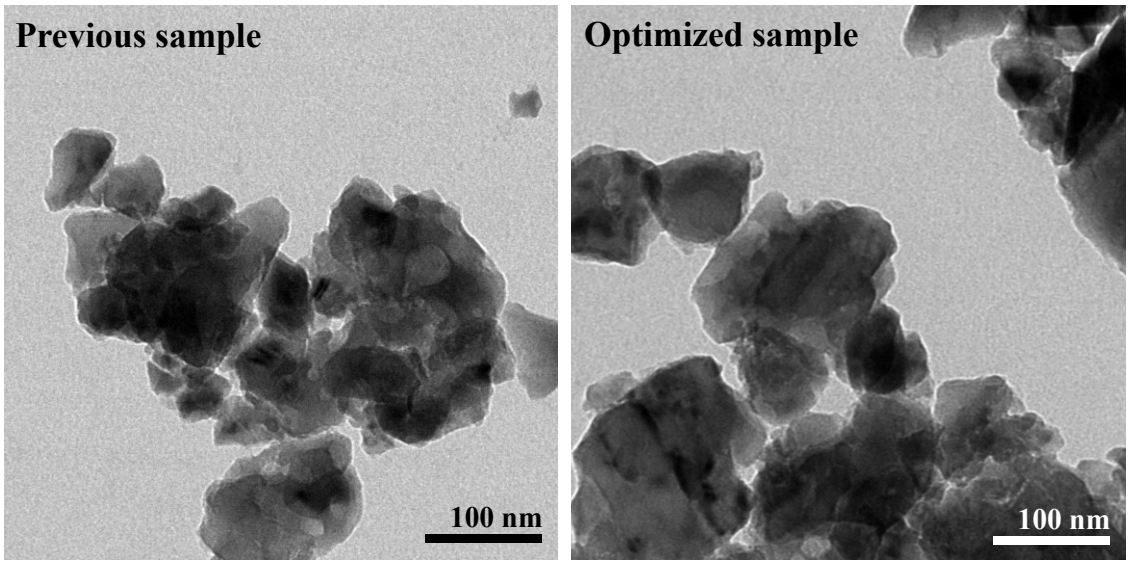

Fig. I-3-3-3 TEM images of previous sample (a) and optimized sample synthesized in this work (b).

Fig. I-3-3-3 and Fig. I-3-3-4 show the TEM images and primary particle distributions of synthesized samples, respectively. The shape that the $LiFePO_4$ particles coated with carbon is not confirmed from these TEM images, the $LiFePO_4$/C synthesized by our method is $LiFePO_4$ and carbon composite. The primary particles size can be confirmed from TEM images are 50 – 150 nm, optimized sample particles seems slightly larger. It is considered that the particle size growth was promoted since thermal conduction to pellet precursor was enhanced by using improved carbon crucible. The

primary particle size distribution of optimized sample is slightly larger compared to the previous sample, which is consistent with the results of TEM observation.

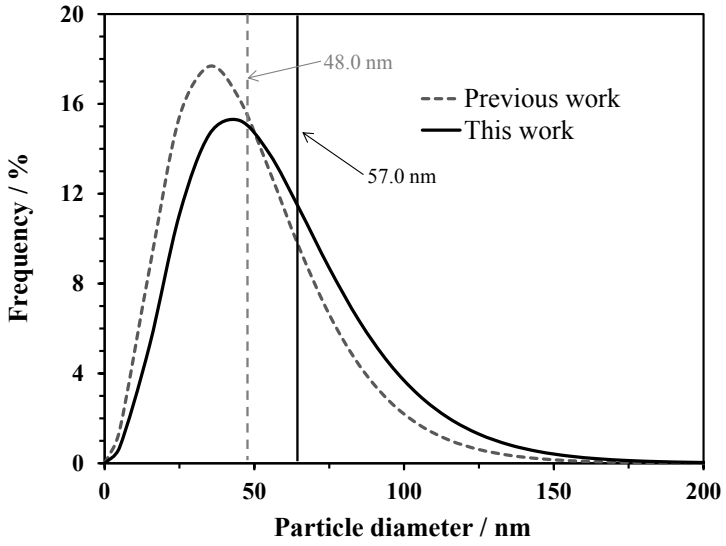

Fig. I-3-3-4 Primary particle size diameter of previous sample (a) and optimized sample synthesized in this work (b)

Table I-3-3-2 Average primary particle diameters and crystallite diameters obtained by Rietveld refinement of previous sample and optimized sample.

Sample	Average primary particle size	Crystallite diameter
Previous sample	48.0 nm	38.5 nm
Optimized sample	57.0 nm	48.0 nm

The average primary particle size and crystallite diameter of both samples are shown in Table I-3-3-2. The crystallite diameter and average primary particle size are similar in both samples, which indicate that a primary particle is single crystal or is composed of a few crystallites. Although the difference between the heating conditions

caused the slight difference in particle size, both samples keep a small particle size that can fully exploit the electrochemical performances of $LiFePO_4$.

Table I-3-3-3 shows the electronic conductivities obtained by fore prove measurement and carbon content measured by XRF of both samples. The electric conductivity of optimized sample is almost identical to that of previous sample even though the carbon content of optimized sample is less than that of previous sample. Since the optimized sample includes the small amounts of Fe_2P (Table I-3-3-1) which is conductive impurity, the optimized sample indicates the equivalent electric conductivity of previous sample despite the small carbon content.

Table I-3-3-3 Electronic conductivities and carbon contents of previous sample and optimized sample.

Sample	Electronic conductivity	Carbon content
Previous sample	1.9×10^{-2} S cm^{-1}	2.74 wt.%
Optimized sample	1.5×10^{-2} S cm^{-1}	2.26 wt.%

Fig. I-3-3-5 shows the charge and discharge curves at 1/10, 1, 5 C-rate of the positive electrodes including previous sample and optimized sample. At the 1/10 C-rate, the positive electrode including previous sample shows the discharge capacity of 156.0 mAh g^{-1} which have not reached theoretical capacity. On the other hand, the positive electrode including previous sample shows the discharge capacity of 162.4 mAh g^{-1}. This specific capacity is normalized by weight including carbon and Fe_2P, the specific capacity normalized by weight of only $LiFePO_4$ is 168.0 mAh g^{-1}, which is 99% of the theoretical capacity. Furthermore, the obtained sample has longer voltage plateau region, which indicates two-phase ($LiFePO_4$/$FePO_4$) coexistence reaction [7], in both charge and discharge curve and the voltage rise and fall at end of charge and discharge occur after almost finishing the charge and discharge. Fig. I-3-3-6 shows the

discharge capacity vs. various charge and discharge rate of the positive electrode containing previous sample and optimized. The positive electrode prepared from

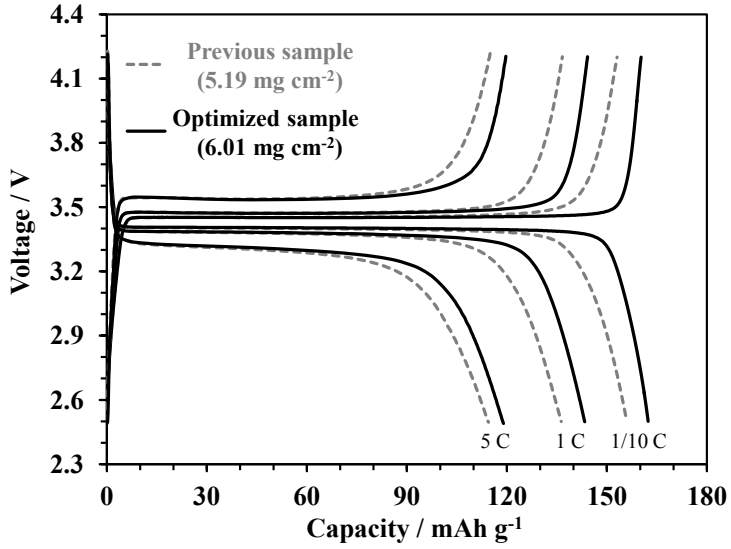

Fig. I-3-3-5 Charge and discharge curves at various C-rate of the positive electrodes prepared from previous sample and optimized sample.

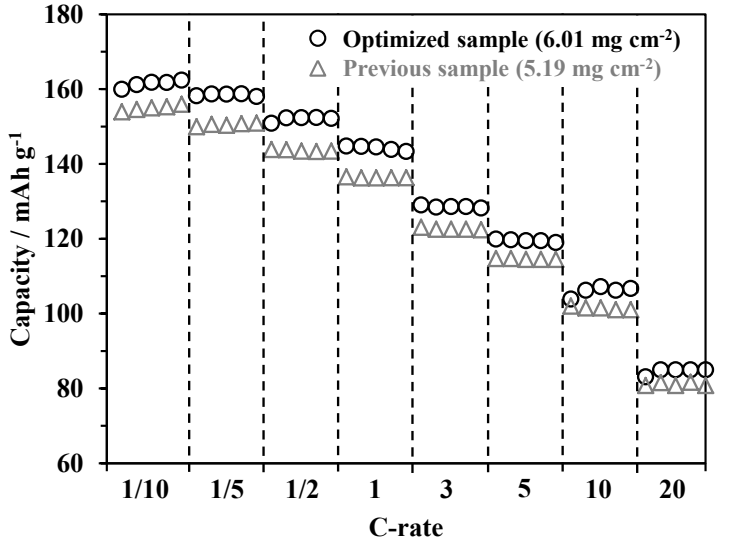

Fig. I-3-3-6 Discharge capacity vs. various charge and discharge rate of the positive electrodes containing previous sample and optimized sample.

optimized sample shows higher capacity than the positive electrode prepared from previous sample in all of 1/10 – 20 C-rates. Since the mass loading of active material on the electrode prepared by using optimized sample is heavier, the rate performance of optimized sample is improved than appearance. Fig. I-3-3-7 shows the discharge capacity vs. cycle number at 5 C-rate. The capacity of positive electrode prepared from previous sample slightly degrades after 110 cycles. The voltage plateau of $LiFePO_4$ is about 3.5 V where electrolyte decomposition does not occur, and there is small amount of time that the electrode potential becomes high potential which may make electrolyte decomposes because this cycle performance test was carried out at a high rate as 5 C-rate. Therefore, capacity degradation in this cycle test seems to be attributed to the deterioration of the $LiFePO_4$. The positive electrode prepared from optimized sample exhibits almost no capacity degradation. The $LiFePO_4$ phase with ideal crystal structure also improves the cycle stability.

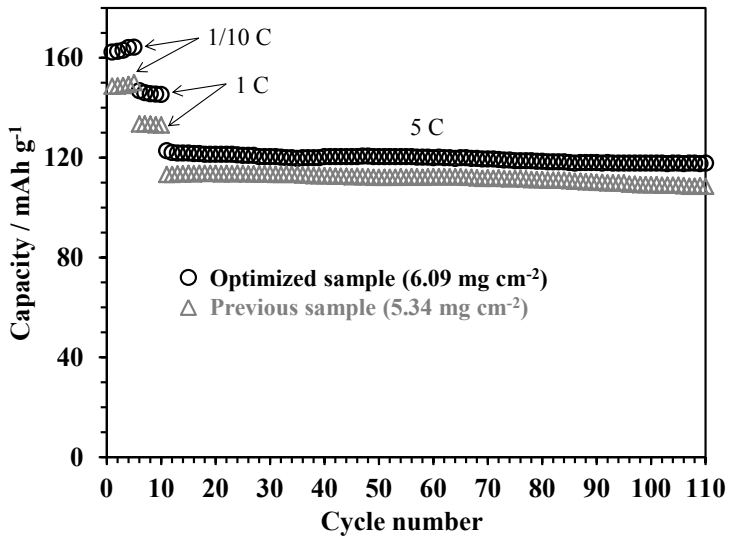

Fig. I-3-3-7 Discharge capacity vs. cycle number of the positive electrodes containing previous sample and optimized sample.

Fig. I-3-3-8 shows the nyqist plots of the positive electrode containing previous sample and optimized sample. The mass loading of active material of each electrodes

using AC impedance measurement is approximately same. The measurement was carried out at equilibrium state after the cell voltage was relaxed enough, the nyqist plots of the cell containing either electrode shows only one semicircle and the straight line with a slope of 45 degrees. It is considered that the semicircle contains both internal charge transfer resistance of the electrode active material and the charge transfer resistance through the electrode/electrolyte interface. The electric conductivity of optimized sample is almost same (or slightly decreases) compared to previous sample and the particle distributions of it increases (in other words, the surface area of it decreases) which causes the increasing in the magnitude of semicircle of the cell containing the electrode prepared from optimized sample. However, it is smaller than the magnitude of semicircle the cell containing the electrode prepared from previous sample. Therefore, we consider that the internal charge transfer resistance of optimized sample decreases together with improving its crystal structure.

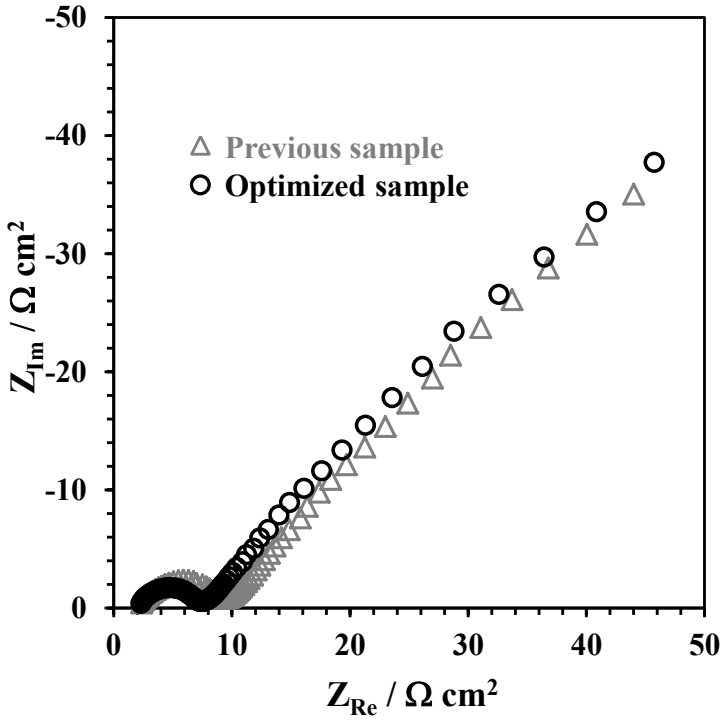

Fig. I-3-3-8 Nyqist plots of the positive electrode containing previous sample and optimized sample measured at half-charging state (80 mAh g^{-1}) in 6 th cycle.

I-3-4. Conclusions

We optimize the heating conditions of high-frequency induction heating method for $LiFePO_4$/C synthesis by using carbon crucible for homogeneously heating the pellet precursor from both sides and obtained the optimized $LiFePO_4$/C with the ideal lattice parameters close to it reported by Padhi et al. Although the optimized sample has slightly larger primary particle size distribution and slightly lower electric conductivity compared to previous sample due to the difference of heating condition, the size of the semicircle on the nyqist plot of the electrode containing optimized sample was reduced compared to that of the electrode containing previous sample. The electrode containing optimized sample shows specific discharge capacity of 168.0 mAh g^{-1}, which achieves 99% of theoretical specific capacity of $LiFePO_4$ phase and the discharge capacity of it in charge and discharge rate performance test is superior to the electrode containing previous sample in all of 1/10 – 20 C-rates. The electrode containing optimized sample also shows excellent cycle stability during 100 cycles at 5 C-rate. These improved results seem to be attributed to the ideal crystal structure of $LiFePO_4$ phase obtained by homogeneous heating conditions. We consider that the $LiFePO_4$/C with ideal crystal structure and excellent electrochemical performances can be synthesized in quite short time heating by achieving the homogeneous heating and believe that high-frequency induction heating method can contribute to significantly reducing the cost of $LiFePO_4$/C.

I-3-5. References

[1] T. Ohozuku, A. Ueda, J. Electrochem. Soc. 141 (1994) 2972.

[2] T. Ohozuku, Y. Makimura, Chem. Lett. (2001) 744.

[3] T. Ohozuku, Y. Makimura, Chem. Lett. (2001) 642.

[4] A.K. Padhi, K.S. Nanjundaswamy, J.B. Goodenough, J. Electrochem. Soc. 144 (1997) 1188.

[5] H. Huang, S.-C. Yin, and L. F. Nazar, Electrochem. Solid-State Lett. 4 (2001) A170.

[6] A. Yamada, S.C. Chung, and K. Hinokuma, J. Electrochem. Soc. 148 (2001) A224.

[7] L. Laffont, C. Delacourt, P. Gibot, M. Y. Wu, P. Kooyman, C. Masquelier, J. M,

Tarascon, Chem. Mater. 18 (2006) 5520.

[8] Z. Chen and J.R. Dahn, J. Electrochem. Soc. 149 (2002) A1184.

[9] C. Delacourt, P. Poizot, S. Levasseur, and C. Masquelier, Electrochem. Solid-State Lett. 9 (2006) A352.

[10] K. F. Hsu, S. Y. Tsay and B. J. Hwang, J. Mater. Chem. 14 (2004) 2690.

[11] M. M. Doeff, Y. Hu, F. McLarnon, R. Kostecki, Electrochem. Solid-State Lett. 6 (2003) A207.

[12] F. Croce, A. D' Epifanio, J. Hassoun, A. Deptula, T. Olczac, B. Scrosati, Electrochem. Solid-State Lett. 5 (2002) A47.

[13] X. Ou, H. Gu, Y. Wu, J. Lu, Y. Zheng, Electrochimca Acta 96 (2013) 230.

[14] J. Ni, M. Morishita, Y. Kawabe, M. Watada, N. Takeichi, T. Sakai, J. Power Sources 195 (2010) 2877.

[15] A. Kuwahara, S. Suzuki, M. Miyayama, Ceram. Int. 34 (2008) 863.

[16] Q. Wang, W. Zhang, Z. Yang, S. Weng, Z. Jin, J. Power Sources 196 (2011) 10176.

[17] H. Deng, S. Jin, L. Zhan, W. Qiao, L. Ling, Electrochimca Acta 78 (2012) 633.

[18] S. Yang, X. Zhou, J. Zhang, Z. Liu, J. Mater. Chem. 20 (2010) 8086.

[19] M. Konarova, I. Taniguchi, J. Power Sources 195 (2010) 3661.

[20] N.A. Hamid, S. Wennig, S. Hardt, A. Heinzel, C. Schulz, H. Wiggers, J. Power Sources 216 (2012) 76.

[21] J. Barker, M. Y. Saidi, J. L. Swoyer, Electrochem. Solid-State Lett. 6 (2003) A53.

[22] H. P Liu, Z. X. Wang, X. H Li, H. J. Guo, W. J Peng, Y. H Zhang, Q. Y Hu, J. Power Sources 184 (2008) 469.

[23] Y. Zhang, H. Feng, X. Wu, L. Wang, A. Zhang, T. Xia, H. Dong, M. Liu, Electrochimca Acta 54 (2009) 3206.

[24] M. Higuchi, K. Katayama, Y. Azuma, M. Yukawa, M. Suhara, J. Power Sources 119-121 (2003) 258.

[25] M. S. Song, D. Y. Kim, Y. M. Kang, Y. I. Kim, J. Y. Lee, H. S. Kwon, J. Power Sources 180 (2008) 546.

[26] M. S. Song, Y. M. Kang, J. H. Kim, H. S Kim, D. Y. Kim, H. S. Kwon, J. Y. Lee, J. Power Sources 166 (2007) 260

[27] S. Uchida, M. Yamagata, M. Ishikawa, Electrochemistry 80 (2012) 825.

[28] C. W. Kim, J. S Park, K. S. Lee, J. Power Sources 163 (2006) 144.

[29] J. F. Martin, A. Yamada, G. Kobayashi, S. Nishimura, R. Kanno, D. Guyomard, N. Dupré, Electrochem. Solid-State Lett. 11 (2008) A12.

CHAPTER II

Improving Cycle Stability of High Capacity Silicon Negative Electrode Composed of μm-Silicon Particles

Section II-1

Electrochemical Properties of Silicon Negative Electrodes Prepared with Polyimide Binder

II-1-1. Introduction

Lithium (Li) -ion batteries are required to become larger and provide further high energy density with the stream of migration to electric vehicles from gasoline vehicles [1]. Currently, the graphite which has high electron conductivity and sufficiently low potential related to intercalation/de-intercalation of Li ion vs. Li/Li^+ is widely used as the negative electrode material of Li-ion batteries [2, 3]. However, the capacity of graphite has been already used close to the theoretical capacity. Namely, it is impossible to increase the specific capacity of negative electrode as long as using graphite. In recent years, silicon (Si) has attracted attention as an alternative material for graphite because Si has the relatively low potential for alloying/de-alloying with Li ion (0.4 V vs. Li/Li^+) and extremely high theoretical capacity of 4200 mAh g^{-1} ($Li_{4.4}Si$) [4], which ten times higher than that of graphite. Therefore, drastically improvement in energy density of Li-ion batteries can be expected by using Si as the negative electrode material. However, the volume of Si significantly expands (up to approximately 400%) and contracts during lithiation and de-lithiation [5, 6]. As a result, the structure of Si negative electrode collapses and hence the capacity decreases rapidly with increasing cycle number [7-9]. In order to solve this problem the electrode prepared using nano-structured Si (c.a. Si nano-particles, Si/C nano-composite, and Si nano-wire) which can reduce the stress with expansion and contraction on Si negative electrode has been studied [10-12]. Although, the cycle performances of these electrodes are significantly improved, practical use of nano-Si is difficult because preparation of these materials requires complex processes [10-13].

In order to apply the Si negative electrodes in commercial Li-ion batteries, the cycle stability of Si negative electrodes should be improved in a simple and inexpensive way as much as possible. Therefore, researchers who study for improving the cycle stability of Si negative electrodes should focus on other materials composing negative

electrode as well as active material. Recently, it has been reported that the cycle stability of Si negative electrodes highly depends on the type of binders and its importance has become evident [14, 15]. In this study, we tried to improve cycle stability of Si negative electrodes composed of untreated micro-sized Si particle (μm-Si) as active material and polyimide (PI) as binder.

II-1-2. Experimental

The Si negative electrode with polyimide binder (PI-Si) was prepared in dry room with dew point of -55°C. The untreated μm-Si was mixed with acetylene black (AB, Denki kagaku kogyo Corp., HS-100) and polyamic acid as a precursor of PI in a respective weight ratio of 80:5:15 or 75:10:15 with an adequate amount of *N*-methyl-2-pyrrolidone (NMP, Kishida Chemical Co., 99.5%) solvent and the obtained slurry was cast onto an Cu-foil current collector and dried at 80°C for 2 h in a vacuum oven to remove NMP. In order to vary the polyamic acid to polyimide via dehydration condensation, the temperature of oven was elevated to 250°C and quenched to room temperature. For comparison, Si negative electrode with styrene-butadiene rubber binder (SBR-Si) was prepared. The untreated μm-Si was mixed with AB, carboxy-methyl cellose, and SBR with a weight ratio of 80:10:5:5 in adequate amount of deionized water and the obtained slurry was cast onto a Cu-foil current collector and dried at 80°C for 10 h in a vacuum oven. The prepared electrode sheets were cut into disks with a diameter of 12 mm for electrochemical measurement. The mass loading of Si in electrodes were approximately 2.0 mg cm^{-2}.

Electrochemical measurements were performed using a two electrode type cell assembled in an argon-filled globe box with the prepared Si electrodes, a Li foil (Honjo Metal Corp.) disk with a diameter of 13 mm, 1 M $LiPF_6$ binaly electrolyte composed of ethylene carbonate and dimethyl carbonate (1:1 v/v) (Kishida Chemical Co., LBG) including 3wt.% of vinylene carbonate (Kishida Chemical Co., LBG), and polyolefin porous film or highly porous polyolefin film coated with ceramic as separator. The charge and discharge measurements were carried out using a galvanostatic charge and discharge unit (Intex Co., BTS2004W). In this paper, the alloying process of Si and Li (i.e. the direction in which the voltage is narrowed) is referred to as “Charge”, and

de-alloying process (i.e. the direction in which the voltage is broaden) is referred to as "Discharge". In the initial cycle, the test cells were charged to 5 mV and discharged to 1500 mV with constant current density of 200 mA g^{-1}. After the second cycle, the test cells were charged to 800 or 1200 mAh g^{-1} as limited capacity and discharged to 1500 mV at constant current density of 800 – 1600 mA g^{-1}. When the cell voltage reaches 5 mV before the charge capacity achieve 800 or 1200 mAh g^{-1}, the charge process is terminated at that point.

The surface morphologies of the Si electrodes before and after cycling were observed using scanning electron microscope (SEM, Hitachi Co., SU-1500).

II-1-3. Results and discussion

Fig. II-1-3-1 shows the particle size distribution of μm-Si and inserted figure shows the morphology of the particles. The primary particle size of μm-Si extends across 0.3 – 20 μm and the average particle size of μm-Si is 4.68 μm. In the case of using such Si particles, it is generally known that the pulverization of Si particles and collapse of electrode structure occur with severe volume expansion and contraction of Si particles. As a result the capacity degradation occurs rapidly. However, we have found that the rapid capacity degradation can be suppressed by using polyimide binder.

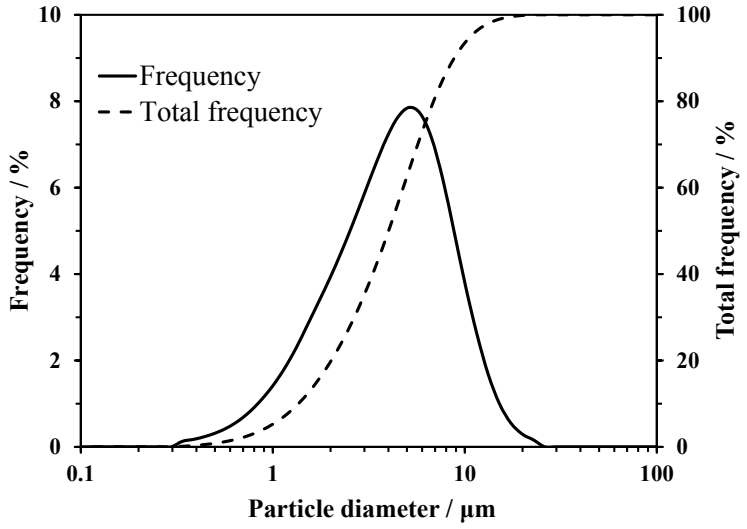

Fig. II-1-3-1 Particle size distribution of μm-Si.

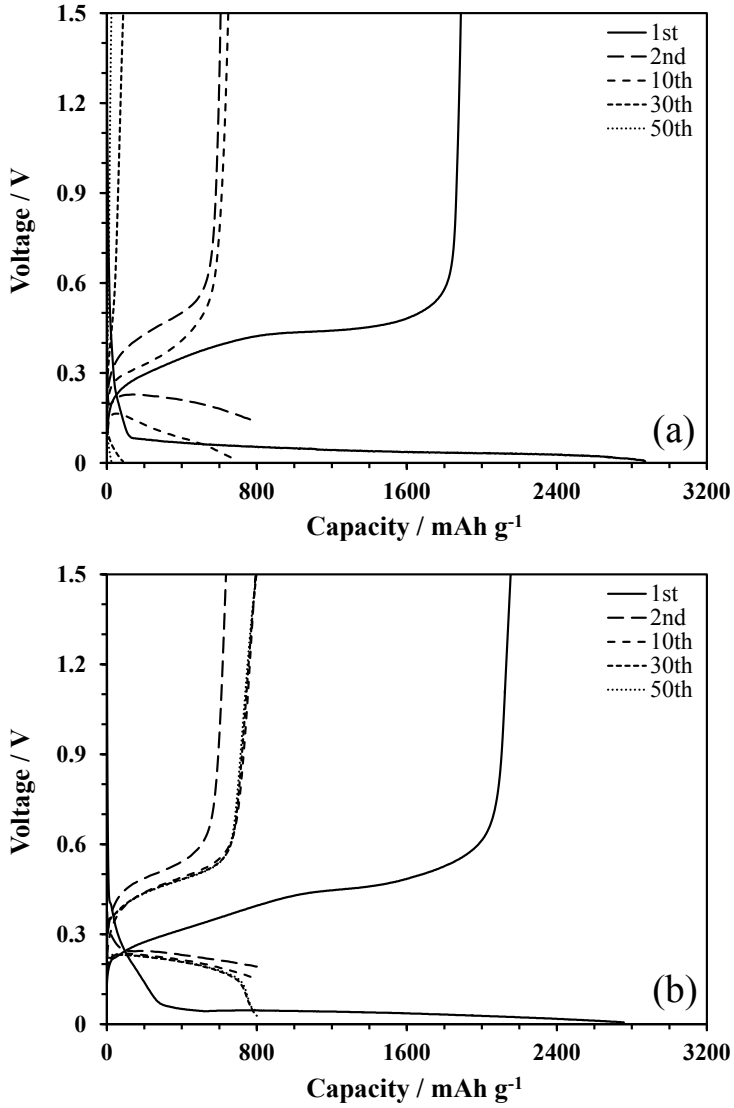

Fig. II-1-3-2 Charge and discharge curves of the cell including (a) PI-Si and (b) SBR-Si electrode.

Fig. II-1-3-2 shows the charge and discharge curves of the cell including (a) PI-Si and (b) SBR-Si electrode. The initial charge capacities of PI-Si and SBR-Si electrodes at low current density (200 mA g^{-1}) were 2756.9 and 2871.6 mAh g^{-1}, respectively; there is no significant difference between these values. On the other hand, the initial discharge capacities of PI-Si and SBR-Si electrodes were 2153.6 and 1888.1 mAh g^{-1}, respectively; the initial cycle efficiency of PI-Si electrode (78.12%) is

significantly higher than that of SBR-Si electrode (65.75%).

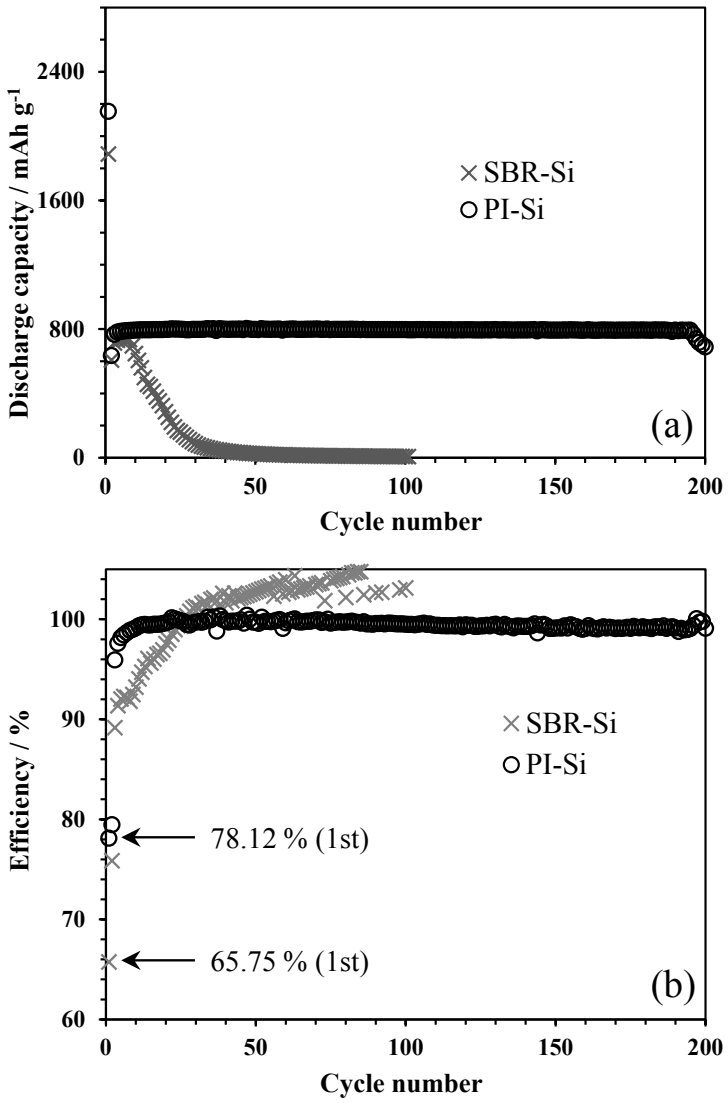

Fig. II-1-3-3 (a) Cycle performances and (b) cycle efficiencies of the cells including PI-Si and SBR-Si electrodes with the charge capacity is limited to 800 mAh g^{-1} (after the 2nd cycle).

After the 2nd cycles of which charge capacity is limited to 800 mAh g^{-1}, the polarization of SBR-Si electrode between charge and discharge continues to increase

with the increase of cycles, while the polarization of PI-Si electrode almost not increase and charge and discharge curves continue to follow almost same trajectory after 30th cycle. Fig. II-1-3-3 shows (a) the cycle performances and (b) the cycle efficiencies of the cells including PI-Si and SBR-Si electrodes with the charge capacity is limited to 800 mAh g^{-1} (after the 2nd cycle). The discharge capacity of SBR-Si significantly reduces predictably and maintains discharge capacity of 800 mAh g^{-1} during only a few cycles, while the cycle stability of PI-Si electrode is excellent and can maintain discharge capacity of 800 mAh g^{-1} during 195 cycles. In addition, the cycle efficiency of PI-Si electrode has maintained always high value and the average cycle efficiency between 11th to 190th cycles is 99.49%. These results mean that the phenomenon which the electronic contacts between the Si particles are lost with the pulverization of Si due to repetition of expansion and contraction of Si particles is less likely to occur.

Fig. II-1-3-4 shows the surface morphology of the PI-Si and SBR-Si electrodes (a) before cycle and (b) after 10 cycles. Before cycle, there is no difference except that the PI-Si electrode seems to be covered in polymer slightly rather than SBR-Si electrode. However, the surface of the PI-Si and SBR-Si electrodes were changed to a completely different form after 10 cycles. Many interspaces are confirmed between the Si particles and the electronic contacts between Si particles are clearly lost. The pulverization of Si particles does not so much occur in the SBR-Si electrode because the Si particles which lost electronic contacts cannot alloy with Li and its utilization is significantly reduced. On the other hand, the pulverization of the Si particles occurs in the PI-Si electrode surface. However, the interspaces between pulverized Si particles are not confirmed and large cracks are clearly observed. The portions surrounded by these large cracks become the shape of like-island, and pulverized Si particles on the island are in close contact with each other. Therefore, it seems that the electronic contact between the Si particles on the same island is sufficiently maintained. Judging from active material density of the PI-Si and SBR-Si before cycle are approximately the same, the difference of electrodes structure after charge and discharge between PI-Si and SBR-Si electrodes as mentioned above was caused by difference in the properties of binders. The PI binder is very hard polymer and has strong adhesion. Even if the curing tape is stuck and peeled off from the surface of the PI-Si electrode, the active material layer does not peeled off

completely. We consider that strong adhesion of PI binder suppress the collapse of the electrode structure.

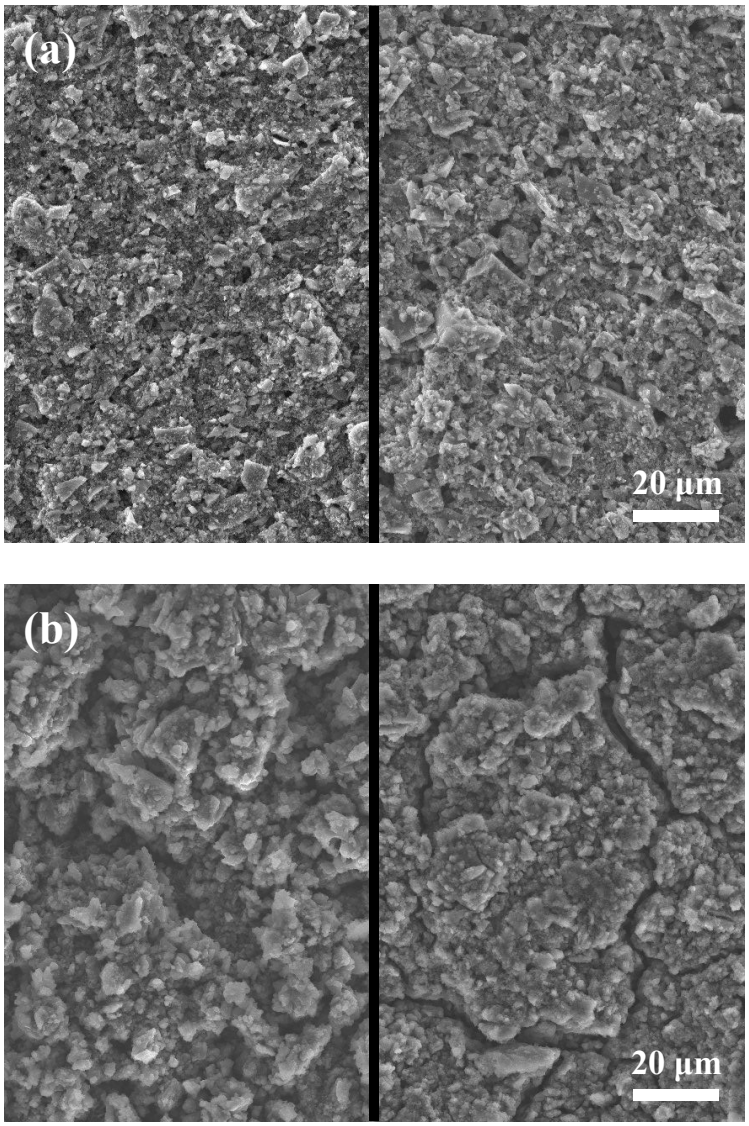

Fig. II-1-3-4 Surface morphology of the PI-Si and SBR-Si electrodes (a) before cycle and (b) after 10 cycles. Left image is SBR-Si electrode. Right image is PI-Si electrode.

The PI-Si electrode prepared in this study contains 15 wt.% of PI binder to suppress the collapse of the electrode structure which is a relatively large amount. It is possible that a large amount of binder adversely affect the charge and discharge at high

current density. We investigate the cycle performance of the PI-Si electrode at high current density Fig. II-1-3-5 shows (a) the cycle performances and (b) the cycle efficiencies of the cells PI-Si electrodes at current density of 1600 mA g^{-1} with the charge capacity is limited to 800 mAh g^{-1} (after the 2nd cycle). The electrode composed of μm-Si, AB and PI in a respective weight ratio of 80:5:15 (Electrode A) can maintain

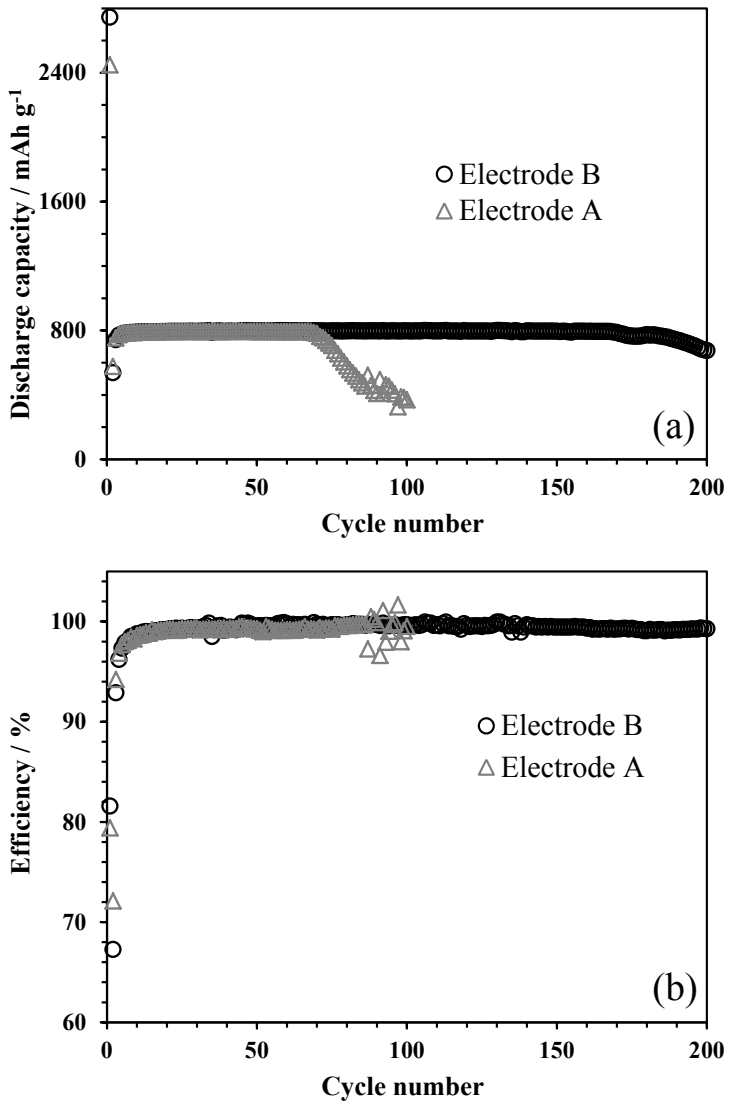

Fig. II-1-3-5 (a) Cycle performances and (b) cycle efficiencies of the cells PI-Si electrodes at current density of 1600 mA g^{-1} with the charge capacity is limited to 800 mAh g^{-1} (after the 2nd cycle).

the discharge capacity of 800 mAh g^{-1} during only 68 cycles and the average cycle efficiency of Electrode A between 11th to 60th cycles (99.19%) slightly reduces compared to that at the current density of 800 mA g^{-1}. We consider that the causes of degradation of the electrodes at high current density are inhomogeneous expansion and contraction of Si particles due to insufficient electric conductivity in the electrode or hindrance of Li ion access to Si particles by large amount of PI binder. If the former is the cause, the percentage of AB in the electrode composition should be increased and if the latter is the cause, the percentage of PI in the electrode composition should be decreased because large amount of PI inhibits the Li ion access to Si particles. Thus, we have prepared the electrode composed of μm-Si, AB and PI in a respective weight ratio of 75:10:15 (Electrode B) and investigate its cycle performance. The Electrode B can maintain the discharge capacity of 800 mAh g^{-1} during 167 cycles at the current density of 1600 mA g^{-1} as long as the cycle performances test at current density of 800 mA g^{-1} and shows the high average cycle efficiency (99.52%) between 11th to 165th cycles. Judging from the fact that the cycle stability in the high current density is improved by using Electrode B containing large amount (10 wt.%) of AB, the cause of degradation of the electrodes at high current density is lack of electric conductivity. Therefore, it seems that the PI binder does not hinder Li ion access to Si particles.

It is considered that smooth Li ion supply to Si particles is also effective to improve the cycle stability of PI-Si electrode because we believe that homogeneous expansion and contraction of Si particles by providing sufficient electric conductivity attribute to suppress of the collapse and improve the cycle stability of the PI-Si electrode. Thus, we have applied highly porous polyolefin film coated with ceramic as separator for smooth Li ion supply from the bulk electrolyte. Fig. II-1-3-6 shows (a) initial charge and discharge curves at low current density (200 mA g^{-1}) without limitation of charging capacity and (b) cycle performances of the cells including Electrode B and highly porous polyolefin separator coated with ceramic at current density of 800 and 1200 mA g^{-1} with charge capacity is limited to 800 and 1200 mAh g^{-1} (after the 2nd cycle), respectively. At the initial cycle without limitation of charge capacity, the cell including Electrode B and highly porous separator shows the charge capacity of 4002 mAh g^{-1} close to the theoretical capacity of Si which significantly

increase compared to that of the cell including conventional separator and its discharge capacity also increases with the charge capacity (3139 mAh g^{-1}) and the initial cycle efficiency is 78.44% which does not decrease despite the increase in the utilization of Si

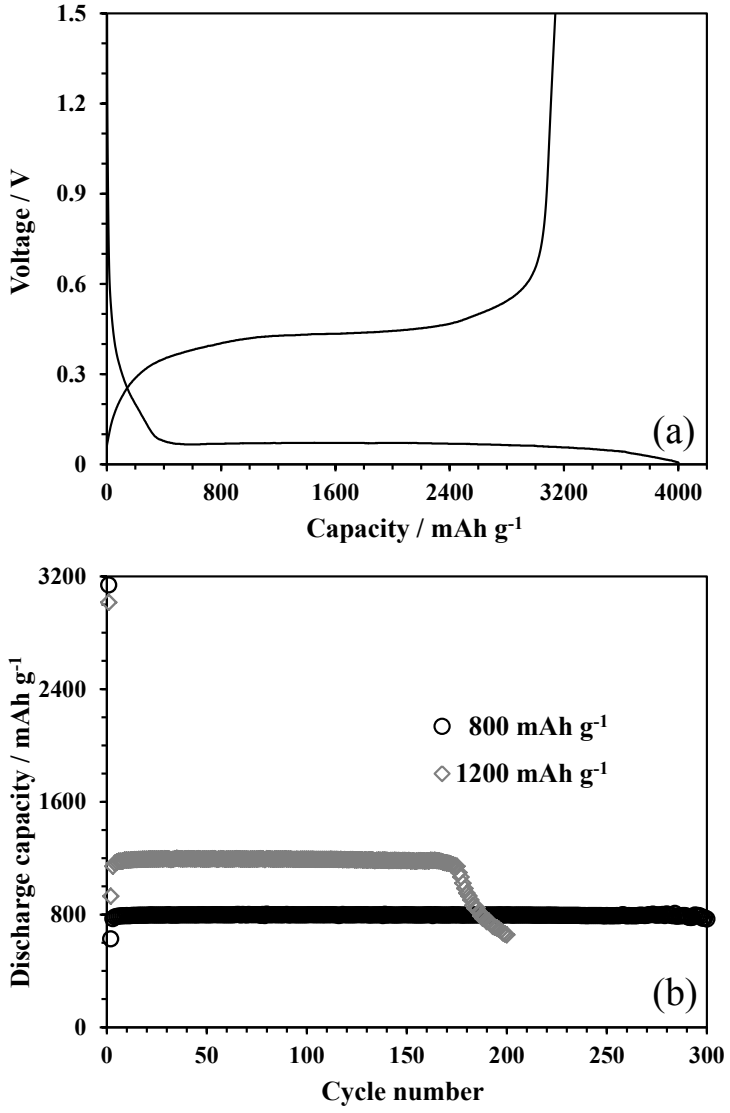

Fig. II-1-3-6 (a) Initial charge and discharge curves at low current density (200 mA g^{-1}) without limitation of charging capacity and (b) cycle performances of the cells including Electrode B and highly porous polyolefin separator coated with ceramic at current density of 800 and 1200 mA g^{-1} with charge capacity is limited to 800 and 1200 mAh g^{-1} (after the 2nd cycle), respectively.

particles. In addition, the cells including Electrode B and highly porous separator shows significantly improved cycle stability compared to that of the cell including conventional separator and maintain the discharge capacity of 800 and 1200 mAh g^{-1} during 300 cycles and 166 cycles, respectively. The separators do not directly contribute to the charge and discharge reaction and role of separator is insulation between positive electrode and negative electrode. However, the above results show that the different types of separators evidently affect cycle stability and utilization of Si particles at least in the case of using μm-Si, which seem to depend on Li ion conductivity of separators derived from its porosity and materials.

II-1-4. Conclusions

We applied the PI as a binder in order to suppress the collapse of electrode structure and improvement of cycle stability of Si negative electrode composed of untreated, conventional Si particles (μm-Si). The PI-Si electrode maintained the discharge capacity of 800 mAh g^{-1} during 196 cycles at the current density of 800 mA g^{-1}. We concerned over the possibility that comparatively large amount of PI binder (15 wt.%) included in our electrodes prevents Li ion access to Si particles and adversely affect the cycle stability of PI-Si electrode at high rate. However, the PI-Si electrode including 10 wt.% of AB (Electrode B) maintained the discharge capacity of 800 mAh g^{-1} during 167 cycles at the current density of 1600 mA g^{-1} and it was found that the cause of degradation of the electrodes at high current density is lack of electric conductivity and the PI binder does not hinder Li ion access to Si particles. The Li ion supply from bulk electrolyte also affected the cycle stability of PI-Si electrode as well as electric conductivity, the cells including highly porous separator maintain the discharge capacity of 800 and 1200 mAh g^{-1} during 300 cycles and 166 cycles, respectively.

We succeeded in improving the cycle stability of Si electrode without use of nano-Si by using PI as a binder and found that the porosity and material selections of separator determine the Li ion conductivity is very important. It is quite interesting that the battery components which do not directly involved in the charge and discharge reactions such as binders and separators significantly affect the battery performances of Si negative electrode. We believe that the effective use of these components can greatly

contribute to the practical application of Si negative electrodes.

II-1-5. References

[1] E. Karden, S. Ploumen, B. Fricke, T. Miller, K. Snyder, J. Power Sources, 168 (2007) 2.

[2] M. Winter, J. O. Besenhard, M. E. Spahr, P. Novak, Adv. Mater. 10 (1998) 725.

[3] D. Aurbach, B. Markovsky, I. Weissman, E. Levi, Y. Ein-Eli, Electrochimica Acta 45 (1999) 67.

[4] R. A. Huggins, J. Power Sources 81-82 (1999) 13.

[5] B. A. Boukamp, G. C. Lesh, R. A. Huggins, J. Electrochem. Soc., 128 (1981) 725.

[6] L. Y. Beaulieu, K. W. Eberman, R. L. Turner, L. J. Krause, J. R. Dahn, Solid-State Lett. 4 (2001) A134.

[7] Y. Oumellal, N. Delpuech, D. Mazouzi, N. Dupre, J. Gaubicher, P. Moreau, P. Soudan, B. Lestriez, D. Guyomard, J. Mater. Chem. 21 (2011) 6201.

[8] J. H. Ryu, J. W. Kim, Y. E. Sung, S. M. Oh, Solid-State Lett. 7 (2004) A306.

[9] S. Pal, S. Damle, S. Patel, M. K. Dutta, P. N. Kumta, S. Maiti, ECS Trans. 41 (2012) 87.

[10] H. Kim, M. Seo, M. H. Park, J. Cho, Angew. Chem. Int. Ed. 49 (2010) 2146.

[11] C. K. Chan, H. Peng, G. Liu, K. Mcilwrath, X. F. Zhang, R. A. Huggins, Y. Cui, Nat. Nanotech. 3 (2008) 31.

[12] L. F. Cui, Y. Yang, C. M. Hsu, Y. Cui, Nano Lett. 9 (2009) 3370.

[13] C. K. Chan, R. Ruffo, S. S. Hong, R. A. Huggins, Yi Cui, J. Power Sources 189 (2009) 34.

[14] S. Komaba, K. Shimomura, N. Yabuuchi, T. Ozeki, H. Yui, K. Konno, J. Phys. Chem. C 115 (2011) 13487.

[15] I. Kovalenko, B. Zdyrko, A. Magasinski, B. Hertzberg, Z. Milicev, R. Burtovyy, I. Luzinov, G. Yushin, Science 334 (2011) 75.

Section II-2

Effect of Electrolyte Additives on Silicon Negative Electrode Prepared with Polyimide Binder

II-2-1. Introduction

High energy density Li-ion batteries (LIBs) are very attractive in various fields, and its applications continue to expand even now. The electric vehicles and large storage systems for renewable power require high performance LIBs with further high power, high energy density, and more safety. In addition, the rapid development of mobile electronic devices such as smart phone, tablet and slim laptop in recent years significantly increases their power consumption, and requires a more high capacity LIBs again.

The energy density of LIBs has been greatly improved so far due to improvement of electrode density or filling method of each component to the package. However, the electrode active materials have not been almost changed from the beginning of development of LIBs; $LiCoO_2$ [1] and $LiMn_2O_4$ [2] are used as positive electrode and graphite [3] is used as negative electrode. To meet the demands of further improving energy density, LIBs should become high capacity based on active materials. It is difficult to significantly increase the weight normalized specific capacity of positive electrode materials because heavy transition metals which are required to obtain a high redox potential are contained in them [1, 2, 4-6]. On the other hand, there is a feasibility of high capacity negative electrode since the candidate for new anode materials often contain light elements as with graphite. Silicon (Si) has quite high theoretical Li storage capacity (4200 mAh g^{-1}) among them which ten times higher than that of graphite (372 mAh g^{-1}) and a relatively low average potential for alloying/de-alloying with Li ion (0.4 V vs. Li/Li^+) [7]. Therefore Si has attracted much attention as next-generation negative electrode material.

The largest problem in the case of using Si as negative electrode for LIBs is collapse of the electrode structure which occurs with large volume change [8] during alloying/de-alloying with Li. The collapse of the electrode structure leads directly to the

loss of electronic contacts, causing a rapid capacity loss with cycles [9-11]. The application of nano-scale Si [12] has been reported as an extremely effective method to solve this problem. The Si nano-wire [13] electrode relaxes the stress due to the volume expansion, which can prevent the collapse of electrode structure. In addition, the efficient electron conductivity is ensured in vertical direction. The Si nano-particles and carbon composite also suppresses the loss of electric conductivity of the electrodes since the stress is relaxed and electric conductivity is enhanced by using Si nano-particles and carbon, respectively [14, 15]. However, the preparation of nano-scale Si requires quite complex method and large amount synthesis of nano-scale Si in practically usable cost is extremely difficult. Thus, the cycle degradation of Si negative electrode should be suppressed by improving other electrode component except active material (Si).

Previously, we reported that the cycle stability of Si electrode composed of μm-ordered Si (μm-Si) particles is drastically improved by using polyimide (PI) as binder [16]. The PI binder suppressed the collapse of electrode structure and the discharge capacity of μm-Si electrode prepared with PI binder was maintained during 300 cycles under the condition that the charge capacity is limited to 800 mAh g^{-1}. However, the pulverizations of Si particles themselves due to the stress caused by volume change, which is another cause of capacity degradation, were not prevented. The surface area of the Si particles increases significantly by pulverization, which leads excessive electrolyte decomposition [17]. As a result, the solid-electrolyte interface (SEI) amount and thickness increase and the resistance of electrode significantly also increase [18]. Since it is considered to be fundamentally impossible to suppress the pulverization of Si particles in the case of using large size Si particles such as μm-Si, the application of electrolyte additives to form effective SEI to suppress decomposition of electrolyte is necessary. In this work, we investigate the effect of electrolyte additives to the μm-Si electrode prepared with PI binder and an effective electrolyte additive is applied to μm-Si and Soft carbon (SC) composite electrode prepared with PI binder. In addition, we try to further improve the cycle stability of Si-SC electrode by optimizing the amount of electrolyte additive.

II-2-2. Experimental

The μm-Si electrode with polyimide (PI-Si electrode) was prepared in dry room with dew point of -55°C. The untreated μm-Si was mixed with acetylene black (AB, Denki kagaku kogyo Co., HS-100) and polyamic acid as a precursor of PI in a respective weight ratio 75:10:15 with an adequate amount of *N*-methyl-2-pyrrolidone (NMP, Kishida Chemical Co., 99.5%) solvent and the obtained slurry was cast onto an Cu-foil current collector and dried at 80°C for 2 h in a vacuum oven to remove NMP. In order to vary the polyamic acid to polyimide via dehydration condensation, the temperature of oven was elevated to 300°C and held for 10 min. After cooling to room temperature, the prepared electrode sheets were cut into disks with a diameter of 12 mm for electrochemical measurement. The μm-Si and SC composite electrode prepared with PI binder (PI-Si-SC electrode) was also prepared in the same procedure. The μm-Si, AB, SC and polyamic acid were mixed with a respective weight ratio 50:25:10:15. The mass loading of active materials (Si or Si + SC) in electrodes were approximately 2.0 mg cm^{-2}. The positive electrode for full-cell test is prepared from $LiNi_{1/3}Mn_{1/3}Co_{1/3}O_2$, AB, and polyvinylidene fluoride (Kureha Co., #1100) with a respective weight ratio of 85:8:7.

The test cells for electrochemical measurements were assembled in an argon-filled globe box using a two electrode type cell (Hosen Co.). The negative half-cells were assembled with the prepared PI-Si or PI-Si-SC electrodes, a Li foil (Honjo Metal Co.) disk with a diameter of 13 mm, 1 mol dm^{-3} $LiPF_6$ in a 1:1 v/v mixture of ethylene carbonate (EC) and dimethyl carbonate (DMC)(Kishida Chemical Co., LBG) without additive and with 3 wt.% of vinylene carbonate (VC, Kishida Chemical Co., LBG) or 3-10 wt.% of fluoro ethylene carbonate (FEC, Kishida Chemical Co., LBG), and highly porous polyolefin film coated with ceramic as a separator.

The charge and discharge cycle performance tests were carried out using a galvanostatic charge and discharge unit (Intex Co., BTS2004W). In this paper, the alloying process of Si and Li (i.e. the direction in which the voltage is narrowed) is referred to as “Charge”, and de-alloying process (i.e. the direction in which the voltage is broaden) is referred to as “Discharge”. Although the cycle performances tests were

carried out under the condition that the charge capacity is limited in our previous report, the charge capacity was not limited in this paper because it is extremely difficult to limit the only charge capacity of negative electrode in full-cell. The negative electrode half-cell was measured in the voltage range of 1.500 – 0.005 V. The charging process proceeded to 0.005 V with constant current (C.C) mode, and then proceeded with constant voltage (C.V) mode at 0.005 V until the current density decreases to 1/10. The discharging process proceeded to 1.500 V with C.C mode. The current densities of initial cycle and after second cycles were 0.2 A g^{-1} and 2.0 – 16.0 A g^{-1}, respectively. The full-cell was measured in the voltage range of 4.200 – 3.000 V and the other conditions are same as that of the half-cell.

The alternative current (AC) impedance spectra measured by using frequency response analyzer (Solartron analytical, 1255B). The cells were cycled until a predetermined cycle and their voltages were relaxed for 10 h at open circuit condition for measurement in steady state. All measurements were carried out in discharge state and measurement frequency range was 100 kHz – 10 mHz.

The surface morphologies of the Si electrodes were observed using scanning electron microscope (SEM, Hitachi Co., SU-1500). The test cells were disassembled in argon-filled globe box after relaxing the cell voltage for 10 h at discharge state of 1st or 10th cycle. The electrodes taken out from the cells were washed carefully in DMC and dried for 12 h in a vacuum state. The dried electrodes were stored in a sealed vial and air exposure was avoided as much as possible to prevent the transformation of electrode surface morphology by oxidation until just before the observation to prevent the transformation of electrode surface morphology.

The chemical composition of the SEI on the electrode surface was analyzed using X-ray photoelectron spectroscopy (XPS, JEOL Ltd., JPS-9010MC) with Mg Kα radiation. The electrodes were removed from the test cells by the same procedure as SEM observation after 10th cycle. The dried electrodes were transferred from glove box into vacuum chamber of XPS apparatus in argon atmosphere using transfer vessel to completely avoid the change in the chemical composition of the SEI. The spectra derived from F 1s (676 – 696 eV), C 1s (274 – 294 eV) and O 1s (522 – 542 eV) were measured in the depth direction using argon etching treatment.

II-2-3. Results and discussion

Fig. II-2-3-1 shows (a) the cycle performances and (b) the cycle efficiencies of PI-Si electrode half-cells containing the electrolytes without additive and with 3wt.% VC or 3wt.% FEC cycled at a current density of 1.0 A g^{-1}. Although the PI-Si electrode shows the relatively good cycle stability even without additive because the collapse of the electrode structure is suppressed by polyimide binder, the addition of VC or FEC

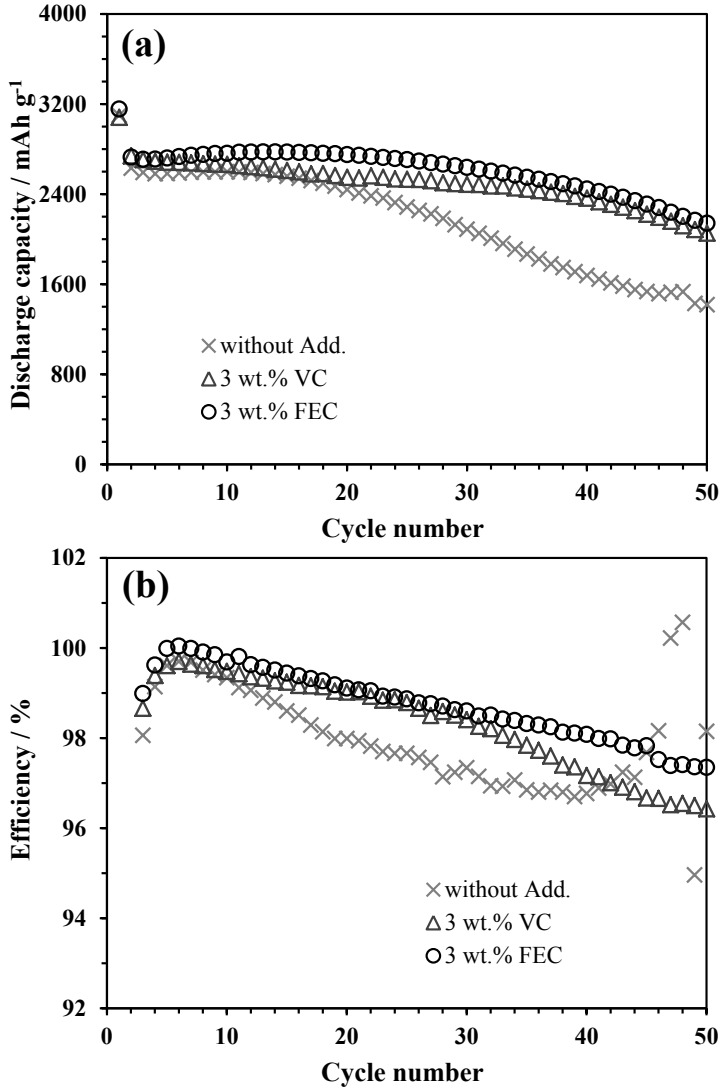

Fig. II-2-3-1 Discharge capacity (a) and cycle efficiency (b) vs. cycle number of PI-Si electrode half-cells including the various electrolytes cycled at a current density of 1.0 A g^{-1}.

further improves the cycle stability of PI-Si electrode. Presence or absence of additives especially affects cycle efficiency. The cycle efficiency of the cell without additive is lower than that with additives even in early cycles, and begins to decrease rapidly around 10th cycle. In addition, the cycle efficiency of the cell with VC also begins to decrease rapidly from around 35th cycle in contrast to that with FEC which is always highest among three cells.

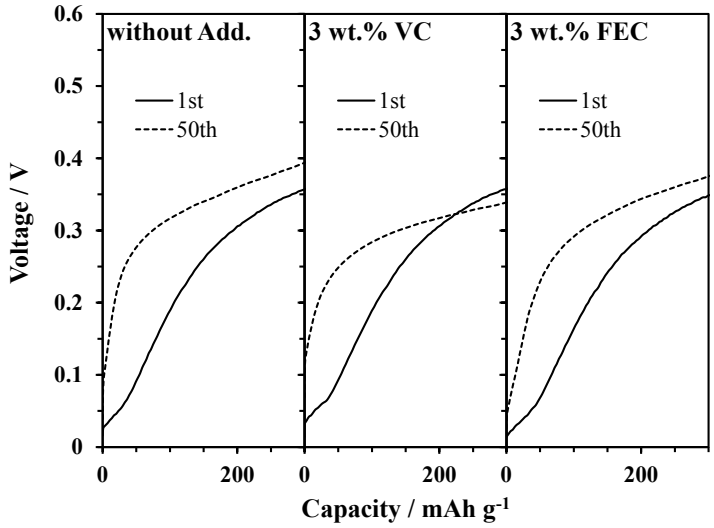

Fig. II-2-3-2 Forepart of the discharge curves of PI-Si electrode half-cells including various electrolytes of 1st and 50th cycles correspond to cycle performance test.

Fig. II-2-3-2 shows the forepart of the discharge curves at 1st and 50th cycles of respective cells. At the beginning of discharge, the discharge curves pursue vertically from 0.005 V, and then begin to incline. The crystalline and amorphous phases coexist in the lithiated Si and their discharge potential is different for each phase [19]. Therefore we cannot discuss the cell resistance unconditionally by using overall degree of polarization between charge and discharge. However, the rising of the voltage that the discharge curves begin to incline (referred to as discharge initiation voltage) reflect the increase in cell resistance. The discharge initiation voltage rises considerably after 50 cycles in the cells without additive and with VC, while the discharge it of the cell with

FEC does not much rise. The increasing the resistance of the cell containing the FEC seems to be significantly smaller compared with other cells. The increase in resistance of the cells relate to cycle efficiency, which seem to derive from the difference in the behavior of electrolyte decomposition brought by the electrolyte compositions.

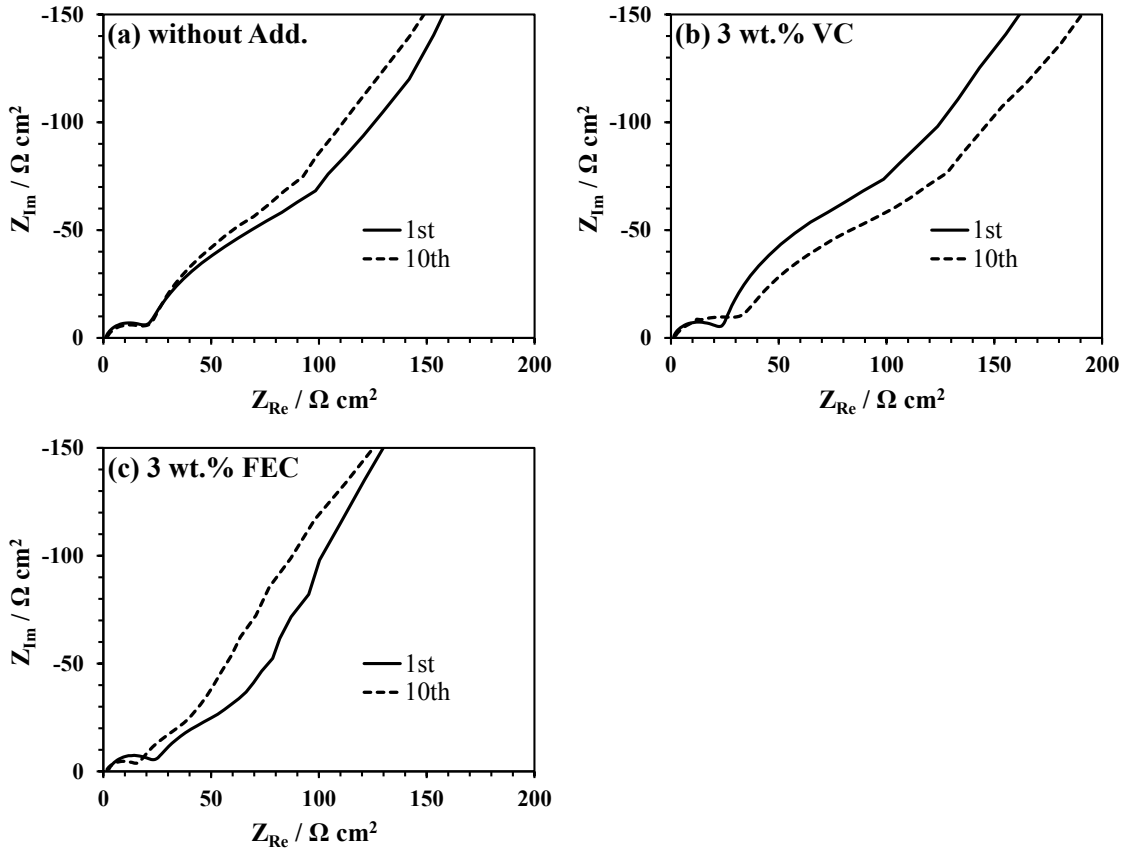

Fig. II-2-3-3 Nyquist plots of PI-Si electrode half-cells including various electrolytes measured at discharge state of 1st and 10th cycles.

In order to identify the origin of the increased cell resistance in detail, we measured the AC impedance of PI-Si electrode half-cells with each electrolyte. Another cells with same configuration as the cells used in cycle performance test were assembled for AC impedance measurement. Fig. II-2-3-3 shows the nyquist plot at discharge state of 1st and 10th cycles. Two semicircles are mainly observed in all the

plots. We consider that the semicircle observed in higher frequency region (left side) includes the resistance of SEI and that in lower frequency region (right side) includes charge transfer resistance. At a discharge state in the 1st cycle, the semicircle in higher frequency region is almost same magnitude in any electrolytes and the semicircle in lower frequency region of the cell containing FEC is clearly smaller than other cells. After 10 cycles, the magnitudes of the semicircle in higher frequency does not change, increase and decrease in the electrolyte without additive, with 3 wt.% VC and with 3 wt.% FEC, respectively. On the other hand, the semicircle in lower frequency becomes larger in the electrolyte without additive and with 3 wt.% VC, but it almost does not change in the electrolyte with FEC. The difference of semicircles observed in lower frequency including charge transfer resistance will be discussed later together with SEM images of PI-Si electrode after charge and discharge, and here we discuss only the difference of semicircle observed in higher frequency region derived from the SEI. The changes of resistance derived from SEI suggest that the amount and thickness of SEI which formed by VC increase, while it formed by FEC deforms into lower resistance form or reduces (this possibility is unlikely) during 10 cycles. From this result, the difference in the degree of rising of discharge initiation voltage seems to be brought down by increasing of SEI amount. Although the resistance derived from SEI in the electrolyte without additive does not change after 10 cycles, it should have been increase if the AC impedance is measured after 50 cycles because the discharge initiation voltage of the cell without additive rises after 50 cycles. Before the measurement, we considered the possibility that the cycle number of the cells is too less as a condition of the AC impedance measurement. Nevertheless, we did not select “after 10th cycle” as a condition of the AC impedance measurement, because distinction of semicircles becomes difficult with increasing cycle number due to degradation of the PI-Si electrode and a Li counter electrode. From these results, it is found that the additives are very effective to improve the cycle stability of the PI-Si electrode and increase in the resistance of SEI formed by FEC is the smallest. However, this result can be discussed only in a continuous cycle test. The commercial Li-ion batteries are often stored at charge state for a long time. In other words, the negative electrodes are always exposed to a lower potential where the electrolyte decomposition easily occur.

Therefore, it should be also investigated that the increase in resistance derived from SEI when PI-Si electrode half-cell stored at charge state. Fig. II-2-3-4 shows the comparison of nyqist plots after discharge at 1st cycle with storage at charge state for 10 hours and without storage. The cells are stored in the open circuit of which voltage is 50-70 mV. The resistance in higher frequency region derived from SEI increases after storage at charge state in the electrolyte without additive and with VC, while it does not increases in the electrolyte with FEC. There is no difference in the degree of pulverization of the Si particles in each cell because charge capacities of each cell are almost same value and Si particle should not expand any more during storage.

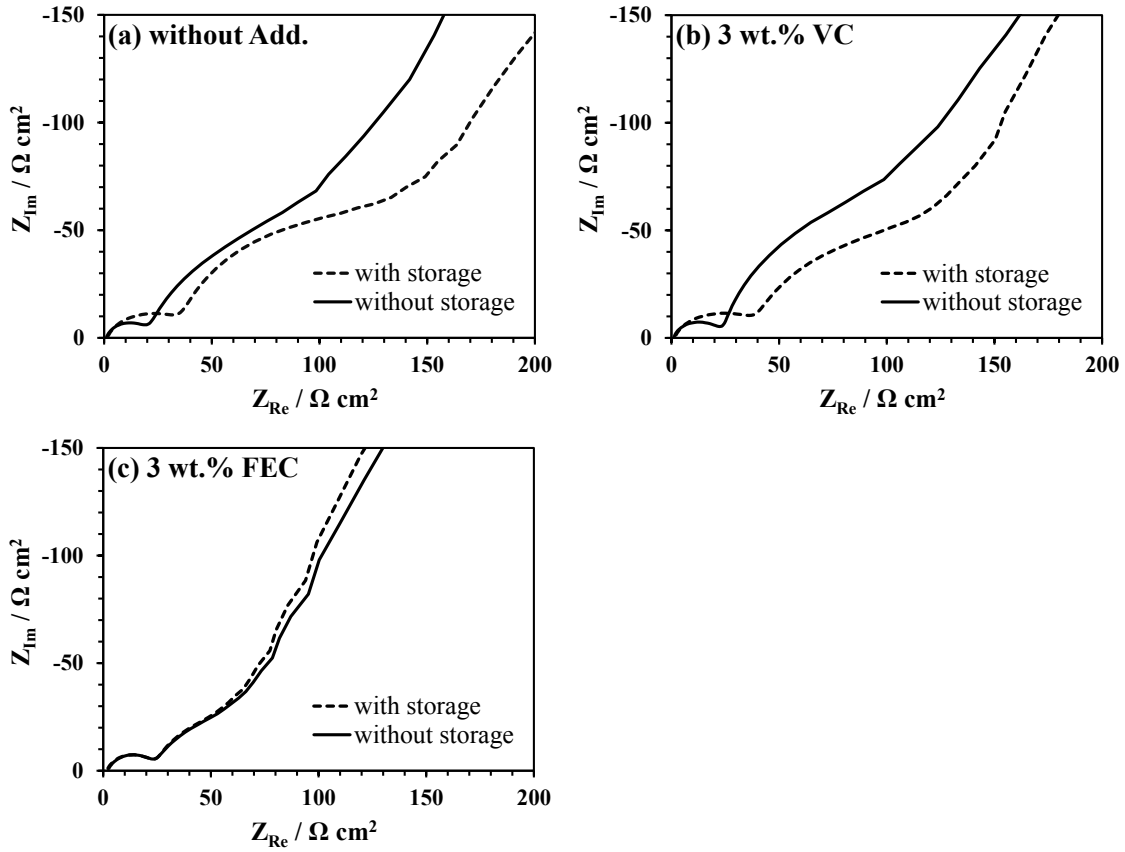

Fig. II-2-3-4 Nyquist plots of PI-Si electrode half-cells including various electrolytes measured at discharge state of 1st cycle with storage at charge state for 10 h and without storage.

This result suggested that further SEI formation progresses in the electrolyte even in situations where pulverization of Si particles does not occur. Thus, we consider that the SEI formed in the electrolyte with VC and without additive does not have much an effect enough to suppress the further SEI formation (i.e., excessive decomposition of the electrolyte). From the results so far, the use of electrolyte additives which affect the SEI formation are very effective to improve the cycle stability of PI-Si electrode and the electrolyte containing FEC has most excellent effect to suppress the decomposition of the electrolyte judging from the change of the magnitude of the semicircle in higher frequency region of AC impedance measurement.

Next, we observed the surface of PI-Si electrodes after discharge to discuss the collapse mechanism of PI-Si electrode. Fig. II-2-3-5 shows the SEM images of the PI-Si electrodes after 1st and 10th cycles. The very wide cracks have already occurred in all PI-Si electrodes after 1st cycle and the portions surrounded by these wide cracks become the shape like islands but the electronic contacts of PI-Si electrodes are maintained because the pulverized Si particles on the island are in close contact each other by extremely strong adhesion of PI binder. Such crack pattern is specific to the PI-Si electrode among composite electrodes containing conductive additive and binder though it often occurs in Si thin film electrode [20]. We consider that the PI-Si electrodes spontaneously clack into like islands by fracture of PI in the early stages of the discharging because the fracture elongation of PI is quite small. When the cracks like islands occur, the tensile stress applies very little to inside of islands and the further collapse of the Si electrode is suppressed as a result. Although there are the reports that the elastic binders are effective to improve cycle stability [21], Li et al. [22] reported that stiff and brittle binder is more effective to improve the cycle stability in Si electrode using commercially available Si particles (-325 mesh). We believe that the collapse mechanism of their electrode similar to our electrode. However, it is notable that the cracks width of the PI-Si electrode in the electrolyte with FEC (Fig. II-2-3-5 (e)) is obviously wide compared with other PI-Si electrode in the electrolyte with VC or without additive (Fig. II-2-3-5 (c) and (a)). The PI-Si electrodes should expand and contract to the same extent in all cells since the charge and discharge capacities are almost same value regardless of electrolyte composition. Nevertheless, the cracks width

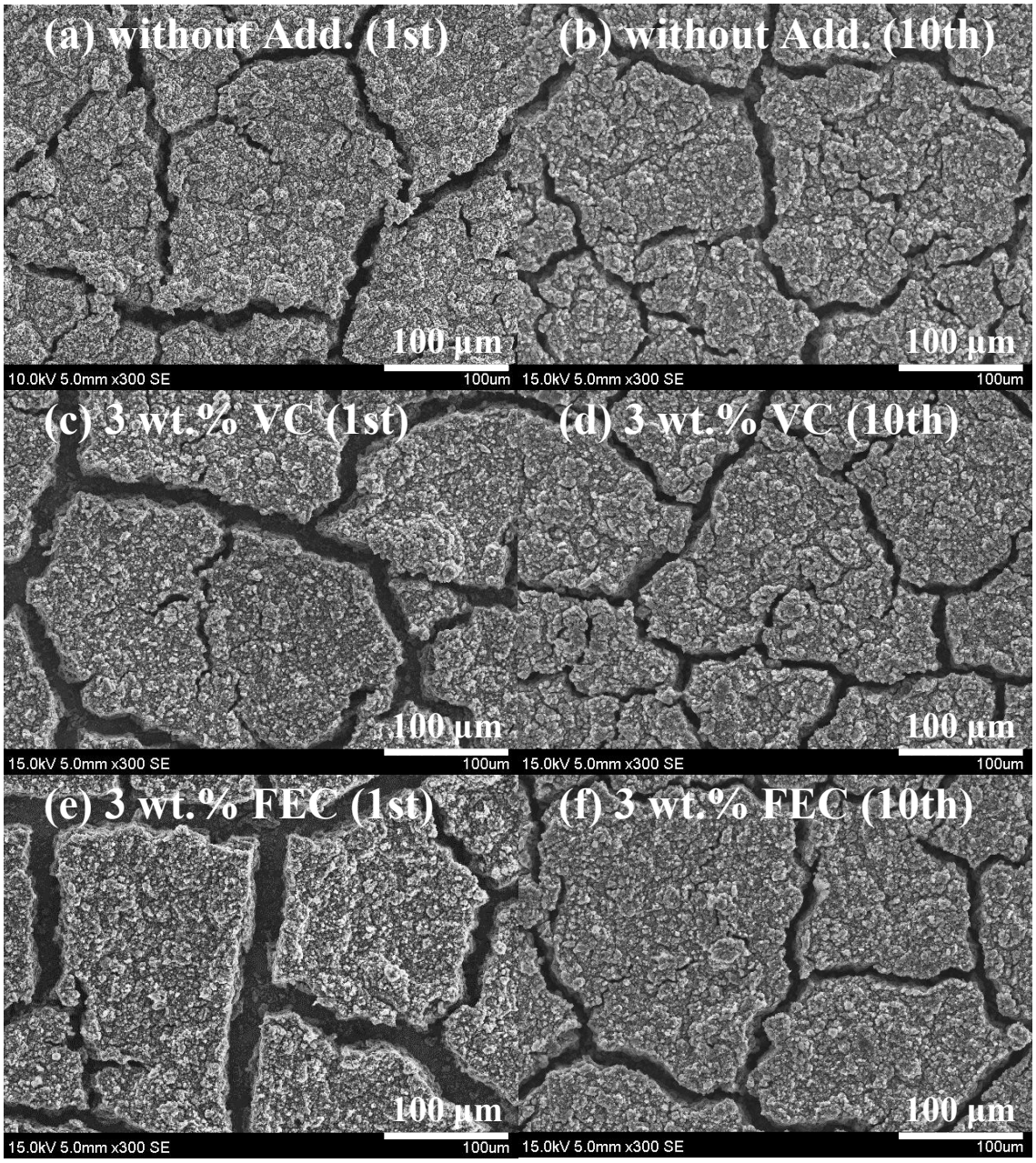

Fig. II-2-3-5 SEM images of PI-Si electrode cycled in electrolyte without additive (a, b) and with 3wt.% VC (c, d) and FEC (e, f) observed at discharge state of 1st (left) and 10th cycles (right).

is different, which indicates the difference in the density of islands. We consider that the islands formed in the electrolyte with VC or without additive include relatively large amount of SEI which exists around pulverized Si particles and inflates the islands. Since large amount of SEI prevents contact between pulverized Si particles on the islands and

electric conductivity of PI-Si electrode seems to decline, our opinion described above well corresponds to the magnitude of the semicircles in lower frequency region of respective cells observed in Fig. II-2-3-3 (or Fig. II-2-3-4). After 10 cycles, the shape of the islands is slightly crumbling in the electrolyte with VC or without additive (Fig. II-2-3-5 (d) and (b)). In contrast, the islands maintain the original shape (Fig. II-2-3-5 (f)) though the difference of the cracks width is lost by repeated expansion and contraction. This result also corresponds to the change of the magnitude of the semicircles in lower frequency region after 10 cycles observed in Fig. II-2-3-3. The effect of electrolyte additives significantly affect the collapse mechanism (as it were electric conductivity) of Si electrode as much as the formation of SEI. Therefore, the select of the electrolyte additives is important as well as select of binder for Si electrode composed of μm-Si.

The reasons which the composition of electrolytes significantly affects the cycle stability of PI-Si electrode is that the chemical compositions of the SEI formed in the respective electrolytes are different. Therefore, elemental analysis of the electrode surface is needed in order to discuss the effect of electrolyte additives. Fig. II-2-3-6 shows the XPS spectra related to F 1s, C 1s and O 1s of PI-Si electrodes surface after 10 cycles. The numbers which shown on the right side of the Fig. II-2-3-6 (a) is the total time (seconds) of Ar etching process and the spectrum shown in more upper part indicates the information of deeper position, which is the same in other figure. The spectra observed in this study are slightly affected by charge-up. Thus, the assigned component and peak position may be slightly different from other literature values. Comparing the Fig. II-2-3-6 (a) and (b), large amount of LiF existed on the surface of PI-Si electrode cycled in the electrolyte with FEC. The advantage of using the FEC as electrolyte additive has been reported that the SEI formed by FEC contains a relatively large amount LiF and its resistance is fairly small [23]. The effective component in our electrodes seems to be same as the component in the previous reports. On the other hand, the peaks assigned to C-O and C=O derived are observed in the spectra related to C 1s (Fig. II-2-3-6 (c) and (d)) and O 1s (Fig. II-2-3-6 (e) and (f)). These peak indicate the existence organic component formed by decomposition of electrolyte and its intensity on surface of PI-Si electrode cycled in the electrolyte with VC is larger.

Therefore, the VC forms the SEI mainly composed of organic components which seems to not have much an effect to suppress the excessive decomposition of the electrolyte and lead to increase in resistance.

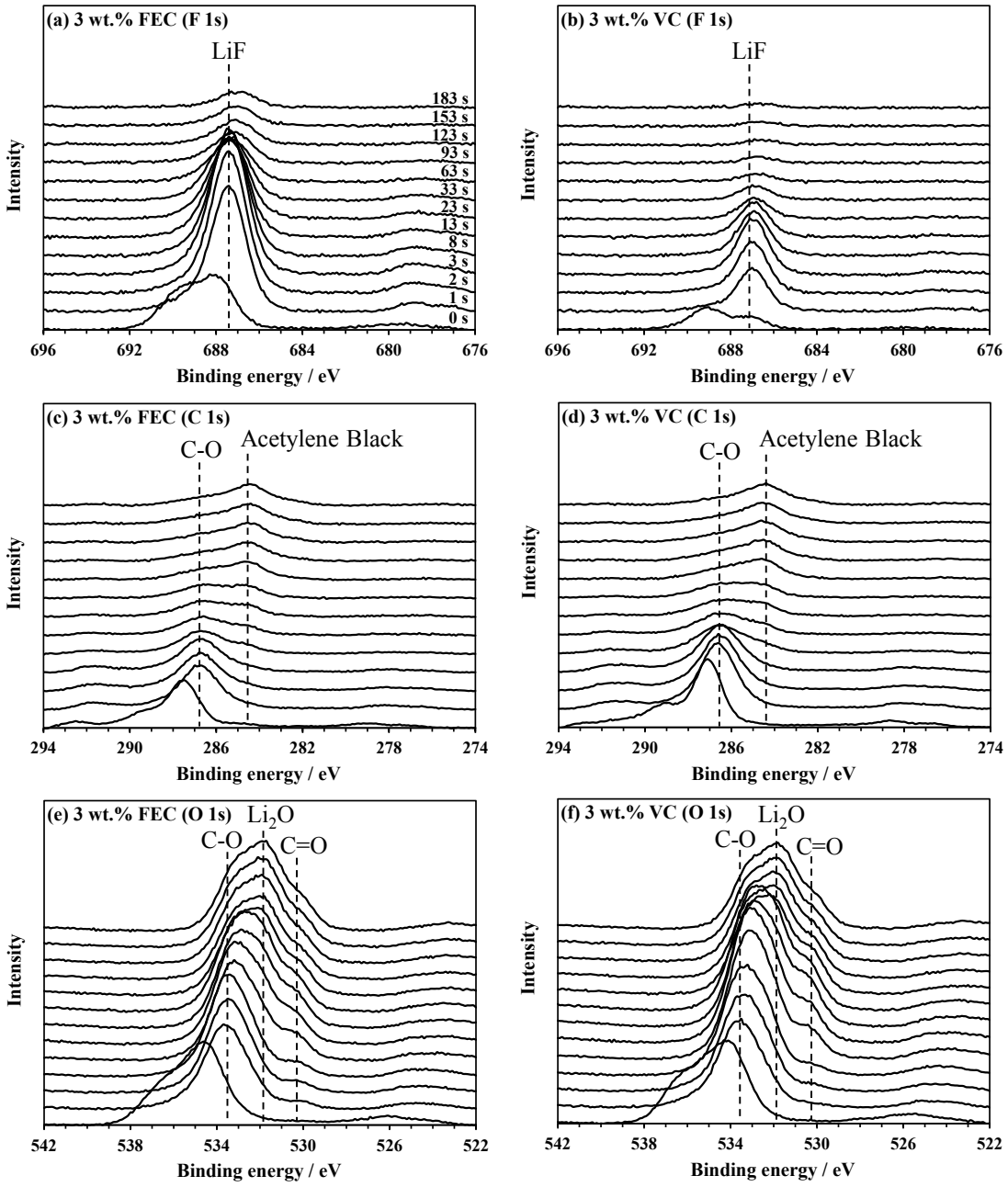

Fig. II-2-3-6 XPS spectra related to F 1s (a, b), C 1s (c, d) and O 1s (e, f) obtained from the surface of PI-Si electrode cycled in the electrolyte containing 3wt.% VC (right) and FEC (left).

The validation results from various angles, we concluded that the FEC is more suitable than VC as an electrolyte additive for PI-Si electrode and applied FEC to the PI-Si-SC electrode in order to further improve cell performances. Fig. II-2-3-7 shows (a) the discharge capacity and (b) the cycle efficiency vs. cycle number of PI-Si-SC electrode half-cells with the electrolyte containing 3 wt.% or 10 wt.% FEC cycled at a current density of 1.0 A g^{-1}.

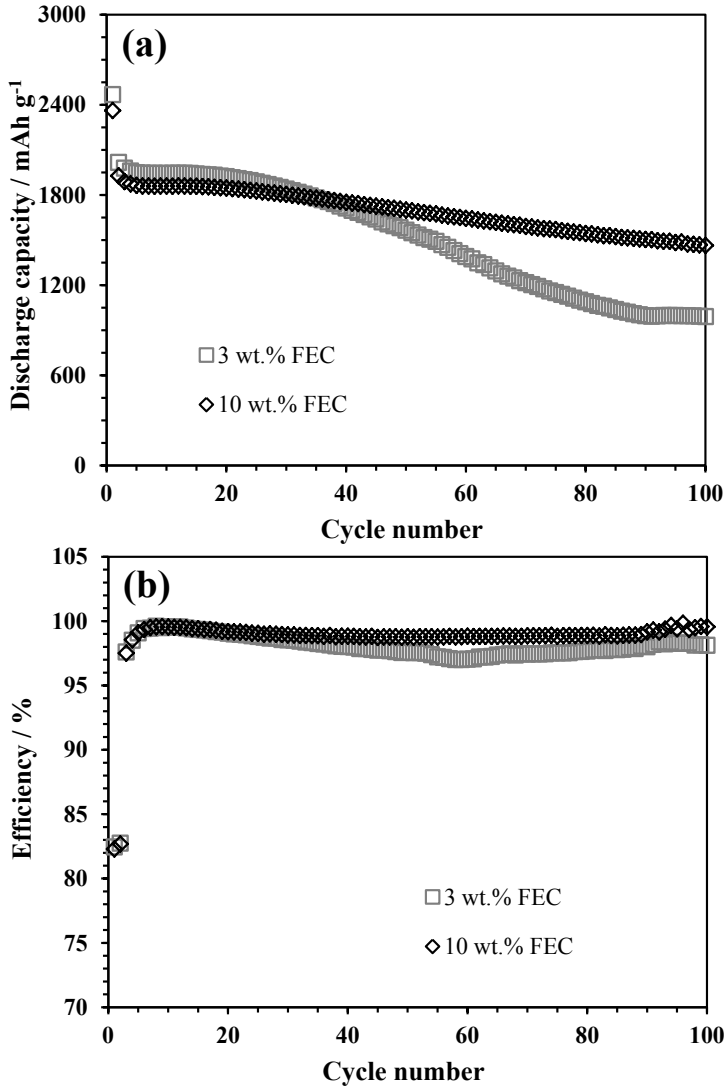

Fig. II-2-3-7 Discharge capacity (a) and cycle efficiency (b) vs. cycle number of PI-Si-SC electrode half-cells with the electrolytes containing 3 wt.% and 10 wt.% FEC. cycled at a current density of 1.0 A g^{-1}.

The initial cycle efficiency improves to 82.45 % by using PI-Si-SC electrode (Initial cycle efficiency of the Si electrode half-cell is 76.48 %, which is not displayed in Fig. II-2-3-1(b)). The electric conductivity and the stress relaxation effect of the electrode seem to be improved by mixing of SC. The discharge capacity retention at 50th cycle relative to the discharge capacity at 10th cycle of PI-Si-SC electrode half-cell with the electrolyte containing 3 wt.% (80.53%) slightly improves compared with that of PI-Si electrode half-cell (77.53%), which is not as much as we expected and the cycle efficiency of PI-Si-SC electrode half-cell with the electrolyte containing 3 wt.% is decreased as with PI-Si electrode half-cell. We considered that the 3wt.% FEC is insufficient to protect the electrode of which surface area increased by pulverization of Si particles against decomposition of electrolyte, and we decided to increase the amount of FEC to 10 wt.%. There is no fear that the increasing in amount of FEC adversely affects the cell performance because the resistance of SEI formed by FEC is quite low. The 10 wt.% FEC drastically improves the cycle stability and the capacity retention of the PI-Si-SC electrode half-cell at 50th and 100th cycles are 91.44% and 78.74%, respectively. Although the mixing of SC reduce the electrode capacity, our electrode (PI-Si-SC) still has a high reversible capacity (1900 mAh g^{-1}), and the mass loading of active materials (Si and SC) on the PI-Si-SC electrode is sufficient to accommodate positive electrode used in commercially Li-ion batteries.

Fig. II-2-3-8 shows the discharge capacity vs. cycle number of PI-Si-SC electrode half-cells with 10 wt.% FEC cycled at various current density (1.0 – 16.0 A g^{-1}). The charging process is carried out using C.C-C.V mode in this measurement as with other charge and discharge measurements. Accordingly, the results in this measurement substantially show the discharge rate performance. The discharge capacity is not reduced so much even though the current density increases to 4.0 A g^{-1} and more the cycle stability is not any degraded. At the quite high current density such as 8.0 and 16.0 A g^{-1}, the PI-Si-SC electrode half-cells containing 10 wt.% FEC maintains high discharge capacity (more than 1200 mAh g^{-1}) and it seems to be stable even after cycles, though the long-term cycle test is not realized due to the short circuit caused by too large current for the half-cells with Li counter electrode.

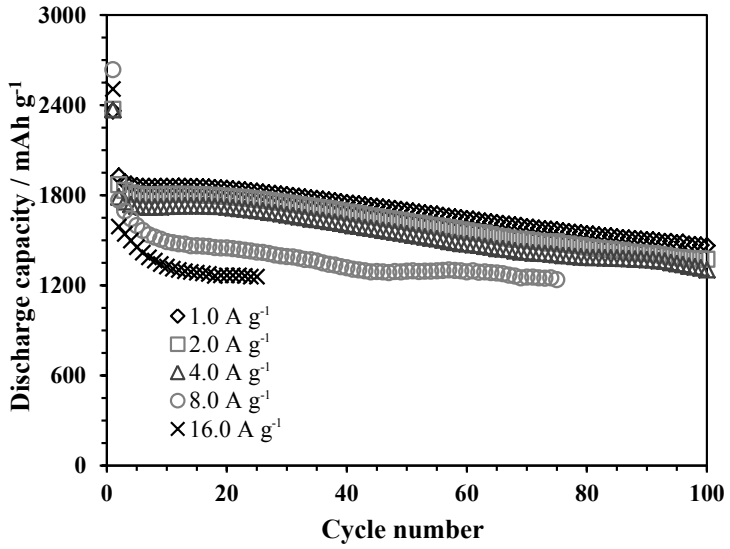

Fig. II-2-3-8 Discharge capacity vs. cycle number of PI-Si-SC electrode half-cells with the electrolyte containing 10 wt.% FEC cycled at various current density (1.0 – 16.0 A g^{-1})

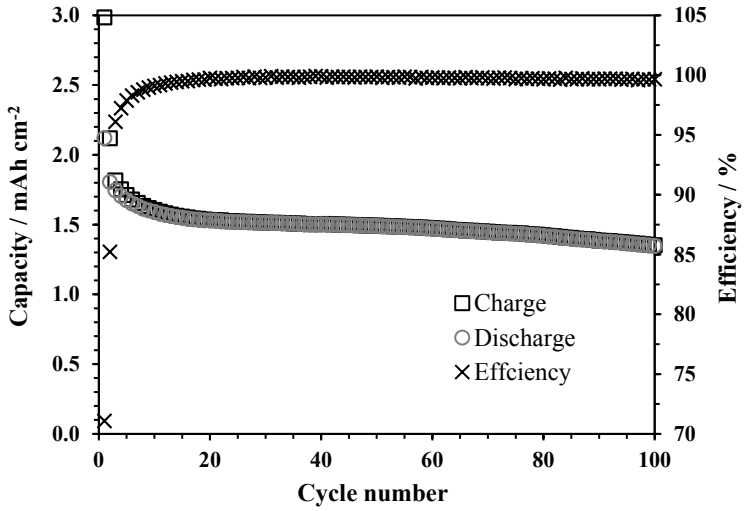

Fig. II-2-3-9 Charge and discharge capacities (correspond to vertical axis on the left side) and cycle efficiency (corresponds to vertical axis on the right side) vs. cycle number of $LiNi_{1/3}Mn_{1/3}Co_{1/3}O_2$/PI-Si-SC cell with the electrolyte containing 10 wt.% FEC cycled at approximately 2.0 A g^{-1} with respect to PI-Si-SC electrode.

We have succeeded in drastically improve the cycle stability of the negative electrode composed of untreated μm-Si particles by optimizing the electrode and electrolyte configuration. Accordingly, we investigated the cycle stability of the full-cell including the PI-Si-SC electrode and the electrolyte containing 10 wt.% FEC. The positive electrode is composed of $LiNi_{1/3}Mn_{1/3}Co_{1/3}O_2$ as active material of which mass loading is approximately 14.5 mg cm^{-2}. The mass loading of the active material (Si + SC) was adjusted to approximately 1.3 mg cm^{-2} which is two-thirds of the PI-Si-SC electrode used in half cells to match the mass loading of the positive electrode. Fig. II-2-3-9 shows the charge/discharge capacities (correspond to vertical axis on the left side) and cycle efficiency (corresponds to vertical axis on the right side) vs. cycle number of $LiNi_{1/3}Mn_{1/3}Co_{1/3}O_2$/PI-Si-SC cell containing 10 wt.% FEC cycled at approximately 2.0 A g^{-1} with respect to PI-Si-SC electrode. The charge and discharge capacities of the $LiNi_{1/3}Mn_{1/3}Co_{1/3}O_2$/PI-Si-SC cell decreases during initial 10 cycles and then it is stable during 90 cycles. The cycle efficiency is maintained at quite high value exceeding 99.6% during 100 cycles except for the initial 10 cycles. This result substantiates that the PI-Si-SC electrode in the electrolyte with 10 wt.% also shows the excellent cycle stability in the full-cell.

II-2-4. Conclusions

The use of electrolyte additives such as VC or FEC further improves the cycle stability of the Si electrode prepared with PI, but the SEI formed by these additives are different from each other. The SEI formed in the electrolyte containing VC is composed of organic components mainly and does not have the effect to suppress the excessive decomposition of electrolyte, which leads to the significantly increase of resistance derived from SEI. In contrast, the SEI formed by FEC of which resistance is quite low includes the large amount of LiF and it is effective to suppress the decomposition of the electrolyte. The Si electrode prepared with PI binder can avoid the significant collapse by forming the cracks like islands as we reported previously. In this work, we found the increase of the SEI also significantly affects the form of islands. Judging from the SEM images, it seems that the amount of SEI formed in the electrolyte containing FEC is quite small and dose not collapses the shape of island. We determined that the FEC is

better as an electrolyte additive than VC, and tried to further improve the cycle stability by combining the electrolyte containing FEC and the PI-Si-SC electrode. Although the 3 wt.% FEC is not sufficient to obtain the enough cycle stability, the addition of 10 wt.% FEC drastically improves the cycle stability of the PI-Si-SC electrode. The combination of PI-Si-SC and the electrolyte containing 10 wt.% FEC shows excellent discharge rate performance and maintains the discharge capacity more than 1200 mAh g^{-1} at high current density as 16.0 A g^{-1}. Moreover, the cycle stability does not degrade at high current density. The $LiNi_{1/3}Mn_{1/3}Co_{1/3}O_2$/PI-Si-SC cell containing 10 wt.% FEC also shows quite good cycle stability during 100 cycles, and the result substantiates that the PI-Si-SC electrode in the electrolyte with 10 wt.% also shows the excellent cycle stability in the full-cell. In this work, we have demonstrated that the quite good cycle stability is obtained by the selection of suitable binder (PI), electrolyte additive and its amount (10 wt.% FEC) even though untreated μm-Si is used as active material. We believe that the result in this work which enables the use of large size Si particles is major step toward the practical application of Si negative electrode.

II-2-5. References

[1] K. Mizushima, P. C. Jones, P. J. Wiseman, J. B. Goodenough, Mat. Res. Bull. 15 (1980) 783.

[2] M. M. Thackeray, P. J. Johnson, L. A de Picciotto P. G. Bruce, J. B. Goodenough Mat. Res. Bull. 19 (1984) 179.

[3] T. Ohzuku, Y. Iwakoshi, and K. Sawai, J. Electrochem. Soc. 140 (1993) 2490.

[4] T. Ohzuku, A. Ueda, M. Nagayama, Y. Iwakoshi, H. Komori, Electrochimica Acta, 38 (1993) 1159.

[5] T. Ohzuku, Y. Makimura, Chem. Lett. 30 (2001) 642.

[6] T. Ohzuku, Y. Makimura, Chem. Lett. 30 (2001) 744.

[7] R. A. Huggins, J. Power Sources 81-82 (1999) 13.

[8] B. A. Boukamp, G. C. Lesh, R. A. Huggins, J. Electrochem. Soc. 128 (1981) 725.

[9] Y. Oumellal, N. Delpuech, D. Mazouzi, N. Dupre, J. Gaubicher, P. Moreau, P. Soudan, B. Lestriez, D. Guyomard, J. Mater. Chem. 21 (2011) 6201.

[10] J. H. Ryu, J. W. Kim, Y. E. Sung, and S. M. Oh, Solid-State Lett. 7 (2004) A306.

[11] S. Pal, S. Damle, S. Patel, M. K. Dutta, P. N. Kumta, S. Maiti, ECS Trans. 41 (2012) 87.

[12] H. Kim, M. Seo, M. H. Park, J. Cho, Angew. Chem. Int. Ed. 49 (2010) 2146.

[13] C. K. Chan, H. Peng, G. Liu, K. Mcilwrath, X. F. Zhang, R. A. Huggins, Y. Cui, Nat. Nanotechnol. 3 (2008) 31.

[14] S. L. Chou, J. Z. Wang, M. Choucair, H. K. Liu, J. A. Stride, S. X. Dou, Electrochem. Commun. 12 (2012) 303.

[15] X. Zhao, C. M. Hayner, M. C. Kung, H. H. Kung, Adv. Energy Mat. 2 (2011) 1079.

[16] In preparation

[17] C. K. Chan, R. Ruffo, S. S. Hong, Y. Cui, J. Power Sources 189 (2009) 1132.

[18] L. Chen, K. Wang, X. Xie, J. Xie, Electrochem. Solid-State Lett. 9 (2006) A512.

[19] M. N. Obrovac, L. Christensen, Electrochem. Solid-State Lett. 7 (2004) A93.

[20] J. Li, A. K. Dozier, Y. Li, F. Yang, Y. T. Cheng, J. Electrochem. Soc. 158 (2011) A689.

[21] Z. Chen, L. Christensen, J.R. Dahn, Electrochem. Commun. 5 (2003) 919.

[22] J. Li, R. B. Lewis, J. R. Dahn, Electrochem. Solid-State Lett. 10 (2007) A17.

[23] V. Etacheri, O. Haik, Y. Goffer, G. A. Roberts, I. C. Stefan, R. Fasching, D. Aurbach, Langmuir 28 (2012) 965.

CONCLUDING REMARKS

In this thesis, the novel key technologies for fabricating advanced Li-ion batteries containing the next generation electrode materials are discussed. Each section is summarized below.

In CHAPTER I, the novel rapid synthesis method for $LiFePO_4$/C composite with sufficient electric conductivity and ideal crystal structure is described.

Section I-1

The $LiFePO_4$/C composite is successfully synthesized using Fe_2O_3 in far less time (within a few minutes) compared to conventional method by combination carbothermal reduction with high-frequency induction heating. The battery performances of synthesized sample are investigated by various measurements. Obtained results are described as follows;

1. The LFP-C synthesized by heating at 700°C for 1 h contains large amount of Fe^{3+} species deriving from Fe_2O_3 because the carbothermal reduction is not completed and the cathode containing LFP-C shows low charge-discharge capacity (118.6 mAh g^{-1}) compared to theoretical capacity.
2. The application of a higher heating temperature to improve the reaction kinetic increases charge-discharge capacity by suppressing the remaining of Fe^{3+} species. The generation of over reduction byproducts such as Fe_2P or Fe_3P can be suppressed by adjustment of heating time.
3. The LFP-90 synthesized in optimized conditions contains no impurities, and the particle size is sufficiently small to achieve the high battery performances. The charge-discharge rate performance and cycle stability of the cathode containing LFP-90 is excellent and the discharge capacity is 153.3 and 100.1 mAh g^{-1} at 1/10 and 10 C-rate, respectively.

Section I-2

The heating condition is adjusted in order to promote carbonization of citric acid as carbon source and improve electric conductivity of $LiFePO_4$/C composite. The

physical properties and battery performances of $LiFePO_4$/C synthesized by adjusted condition is investigated by various measurement. The obtained results are described as follows;

1. The electrical conductivity of $LiFePO_4$/C can be improved from 8.7 x 10^{-3} to 1.9 x 10^{-2} S cm^{-1} by introducing the short-time annealing process at 700°C following the sintering process at 900°C.
2. The discharge capacities of the annealed $LiFePO_4$/C cathode at 1/10, 1, and 10 C-rates are 156.0, 136.3, and 100.1 mAh g^{-1}, respectively, which are somewhat larger than those of the non-annealed $LiFePO_4$/C cathode. In addition, the polarization between charge and discharge of the annealed $LiFePO_4$/C cathode is much smaller than that of the non-annealed cathode.
3. The difference in these electrochemical properties seems to be derived from a difference in the electrical conductivity of residual carbon at the surface of $LiFePO_4$ particles because formation of Fe_2P as impurity and increase in primary and secondary particle sizes are not observed during annealing.

Section I-3

The shape of carbon crucible is optimized for homogeneously heating condition to obtain ideal crystal structure of $LiFePO_4$ phase. The physical properties, crystal structure and battery performances of $LiFePO_4$/C synthesized by optimized carbon crucible for homogeneously heating the pellet precursor from both sides is investigated by various measurement. The obtained results are described as follows;

1. The optimized $LiFePO_4$/C has ideal lattice parameters close to it reported by Padhi et al.
2. Although the optimized sample has slightly larger primary particle size distribution and lower electric conductivity compared to previous sample due to the difference of heating condition, the size of the semicircle on the nyqist plot of the electrode containing optimized sample was reduced compared to that of the electrode containing previous sample.

3. The electrode containing optimized sample shows specific discharge capacity of 168.0 mAh g^{-1}, which achieves 99% of theoretical specific capacity of $LiFePO_4$ phase and the discharge capacity of it in charge and discharge rate performance test is superior to the electrode containing previous sample in all of 1/10 – 20 C-rates.

In CHAPTER II, the improvement method for cycle stability of Si electrode without optimizing Si active material by focusing on binder and electrolyte additives is described.

Section II-1

The cycle stability of Si electrode without use of nano-Si is improved by using PI as a binder and highly porous polyolefin film coated with ceramic as a separator. It is quite interesting that the battery components which do not directly involved in the charge and discharge reactions such as binders and separators significantly affect the battery performances of Si negative electrode. The obtained battery performances of μm-Si electrode prepared with PI binder are described as follows;

1. The PI-Si electrode maintains the discharge capacity of 800 mAh g^{-1} during 196 cycles at the current density of 800 mA g^{-1}.
2. The PI-Si electrode including 10 wt.% of AB (Electrode B) maintains the discharge capacity of 800 mAh g^{-1} during 167 cycles even at high current density (1600 mA g^{-1}). Therefore, the cause of degradation of the electrodes at high current density is lack of electric conductivity and the PI binder does not hinder Li ion access to Si particles.
3. The Li ion supply from bulk electrolyte also affected the cycle stability of PI-Si electrode as well as electric conductivity. The cells including highly porous separator maintain the discharge capacity of 800 and 1200 mAh g^{-1} during 300 cycles and 166 cycles, respectively.

Section II-2

In order to select an electrolyte additive to form effective SEI layer which can

prevent excessive electrolyte decomposition together with pulverization of Si particles, the effect of electrolyte additives on μm-Si electrode prepared with PI binder is investigated by using various measurements. The obtained results are described as follows;

1. The SEI formed in the electrolyte containing VC is composed of organic components mainly and does not have the effect to suppress the excessive decomposition of electrolyte. In contrast, the SEI formed by FEC of which resistance is quite low includes the large amount of LiF and it is effective to suppress the electrolyte decomposition.
2. It was found that the increase of the SEI significantly affects the form of islands. Judging from the SEM images, it seems that the amount of SEI formed in the electrolyte containing FEC is quite small and dose not collapses the shape of island.
3. Although 3 wt.% FEC is not sufficient to obtain the enough cycle stability, 10 wt.% FEC drastically improves the cycle stability of the PI-Si-SC electrode. The combination of PI-Si-SC and the electrolyte containing 10 wt.% FEC shows excellent discharge rate performance and maintains the discharge capacity more than 1200 mAh g^{-1} at high current density as 16.0 A g^{-1}. Moreover, the cycle stability does not degrade at high current density.
4. The $LiNi_{1/3}Mn_{1/3}Co_{1/3}O_2$/PI-Si-SC cell containing 10 wt.% FEC also shows quite good cycle stability during 100 cycles.

PUBLICATIONS LIST

CHAPTER I

Section 1

Satoshi Uchida, Masaki Yamagata and Masashi Ishikawa
"A Novel Rapid Synthesis Method of $LiFePO_4$/C Cathode Material Using High-Frequency Induction Heating"
Journal of Power Sources, **243**, 481 (2013)

Section 2

Satoshi Uchida, Masaki Yamagata and Masashi Ishikawa
"Improvement of Synthesis Method for $LiFePO_4$/C Cathode Material by High-frequency Induction Heating"
Erectrochemistry, **80**, 825 (2012).

Section 3

Satoshi Uchida, Masaki Yamagata and Masashi Ishikawa
"Optimized Heating Condition of High-Frequency Induction Heating for $LiFePO_4$ with Ideal Crystal Structure"
Journal of Power Sources, **243**, 617 (2013)

CHAPTER II

Section 1

Satoshi Uchida, Megumi Mihashi, Masaki Yamagata and Masashi Ishikawa
"Electrochemical Propaties of Silicon Negative Electrodes Prepared with Polyimide Binder"
Journal of Power Sources, in press

Section 2

Satoshi Uchida, Masaki Yamagata and Masashi Ishikawa
"Effect of Electrolyte Additive on Si Negative Electrode Prepared with polyimide binder"
Journal of The Electrochemical Society, submitted

ACKNOWLEGMENTS

The author wishes to express my most sincere appreciation to Professor Masashi Ishikawa, Department of Chemistry and Material Engineering, Faculty of Chemistry, Material and Bioengineering, Kansai University, for his thorough guidance and hearty encouragement for achievement of this work.

The author wishes to my sincere appreciation to Professor Ryuichi Arakawa and Professor Yoshinori Arachi for their helpful suggestions in preparing this thesis.

The author wishes to my sincere appreciation to Associate Professor, Masaki Yamagata, Dr. Yuichi Honda, Shigeaki Yamazaki and Toshinori Sugimoto for their kind guidance and helpful suggestions for achievement of this work.

Sincere gratitude is made to Professor Hiroyuki Aota, Yuichi Ohya, Hideya Kawasaki, Mitsukazu Ochi, Yutaka Nishiyama, Koichi Tanaka, Yasuo Nakabayashi, Hiromitsu Kozuka and other faculty members of chemistry, materials and bioengineering for their warm encouragement.

Thanks are given to the author's co-workers, especially Ms. Megumi Mihashi, graduates and members of the electrochemistry laboratory for their help, valuable suggestions and friendships.

Finally, the author wishes to my deepest gratitude to his father, his mother, his grandfathers, his grandmothers and all the people who support him for giving me good advice, encouragement, mental and financial supports in accomplishment of this work.

September 2013

Satoshi Uchida